Lappeenranta
University of Technology

Riina Salmimies

ACIDIC DISSOLUTION OF IRON OXIDES AND REGENERATION OF A CERAMIC FILTER MEDIUM

Thesis for the degree of Doctor of Science (Technology) to be presented with due permission for public examination and criticism in the Auditorium 1383 at Lappeenranta University of Technology, Lappeenranta, Finland on the 14th of December, 2012, at noon.

Acta Universitatis
Lappeenrantaensis 495

Supervisors

Professor Emeritus Juha Kallas
LUT Chemistry
Lappeenranta University of Technology
Finland;
Professor Emeritus
Laboratory of Inorganic Materials
Tallinn University of Technology
Estonia

Professor Antti Häkkinen
LUT Chemistry
Lappeenranta University of Technology
Finland

Reviewers

Professor Richard Wakeman
Department of Chemical Engineering
Loughborough University
Great Britain

Leading Research Scientist Rein Kuusik
Department of Chemical Engineering
Tallinn University of Technology
Estonia

Opponent

Professor Richard Wakeman
Department of Chemical Engineering
Loughborough University
Great Britain

Custos

Professor Antti Häkkinen
LUT Chemistry
Lappeenranta University of Technology
Finland

ISBN 978-952-265-331-4, ISBN 978-952-265-332-1 (PDF), ISSN 1456-4491

Lappeenrannan teknillinen yliopisto

Yliopistopaino 2012

“Intelligence plus character – that is the goal of true education.”

Martin Luther King, Jr.

Abstract

Riina Salmimies

Acidic dissolution of iron oxides and regeneration of a ceramic filter medium

Lappeenranta 2012
51 p.

Acta Universitatis Lappeenrantaensis 495
Diss. Lappeenranta University of Technology

ISBN 978-952-265-331-4, ISBN 978-952-265-332-1 (PDF), ISSN 1456-4491

The dewatering of iron ore concentrates requires large capacity in addition to producing a cake with low moisture content. Such large processes are commonly energy intensive and means to lower the specific energy consumption are needed. Ceramic capillary action disc filters incorporate a novel filter medium enabling the harnessing of capillary action, which results in decreased energy consumption in comparison to traditional filtration technologies. As another benefit, the filter medium is mechanically and chemically more durable than, for example, filter cloths and can, thus, withstand harsh operating conditions and possible regeneration better than other types of filter media.

In iron ore dewatering, the regeneration of the filter medium is done through a combination of several techniques: (1) backwashing, (2) ultrasonic cleaning, and (3) acid regeneration. Although it is commonly acknowledged that the filter medium is affected by slurry particles and extraneous compounds, published research, especially in the field of dewatering of mineral concentrates, is scarce. Whereas the regenerative effect of backwashing and ultrasound are more or less mechanical, regeneration with acids is based on chemistry.

The chemistry behind the acid regeneration is, naturally, dissolution. The dissolution of iron oxide particles has been extensively studied over several decades but those studies may not necessarily be directly applicable in the regeneration of the filter medium which has undergone interactions with the slurry components.

The aim of this thesis was to investigate if free particle dissolution indeed correlates with the regeneration of the filter medium. For this purpose, both free particle dissolution and dissolution of surface adhered particles were studied. The focus was on acidic dissolution of iron oxide particles and on the study of the ceramic filter medium used in the dewatering of iron ore concentrates.

The free particle dissolution experiments show that the solubility of synthetic fine grained iron oxide particles in oxalic acid could be explained through linear models accounting for the effects of temperature and acid concentration, whereas the dissolution of a natural magnetite is not so easily explained by such models. In addition, the kinetic experiments performed both support and contradict the work of previous authors: the suitable kinetic model here supports previous research suggesting solid state reduction to be the reaction mechanism of hematite dissolution but the formation of a stable iron oxalate is not supported by the results of this research. Several other dissolution mechanisms have also been suggested for iron oxide dissolution in oxalic acid, indicating that the details of oxalate promoted reductive dissolution are not yet agreed and, in this respect, this research offers added value to the community.

The results of the regeneration experiments with the ceramic filter media show that oxalic acid is highly effective in removing iron oxide particles from the surface of the filter medium. The dissolution of those particles did not, however, exhibit the expected behaviour, i.e. complete dissolution.

The results of this thesis show that although the regeneration of the ceramic filter medium with acids incorporates the dissolution of slurry particles from the surface of the filter medium, the regeneration

cannot be assessed purely based upon free particle dissolution. A steady state, dependent on temperature and on the acid concentration, was observed in the dissolution of particles from the surface even though the limit of solubility of free iron oxide particles had not been reached. Both the regeneration capacity and efficiency, with regards to the removal of iron oxide particles, was found to be temperature dependent, but was not affected by the acid concentration. This observation further suggests that the removal of the surface adhered particles does not follow the dissolution of free particles, which do exhibit a dependency on the acid concentration.

In addition, changes in the permeability and in the pore structure of the filter medium were still observed after the bulk concentration of dissolved iron had reached a steady state. Consequently, the regeneration of the filter medium continued after the dissolution of particles from the surface had ceased. This observation suggests that internal changes take place at the final stages of regeneration. The regeneration process could, in theory, be divided into two, possibly overlapping, stages: (1) dissolution of surface-adhered particles, and (2) dissolution of extraneous compounds from within the pore structure.

In addition to the fundamental knowledge generated during this thesis, tools to assess the effects of parameters on the regeneration of the ceramic filter medium are needed. It has become clear that the same tools used to estimate the dissolution of free particles cannot be used to estimate the regeneration of a filter medium unless only a robust characterisation of the order of regeneration efficiency is needed.

Keywords: Ceramic filter medium, Regeneration, Oxalic acid, Dissolution

UDC 66.067.1/.3:66.061:661.743.1:547.461.2

Acknowledgements

Firstly, I wish to acknowledge all those who funded this research: the Graduate School for Chemical Engineering, Outotec (Filters) Oy, the LUT Foundation, LUT CST, the Emil Aaltonen Foundation, and the Magnus Ehrnrooth Foundation, and would like to thank LUT Chemistry and the Laboratory of Separation Technology where this work was done. I also wish to give extra special thanks to Outotec (Filters) Oy. Without their input in providing me with the necessary samples this work could have never been realised. Especially Mr Bjarne Ekberg deserves to be acknowledged for all his input in this thesis. He has been exemplary in his actions in demonstrating how the co-operation between a university and an industrial partner should work.

This research has been enabled by the continuous support of my supervisors. Professor Emeritus Juha Kallas has been the most encouraging influence for me for the past five years and truly is inspirational both as an expert as well as a person. He has a special gift of looking at the big picture and finding words of encouragement even when going gets tough. Professor Antti Häkkinen has been a role model for me throughout this thesis. He commands my absolute professional respect and I would be very fortunate to work with him in the future. There are no words for Antti and I'm very rarely left speechless. I could not imagine anyone doing a better job than my supervisors and for that I shall be ever grateful.

I would also like to thank the reviewers of this thesis, leading research scientist Rein Kuusik from Tallinn University of Technology and Professor Richard Wakeman from Loughborough University. The comments that I received enabled me to further improve this work and I was priviledged to have such prestige reviewers for this thesis. In addition, I would like to acknowledge the hard work of Mr Peter Jones and Mr Trevor Sparks in revising the linguistics of this thesis and of several of my papers.

I have been lucky enough to find numerous friends through my years in the Graduate School for Chemical Engineering. I cannot express how much I've enjoyed our seminars, where, in addition to the scientific programme, I've been blessed with some unforgettable evenings. Pasi, Kalle, Juho, Sanna, Kaarina: thank you for being special people.

My colleagues at the university obviously deserve to be praised. I've been fortunate to work in the research group of solid/liquid – separation for these past five years. Although so many of my colleagues have influenced me in a positive way and have been a part of this thesis in one way or the other, two of them truly stand out for me: Marju and Mikko. Marju is a cheerful person whose help I've always been able to count on. I've experienced everything from organising conferences to discussing my own research results with her. I cannot thank you enough, Marju. What of Mikko then? He has, and most likely will be in the future, a challenge for me. He very often sees things differently than I do and has given me valuable, although sometimes very annoying, perspectives on issues which I thought were straightforward. Even in the final days before this thesis had to go to print he helped me with finishing one of my articles. His brilliant advice, literally, got me through.

Also colleagues at Outotec (Filters) Oy, Mr Jason Palmer and Mr Guido Görres, are kindly acknowledged for their input in several of my papers. In addition, I've been priviledged in having good discussions regarding my work with Mr Rolf Hindström, Mr Mika Illi, and Mrs Lena Kaipia.

My visit to the Norwegian University of Science and Technology in Trondheim in year 2010 was one of the most amazing experiences of my life. The people to thank for that opportunity are associate professor Jens-Petter Andreassen and post-doctoral researcher Ralf Beck. Thank you for welcoming me into your group, and thank you for including me in the orientation programme for the Erasmus exchange students. Special thanks also goes to Dr Julian Tolchard who was kind enough to help me learn more about my samples through the analysis work I did in Trondheim. He surely knows how to make a person feel welcome with his quirky sense of humour. I met the most wonderful people during my first few weeks: Maja, Ciska, Julian, Bastian, Thibault, Joanna. Even one of my flat mates, whose name shall not be mentioned here, sort of grew on me although I hated him for doing his laundry in the shower. Of all those people, Paul, my ever so English flat mate, was the most special in my eyes.

He taught me how to hug people, how to cook, and how I seriously knew nothing about men. I still don't and I always call him for advice. Most of the time he just tells me what twats men are or what a muppet I've been.

The support of my friends, when I've been at the brink of insanity, has gotten me through these past five years. The time spent with them at movies, out having coffee, or partying has *literally* made me forget about the pain of being a doctoral student. My friend Kati, a doctoral student at the department of industrial management at LUT, will also be defending her thesis soon and has surely been the person who understands my pain the best. In addition, she has been my rock through hardship in my personal life. There are no words to thank her enough. My friend Sanna could take the credit for being the party animal, which we all so desperately need. Our twilight experiences have always reminded me that there's more to life than being rational. I'm also forever grateful to Jarkko for those times he would laugh at me for going bonkers over work, for those times when he made me laugh too, and especially for those times when I was tired and only needed him to hold me and say nothing. Sometimes those special people are just a loan and, at the end, there's nothing else you can do but to appreciate the time you had with them. I've been blessed with extraordinary people in my life, and they are where I derive my strength from.

Last, but hopefully not least, I wish to thank myself. Without enduring failure and getting up again, this work would have never been finished. Those times, when my papers got rejected were always moments of disappointment. Those times were, however, also the ones that built character. Next time I will do better, I would say to myself. Reaching for the stars means that you will fall, but not to fall means that you haven't reached high enough.

All these people have a special place in my heart. From underneath the rough exterior that is I, overwhelming gratitude pushes out as I'm writing this. What I wish to leave on the table after this journey is simple: I thank you.

List of publications

This work is based on the following peer reviewed scientific journal articles which will also be referred to in the thesis:

I *Salmimies, R.*, Mannila, M., Kallas, J., and Häkkinen, A.*, 2011. Acidic dissolution of magnetite: experimental study on the effects of acid concentration and temperature, *Clays and Clay Minerals*, 59, 136 – 146.

II *Salmimies, R.*, Mannila, M., Kallas, J., and Häkkinen, A.*, 2012. Acidic dissolution of hematite: kinetic and thermodynamic investigations with oxalic acid, *International Journal of Mineral Processing*, 110 – 111, 121 – 125.

III *Salmimies, R.*, Kallas, J., Ekberg, B., Häkkinen, A.*, 2012. Scale growth in the dewatering of iron ore, *International Journal of Mining Engineering and Mineral Processing*, 1, 69 – 72.

IV *Salmimies, R.*, Kallas, J., Ekberg, B., Andreassen, J.-P., Häkkinen, A.*, 2012. Long-term fouling of ceramic filter media used in the dewatering of hematite, *Filtration*, 14, 219 – 222.

V *Salmimies, R.*, Häkkinen, A., Kallas, J., Ekberg, B., Andreassen, J.-P., and Beck, R.*, Characterisation of long-term scaling effects of ceramic filter media used in the dewatering of a magnetite concentrate, *International Journal of Mineral Processing* (revision submitted)

VI *Salmimies, R.*, Huhtanen, M., Kallas, J., and Häkkinen, A.*, Empirical modelling to describe the solubility of magnetite in oxalic acid, A., *Journal of Powder Technology* (revision submitted)

VII *Salmimies, R.*, Kinnarinen, T., Kallas, J., Ekberg, B., and Häkkinen, A.*, Oxalic acid regeneration of ceramic filter medium fouled in the dewatering of iron ore, *ISRN Chemical Engineering*, 2012.

Author's contribution

The author has been the primary contributor in all publications. The author has done most of the experimental work, the analysis of the data, and the writing of the manuscript. The author has also handled the correspondence with the journals to which the manuscripts have been submitted.

In addition to the scientific peer reviewed publications mentioned above, the author has presented her work at eight international conferences in 2008 – 2012.

Related publications

I *Salmimies, R., Louhi-Kultanen, M., Ekberg, B., Häkkinen, A., Kallas, J., Huhtanen, M.,* 2008. Fouling of filter media: solubility of oxalate solutions, Proceedings of *the 10th World Filtration Congress*, Leipzig, Germany, 14 – 19 April.

II *Salmimies, R., Kallas, J., Häkkinen, A.,* 2008. Magnetite particle dissolution in acidic conditions, Proceedings of the *European Symposium on Comminution and Classification*, Espoo, Finland, 15 – 18 September.

III *Salmimies, R., Häkkinen, A., Ekberg, B., Kallas, J.,* 2009. Dissolution of magnetite particles in acidic conditions, Proceedings of *Filtech 2009*, Wiesbaden, Germany, 13 – 15 October.

IV *Salmimies, R., Häkkinen, A., Ekberg, B., Kallas, J., Andreassen, J.-P.,* 2010. Characterization of filter media used in the dewatering of iron ore, Proceedings of the *13th Nordic Filtration Symposium*, Lappeenranta, Finland, 10 – 13 June.

V *Salmimies, R., Häkkinen, A., Ekberg, B., Kallas, J., Andreassen, J.-P., and Beck, R.,* 2011. Removal of calcium scales from the surface of a ceramic filter medium, Proceedings of *Filtech 2011*, Wiesbaden, Germany, 22 – 24 March.

VI *Salmimies, R., Häkkinen, A., Kallas, J., Ekberg, B., Andreassen, J.-P., Beck, R.,* 2011. Characterisation of long-term scaling effects of ceramic filter media used in the dewatering of iron ore, Proceedings of *Iron Ore 2011*, Perth, Australia, 11 – 13 July.

VII *Salmimies, R., Häkkinen A., Ekberg, B., Kallas J., Andreassen, J.-P.,* 2012. Long-term fouling of ceramic filter medium in the dewatering of hematite concentrate, Proceedings of the *11th World Filtration Congress*, Graz, Austria, 16 – 20 April.

VIII *Salmimies, R., Kallas, J., Ekberg, B., Häkkinen, A.,* 2012. Regeneration of ceramic filter media used in the dewatering of iron ore, Proceeding of the *14th Nordic Filtration Symposium*, Aalborg, Denmark, 30 – 31 August.

TABLE OF CONTENTS

Nomenclature

A	Mean (with appropriate unit in Eq.(19))	-
a	Constant	-
B	Constant (with appropriate unit in Eq.(20))	-
c_{acid}	Concentration of acid	mol/L
c_{Fe}	Concentration of dissolved Fe	mg/L
d	Distance between crystal planes	m
F	Bubble flow	cm^3/min
H	Permeability	$L/(m^2\ h\ bar)$
k	Reaction rate coefficient	1/s
n	Order of diffraction	-
P	Pressure	Pa
t	Time	min
T	Temperature	°C
x_a	Autoscaled value (with appropriate unit)	-
x_c	Centered value (with appropriate unit)	-
x_i	Initial value (with appropriate unit)	-
α	Extent of reaction	-
λ	Wavelength	m
θ	Diffraction angle	°

Abbreviations

AAS	Atomic absorption spectroscopy
DHEDPA	1,2-dihydroxyethane-1,1-diphosphonic acid
EDS	Energy dispersive X-ray spectroscopy
EDTA	ethylene diamine tetra acetic acid
FAAS	Flame atomic absorption spectroscopy
FTIR	Fourier transform infrared microscopy
HEDPA	1-hydroxyethane-1,1-diphosphonic acid
ICP-OES	Inductively coupled plasma optical emission spectroscopy
NTA	Nitrilotriacetic acid
PMI	Porous Materials Incorporated
SEM	Scanning electron microscopy
SFS	Formaldehydesulfoxylate
TOC	Total organic carbon
VDPA	Vinylidene-1,1-diphosphonic acid
XRD	X-ray diffraction

1 INTRODUCTION

Iron oxides, referring to both oxides and hydroxides, are present in numerous environmental and industrial systems and attract multidisciplinary attention from geologists, soil scientists, engineers, material scientists, and medicine. Whereas hematite can be found e.g. in cosmetics as a pigment or as the primary component in iron ore, magnetite can be used for e.g. catalysis and is also a primary iron ore component. Iron oxides, e.g. goethite, are common products of iron and steel corrosion making them familiar to most of earth's population.

The dissolution of iron oxides has been extensively studied for several decades but it appears that a general consensus on the reaction mechanisms or the applicable kinetic models has not yet been achieved in the scientific community. Discrepancies between existing studies show that even the dissolution of solid particles is not fully understood. Furthermore, most studies are done by using pure iron oxides and the results do not necessarily directly apply to industrial iron ore concentrates, which contain impurities even after the concentration process.

The dissolution of iron oxides is especially important in understanding the regeneration process of the ceramic filter medium commonly used in the dewatering of iron ore. The regeneration is done with acids, as iron oxides have been shown to dissolve in acidic media better than in bases. The regeneration acid is thus specifically targeted at dissolving the slurry particles. With effective regeneration of the filter medium, the lifetime of the filter medium can be extended and, consequently, the cost of operation for the process owner can be reduced.

Ceramic capillary action disc filters represent a novel filtration technology, providing more energy efficient dewatering than conventional filtration technologies. Although the actual filtration process is well understood and widely accepted theories of filtration can be applied, the regeneration of the filter medium has, so far, had less attention. In general, the regeneration of any filter medium has so far received little attention in either textbooks or research publications. The ceramic filter medium has been in use in membrane filtration for a much longer time, but the application of the medium in cake filtration has been more limited until the introduction of the full-scale ceramic capillary action disc filters. Although research done in the field of cross flow filtration can provide useful information, the required separation, the suspension composition, and the fluid flow conditions differ significantly from those in mineral concentrate dewatering.

The choice acid used for cleaning is mostly based on literature describing the performance of the chemical in dissolving iron oxide particles, and on some test work. However, actual research on whether the performance of the cleaning chemical in dissolving particles from the surface, and possibly from inside the filter medium, can be assessed based on free particle dissolution is scarce. In addition, long-term use of the ceramic filter medium can result in effects, which are difficult to identify through laboratory experiments and, to the best knowledge of the author, studies on those long-term effects have not been published.

1.1 The research question

The primary research question for this thesis was:

> Can the cleaning performance of a specific chemical, in the regeneration of a ceramic filter medium, be predicted by free particle dissolution experiments?

The focus was on the study of acidic dissolution of both free and surface adhered particles.

During this thesis, it became clear even the dissolution of free particles of iron oxides have not been agreed within the scientific community and more effort in the development of tools to describe this

dissolution were required. The acquisition of the dissolution data for free particles was, however, found to be very time-consuming.

1.2 Outline of the thesis

This thesis comprises 7 international journal publications, and is essentially divided in two parts: a review of the existing literature and an experimental part based on the previously introduced research question.

Theoretical and previously published aspects of iron oxide dissolution, with an emphasis on acidic dissolution, and filtration are discussed in the first four Chapters. Chapter 2 introduces some basic characteristics of iron oxides, emphasising those of magnetite and hematite. Subsequently, Chapter 3 is used to discuss the specific aspects of dissolution, e.g. dissolution mechanisms, related to iron oxides, again emphasising the behaviour of magnetite and hematite. Chapter 4 familiarises the reader with the basic concepts of filtration of mineral slurries, starting with the fundamentals of vacuum filtration and moving on to discuss, in general, the blinding of the filter medium, which is one of the most important themes of this thesis. Finally, ceramic capillary action technology and the related disc filters are discussed briefly. Chapter 5 introduces the analytical techniques which form the foundation for the following experimental work.

The experimental part and results of this thesis are discussed by referring to the peer reviewed articles and by including additional, previously unpublished, data. Chapter 6 briefly describes the experimental methods used in this thesis. The results, starting with Chapter 7, comprise three distinct steps. Firstly, observations of free particle dissolution, included in Paper I and II, are discussed as the dissolution of free particles is easily studied at the laboratory scale and would be a useful tool for estimating the efficiency of specific chemicals in dissolving those same particles from solid surfaces. Secondly, to reinforce the research question and demonstrate to the reader that solid iron oxide particles do indeed influence the filter medium in an iron ore dewatering process, characteristics of used filter media are presented with references to Paper III, IV, and V. Thirdly, some aspects of the dissolution of those solid particles from the surface of a ceramic filter medium, included in Paper VI, are presented. Chapter 8 is then used to discuss whether free particle dissolution experiments can indeed be used to estimate the dissolution of those same particles from surfaces or not. This ties together the information produced in the three experimental steps.

I THEORY

Numerous published papers exist on the dissolution of iron oxides. Those research papers, however, do not necessarily agree on the mechanisms of dissolution, making the direct application of those results slightly challenging. Published literature on the acidic dissolution of iron oxide particles is discussed here.

In addition to describing the principle operation of vacuum disc filters the reader is introduced to numerous studies on the blinding of the filter medium, mostly regarding cross flow membrane filtration, and several analytical techniques used to study blinding. Finally, the analytical techniques chosen for this thesis are introduced, to justify their selection and to identify some limitations related to those techniques.

2 IRON OXIDES

Before going into details about the dissolution of iron oxides, certain basic characteristics of these compounds should be introduced. This chapter does not cover all iron oxides but only those relevant to this thesis: hematite and magnetite. A brief description is also given of goethite, as the dissolution of goethite has been described by several authors. An extensive review of the characteristics of all iron oxides, including their crystal structure, has been given by Cornell and Schwertmann (2003).

Hematite, α-Fe_2O_3, is an Fe(III) oxide having a corundum structure, resembling that of α-alumina, α-Al_2O_3. The most common morphologies of hematite crystals are hexagonal plates and rhombohedra, although several other morphologies exist. All iron oxides containing Fe(III) can be subject to isomorphous cation substitution, i.e. the substitution of lattice Fe(III) with another metal cation, commonly having the same oxidation state, but cations with other oxidation states can also substitute Fe(III). Possible metals that can substitute Fe(III) include aluminium (Al(III)), chromium (Cr(III)), and manganese (Mn(III)). The substitution does not change the structure of the oxide, but does affect the dimensions of the unit cell and, for example, the dissolution behaviour (Wells *et al.*, 2001). Cation substitution can be observed by several analytical techniques, of which one is the shift of X-ray peaks in comparison to non-substituted oxides.

Magnetite, Fe_3O_4, is an iron oxide comprising both bi- and trivalent iron in its lattice. Magnetite has a spinel structure similar to several other minerals. Magnetite, in addition to titanomagnetite, is responsible for the magnetic properties of rocks. The principal morphology of magnetite crystals is octahedral, although, again, other morphologies also exist. Magnetite is also susceptible to cation substitution, as it contains both lattice Fe(III) and Fe(II). Both bi- and trivalent cations, including Al(III), Mn(II), copper (Cu(II), and zinc (Zn(II), can substitute the Fe-atoms within the structure. Magnetite is one of the few iron oxides exhibiting ferrimagnetic properties.

Goethite, α-FeO(OH), is a widespread compound throughout the global ecosystem. Being one of the most thermodynamically stable iron oxide compounds at ambient temperature, goethite is usually, depending on the precursor, the first or the last iron oxide to form on the reaction pathway consisting of different formation and transformation reactions. The coloration of goethite varies from dark brown or black for crystal aggregates to yellow for powder. Goethite is isostructural to diaspore (α-AlO(OH)) and is thus said to have a diaspore structure. The crystals commonly exhibit an acicular morphology. Due to the isostructural correlation with other compounds, goethite also exhibits isomorphous cation substitution. The most common Fe(III) substituting cation is Al(III) which can substitute up to one third of the total Fe(III) in goethite. The reductive dissolution kinetics can be decreased with increasing Al(III) substitution (Gonzalez *et al.*, 2002). The changes in the mineralogical properties, especially in unit cell dimensions, of goethite as a result of cation substitution have been described by Wells *et al.* (2006).

Due to their intense colour, all of the previously mentioned iron oxides can, and are, used as pigments for cosmetics and paints. Those oxides are also common staining compounds in e.g. ceramics. Iron oxides can also be used as catalysts and adsorbents. In addition to the chemical industry, all these oxides are present in iron ore. Hematite and magnetite are the two most important iron ores in the world, whereas the beneficiation of goethite has so far been less extensive.

3 DISSOLUTION OF IRON OXIDES

The two most important iron oxides in iron ores are hematite (α-Fe_2O_3) and magnetite (Fe_3O_4). Hematite comprises only trivalent iron (Fe(III)) whereas magnetite contains both Fe(II) and Fe(III). Hematite, in general, is more stable than magnetite and is more difficult to dissolve. Both Fe(III) and Fe(II) have low solubility and the total dissolved iron in pH 4-10 is below 1 μM (Cornell and Schwertmann, 2003). Dissolution kinetics, in general, are slow.

On an industrial scale, dissolution of iron oxides plays an important role in the leaching of iron ores (Chiarizia and Horwitz, 1991), in dissolving iron oxide scales from heat exchangers (Bruyere and Blesa, 1985) and impurities from clay and silica minerals (Taxiarchou *et al.*, 1997a; Taxiarchou *et al.*, 1997b; Mandal and Banerjee, 2004).

The dissolution process can be affected by several factors. The properties of the system, e.g. temperature and lighting conditions, the properties of the solid phase, e.g. particle size distribution, surface area and chemical composition, and the composition of the liquid phase, e.g. pH, redox potential and concentration of the solvent, can all, to some extent, be regarded as variables for a dissolution process. In most studies some of these are fixed, e.g. the chemical composition of the solid, and research is focused on determining the effects of only a few variables on the dissolution process.

When metal oxides are exposed to water, the oxide surface groups transform into hydrated oxides or hydroxides which can adsorb different ions (Stumm and Furrer, 1987). The surface charge of the solid depends on proton transfer and is thus pH dependent. Although the theory of the electric double layer can account for dispersion and aggregation of particles, only chemical reactions can explain the interactions of the surface and the solute species.

In this Chapter, the basic mechanisms of dissolution of iron oxides are discussed. The emphasis is on reporting previous results of dissolution of iron oxides in different acids and other dissolution methods, for example using microbes, are overlooked here. Furthermore, specific investigations and earlier studies on the dissolution of hematite and magnetite are presented. Alkaline leaching is not considered as an extensive review of existing literature (Stefanova and Aromaa, 2012) has shown that iron oxides do not dissolve in alkaline media.

3.1 Mechanisms of dissolution

The mechanisms of dissolution of metal oxides have been discussed extensively by Stumm and Furrer (1987). The kinetics of dissolution have, in turn, been presented by Brown *et al.* (1980) in general for different solids. Cornell and Schwertmann (2003) have further discussed the mechanisms and kinetics of dissolution of iron oxides.

Iron oxides are dissolved through three distinct mechanisms: (1) protonation, (2) complexation, and (3) reduction. In general, protonation is the slowest and reduction, in turn, the fastest mechanism. Individual solvents do not necessarily exhibit only one of these mechanisms but rather, as dissolution proceeds, the mechanism can change. Banwart *et al.* (1989) have also suggested that two supporting mechanisms can co-exist and that ligand-promoted reductive dissolution, combining both complexation and reduction, would result in the most desired effect for kinetics of dissolution.

The surface of an iron oxide commonly undergoes surface modification when placed in an aqueous medium. The Fe atoms in the oxide can act as Lewis acids which, in aqueous systems, associate with hydroxyl ions or water molecules. Once water is adsorbed, the molecule commonly dissociates and the surface is left with hydroxyl groups. Thus, most of the reactions presented below, will start with a surface containing hydroxyl groups.

3.1.1 Protonation

Protonation, as could be assumed, is a reaction between the protons and the surface groups of the solid iron oxide. The general reaction between Fe(III) oxides and protons proceeds according to Eq. (1):

$$FeO(OH)_{aq} + nH^+ \rightarrow [Fe(OH)_{(3-n)}]^{n+}{}_{aq} + (n-1)\ H_2O \quad (1)$$

Although Eq. (1) seems simple enough, the reaction mechanism consists of several steps. According to Stumm and Furrer (1987), the reaction is initiated at the surface where an Fe atom is coordinated to a neutral OH/OH_2 pair. The OH group adsorbs a proton, changing the neutral surface group into a positively charged group, $Fe(III)(OH_2)_2^+$. Two more protons are then adsorbed, which promotes the polarisation and consequent weakening of the Fe-O bond. Once the bond is weak enough, Fe is detached from the lattice. The adsorption of protons onto the surface of the oxide is commonly very fast and the actual rate determining step is the detachment of the iron from the lattice.

Dissolution in e.g. hydrochloric acid (HCl) or nitric acid (HNO_3) is governed by protonation but the anions of the acids are not without importance. The anions can promote the dissolution of iron oxides by replacing the surface OH groups and further facilitating the detachment of Fe atoms, as was suggested by Sidhu *et al.* (1981) when dissolving different iron oxides with HCl and perchloric acid ($HClO_4$). It has been proposed that chloride ions accelerate the dissolution, by forming complexes with the Fe atoms, which consequently enhance the interaction between the oxide surface and the protons. Observed dissolution rates were higher for magnetite than for hematite and were suggested to result from differences in the crystal structure of the two oxides: Fe occurs in both octahedral and tetrahedral sites in magnetite but only in octahedral sites in hematite.

3.1.2 Complexation

Complexation, or ligand-promoted dissolution, is a reaction between the surface groups of the oxide and the complexing ligands of the solvent that, in turn, promotes the detachment of the iron together with the ligand from the surface of the solid.

$$Fe(III)OH_s + L^- + H^+ \rightarrow Fe(III)L_s + H_2O \rightarrow Fe(III)L_{aq} + H_2O \quad (2)$$

The complete dissolution of iron oxides in carboxylic acids has essentially been suggested (Panias *et al.*, 1996) to comprise three simultaneous mechanisms: (1) adsorption of the ligands, (2) non-reductive dissolution, and (3) reductive dissolution. Complexation is initiated by the adsorption of the ligand onto the surface, much like the adsorption of protons in protonation, and followed by the detachment, or desorption, of the metal with the ligand and their subsequent transfer into the solution phase. At this stage, the surface is left with reactive O^- and OH^- sites which are protonated and the surface is restored. Reductive dissolution takes place once Fe(II) ions have been generated in the solution after an induction period. Fe(II) is present in the lattice in magnetite, so Fe(II) can be generated through dissolution but for hematite, containing no lattice Fe(II), the generation of Fe(II) is through electron transfer from the ligand to the Fe(III) ions. Once Fe(II) has been generated, the dissolution process becomes autocatalytic and the rate of dissolution is increased significantly. The

factors affecting the dissolution mechanism include the pH of the initial solution, temperature, illumination of the solution with UV light and the addition of bivalent iron to the initial solution.

Oxalic acid, by dissociation, produces a strong complexing agent, the oxalate ion, which can be adsorbed onto the surface of the oxide to form a strong surface complex (Eq. (3)). After the metal atom detaches from the surface with the ligand, the negative surface is restored by protonation.

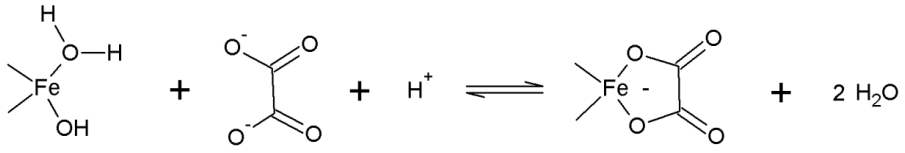

(3)

Further attachment of protons and hydrogen oxalate species has been described by Blesa *et al.* (1987). The speciation of oxalic acid is, however, very much pH dependent, which could explain the existence of an optimum pH for the rate of oxalate promoted dissolution. The speciation of oxalic acid at different pH has been considered by several authors (Lee *et al.*, 2007; Panias *et al.*, 1996, Cornell and Schindler, 1987).

3.1.3 Reduction

Reduction is a process where the lattice Fe(III) is reduced to Fe(II). The process requires electron transfer, which can take place either through the adsorption of an electron donor, through cathodic polarisation of a supporting electrode, or through electron transfer from a ternary surface complex. Consequently, reduction is slightly more complicated in comparison to the other two dissolution mechanisms and can not be described by a simple generic reaction equation. As Fe(III) is reduced to Fe(II), the loss of charge and the change in the physical size of the Fe atom facilitate the detachment of Fe(II) from the lattice.

Determining the specific stage where Fe(III) is reduced to Fe(II) has been shown to be challenging. The reduction can take place as an Fe(III) ligand is formed and Fe(II) can detach from the lattice or the Fe(III) ligand can initially be dissolved and further reduced in the solution (Borghi *et al.*, 1991).

Several different reductants for the dissolution of iron oxides have been investigated. Dithionite (Rueda *et al.*, 1992) has been shown to be an efficient dissolving agent for iron oxides but it decomposes rapidly, producing hydrogen sulphide, in an acidic medium.

3.2 Kinetics of dissolution

The rate of dissolution has been described by several different equations. Commonly used equations have been the cube root law (Hixson and Crowell, 1931), the Kabai equation (Kabai, 1973), the Avrami-Erofe'ev equation, the first order nucleation (Mampel, 1940), and the shrinking core model (Levenspiel, 1999). Brown *et al.* (1980) have discussed 12 different equations for dissolution (Table I), including the previously mentioned equations.

All the equations could be applied to the dissolution of any solids, not just Fe oxides. Several of them have, however, been shown to apply for numerous Fe oxides (Cornell and Schwertmann, 2003). The equations can be roughly divided into two categories: diffusion and reaction controlled. For diffusion, the rate determining phenomenon is the transportation of reactants of reaction products to or from the reaction site. For chemical reaction, the rate determining step is, in turn, the actual chemical reaction taking place at the reaction site. The influence of mixing in determining the rate limiting step of any dissolution process should always be considered. An increased influence of mass transfer can be

observed in various hydrometallurgical systems if sufficient mixing is not induced. The shape of the dissolution curve can also be used to evaluate the suitability of a kinetic model. Deceleratory dissolution curves are characteristic of diffusion controlled dissolution whereas sigmoidal behaviour can be observed for autocatalytic reactions.

Table I Equations for dissolution, the shapes of the dissolution curves, and the physical background of the equations (tabulated from Cornell and Schwertmann, 2003).

No.	Equation	Curve[1]	Physical background[2]
4	$\alpha^2 = kt$	D	1D diffusion parabolic
5	$(1-\alpha)\ln(1-\alpha)+\alpha = kt$	D	2D diffusion for cylinder
6	$\left[1-(1-\alpha^{1/3})\right]^2 = kt$	D	3D diffusion for sphere
7	$(1-2/3\alpha)-(1-\alpha)^{2/3} = kt$	D	3D diffusion for sphere
8	$-\ln(1-\alpha) = kt$	D	1st order random nucleation
9	$[-\ln(1-\alpha)]^{1/2} = kt$	V	Random nucleation
10	$[-\ln(1-\alpha)]^{1/3} = kt$	V	Random nucleation
11	$\ln\ln(1-\alpha) = a\ln k + a\ln t$	V	1st order random nucleation (modified)
12	$1-(1-\alpha)^{1/2} = kt$	G	Phase boundary control, shrinking disc
13	$1-(1-\alpha)^{1/3} = kt$	G	Phase boundary control, contracting sphere
14	$\alpha^{1/n} = kt$	A	-
15	$\ln\alpha = kt$	A	-

[1] D = deceleratory, V = variable, G = geometric, A = acceleratory
[2] 1D, 2D, 3D = 1-, 2-, and 3-dimensional

The extent of reaction, α, is calculated by the division of the dissolved mass at time *t* by the initial mass of the oxide. The reaction rate coefficient is represented by *k* and *a* is a material constant.

The above mentioned cube root law, Kabai equation, Avrami-Erofe'ev equation, 1st order rate law and shrinking core model are Eq. (14) (where n = 3), (11), (9), (8), and (13) presented in Table I. Furthermore, Eq. (6) (Jander, 1927) and (7) (Ginstling and Brounhstein, 1950) are developments of Eq. (13) and have also been referred to as the shrinking core model. Chiarizia and Horwitz (1991) have described that Eq. (6) commonly applies to reactions where a solid product layer forms on the surface of the dissolving particle and the reactant needs to diffuse through that layer.

The suitability of different kinetic models does not directly correlate with the mechanisms of dissolution, as some of the kinetic models represent more or less mathematical models instead of chemical reactions. The dissolution of the same iron oxide, dissolved with the same acid, could be described with several kinetic models as indicated by the extensive review by Cornell and Schwertmann (2003).

3.3 Hematite

The dissolution of hematite in an acidic solution, where protonation is the prevailing mechanism of dissolution, proceeds according to Eq. (16):

$$Fe_2O_3 + H^+ \rightarrow 2Fe^{3+} + 2H_2O \quad (16)$$

The dissolution of hematite in HCl has been shown to follow the Avrami-Erofe'ev equation and was suggested not to be dependent on the crystal morphology or method of preparation (Cornell and Giovanoli, 1993): all crystal faces are dissolved equally. The acidic dissolution of hematite has also been studied by Wells *et al.* (2001). The rate of dissolution of metal-substituted hematites in HCl was found to be described by the Avrami-Erofe'ev equation. As mentioned in Section 3.1, Sidhu *et al.* (1981) studied the dissolution of several Fe oxides, including hematite, in HCl at 60°C and found that, after goethite, hematite had the lowest rate of dissolution per unit surface area. The cube root law was successfully used to describe the kinetics of dissolution, although the authors observed sigmoidal dissolution curves, which is not typical for dissolution kinetics described by the cube root law.

In addition to the study of hematite dissolution in HCl, other acids acting through protonation have also been investigated. Gorichev and Kipriyanov (1984) have given an extensive review on the dissolution of metal oxides in acidic media. The review contains discussion on the influence of protons on the dissolution as well as the anions of the acids. For Fe oxides, the dissolution increases with increasing proton concentration. For hematite dissolution in both HNO_3 and H_2SO_4, the order of reaction with respect to hydrogen ions is roughly 0.5 – 0.6. The anions of the acid can form complexes with the with the oxide surface and thus increase the rate of dissolution. For NO_3^- and SO_4^{2+} the orders of reaction have been found to be 0.30 and 0.35, respectively, when dissolving hematite.

Banwart *et al.* (1989) suggested that the dissolution of hematite in the presence of oxalate is purely ligand-promoted and does not involve redox reactions. In the presence of ascorbate, a reducing agent, the addition of oxalate can increase the rate of reductive dissolution significantly. The authors reported not to have observed an increase in pH of the solution during the course of dissolution.

As previously discussed in Section 3.1.2, Panias *et al.* (1996) have suggested, through a review of existing literature, that the dissolution of iron oxides with oxalic acid includes a step of reductive dissolution, and that the mechanism is not merely based on ligand formation. Taxiarchou *et al.* (1997a, 1997b) also studied the effects of temperature, oxalate concentration, and pH on the dissolution of hematite, and found that the dissolution rate of hematite was dependent on temperature and on the pH, but was not affected by the oxalate concentration between 0.1 and 0.5 mol/L oxalate at pH 1. The authors suggested that the concentration of the bivalent iron in the solution is a significant factor for the dissolution of hematite, and that the oxidation of Fe^{2+} to Fe^{3+} is highly dependent on pH.

Lee *et al.* (2006) have, in turn, suggested that the dissolution of hematite in oxalic acid is not governed by complexation but solid-state reduction of the lattice Fe(III). The rate of dissolution was described by a diffusion-controlled shrinking core model where the concentration of the oxalate was, in turn, found to be a significant factor. Lee *et al.* (2007) have also shown that the formation of a solid Fe(II) oxalate can inhibit the dissolution of hematite. The formation of the solid oxalate, however, occurs in a limited pH range, of roughly 1.6 – 3.2.

Where the effects of pH and oxalate concentration have been investigated, the reader should not assume these two to be co-dependent. The oxalate concentration has been adjusted with oxalic acid, which does affect the pH but rather the pH was determined by the addition of e.g. NH_4OH. The effect of pH has thus been studied at constant oxalic acid concentration, by varying the quantity of the base.

The dissolution of hematite by oxalic acid can be further enhanced by ultraviolet wavelengths (Siffert and Sulzberger, 1991). The phenomenon is called photochemical dissolution and is based on reduction of the solid phase Fe(III). The reduction of the Fe(III) in the solid phase results in destabilisation of the bond between the Fe and O atoms through bringing the necessary energy into the system to overcome the activation energy of electron transfer. The photochemical, or light-induced, dissolution of hematite, however, requires the elimination of oxygen as it can strongly inhibit the dissolution by reoxidizing the Fe(II) before it is transferred into the solution. Thus the effect of

light in an industrial process operated in a normal atmosphere would most likely be small, or even insignificant.

Several chelating, or complexing, agents can be used to enhance dissolution. Chang and Matijevic (1983) studied several of these chelating agents and have found that different chelating agents, although originating from the same group of compounds, can act very differently, depending upon pH. Whereas EDTA was shown to enhance dissolution at low temperatures in basic systems and at high temperatures in acidic systems, NTA was found most effective in acidic systems and virtually inactive in basic systems. The authors concluded that the differences between the dissolving agents were most likely due to small differences in the molecular structure of the reagents. The size of the molecule was considered to be especially significant, as the size was seen as an indicator of the bond sites occupied by the molecule: a large molecule (EDTA) occupies several sites and necessitates the breakage of several lattice bonds whereas the number of bonds to be broken would be less for a smaller molecule.

3.4 Magnetite

The dissolution of magnetite is faster because the lattice comprises both Fe(II) and Fe(III). Fe(II) can catalyse the dissolution reaction and thus increase the reaction rate significantly, which means that when performing any dissolution experiments with hematite, the material should be free from magnetite. Because of the presence of both Fe(II) and Fe(III), the dissolution of magnetite is slightly more challenging to explain than the dissolution of hematite, which contain only Fe(III).

Bruyere and Blesa (1985) have suggested that the reductive dissolution of magnetite with H_2SO_4 is controlled by the rate of electron transfer from adsorbed Fe(II) to Fe(III) on the surface of magnetite. As this requires the generation of Fe(II) in solution, a short induction period should be observed. Some of the dissolution profiles presented in the paper show a change in the slope of the curve but, as the authors also concluded, all the dissolution profiles were not similar, i.e. the induction period could not be seen in all the experiments. The reaction mechanism for concentrated H_2SO_4 has been explained to include the adsorption of anions onto the surface of the oxide thus accelerating the dissolution.

The dissolution of magnetite in oxalic acid in the presence of ferrous ions has been investigated by Blesa *et al.* (1987). Sigmoidal dissolution curves were observed in the study and a 3D contracting-geometry rate law was used to describe the dissolution profile. The authors also showed that beyond a certain oxalic acid concentration (roughly 0.85 mol/L) the initial reaction rate no longer increased. Adsorption saturation, according to the authors, takes place at oxalate concentrations beyond 0.15 mol/L, i.e. the oxalic acid concentration affects the dissolution process by other means than just adsorption. The reaction order with respect to protons was suggested to be roughly 0.5. In addition to protons, ferrous ions were shown to accelerate the initial dissolution rate.

EDTA can also act as a complexing agent also in the dissolution of magnetite (Blesa *et al.*, 1984). The number of bond sites occupied by the large EDTA molecule has been found to be dependent on pH. The competition for EDTA between the surface iron ions and the iron ions in the solution strongly influences the dissolution process.

In the dissolution of magnetite with mercaptocarboxylic acids, ligand promoted dissolution is again the key (Borghi *et al.*, 1991). In contrast to oxalic acid, the ligands are formed between the surface Fe(III) and both the carboxylate ion and the sulphur ion. No pH control was employed and the authors reported not to have observed change in pH during their experiments.

Sun *et al.* (1998) studied the dissolution of magnetite at pH 4.5 in 0.1 M $NaClO_4$ at 25 °C and found the equilibrium to be reached after 20 days. No discussion of the mechanisms of dissolution was undertaken by the authors in this case.

The dissolution of magnetite has been studied to a much lesser extent than that of e.g. hematite or goethite. Sweeton and Baes (1970) conducted extensive research on the solubility of magnetite in dilute aqueous solutions containing KOH and HCl. Although the authors deserve appreciation for investigating the thermodynamics of these dilute systems, the data provides little assistance in estimating the solubility of magnetite in more concentrated acid solutions. Furthermore, whereas kinetic experiments have been popular for several decades, thermodynamic solubility data is still scarce.

References for the dissolution of magnetite in HNO_3 were not found. The dissolution of magnetite in HNO_3 can, however, be expected to be similar to the dissolution of magnetite in H_2SO_4 with slight exceptions in the anion complex formation, as described earlier for hematite in these two acids.

3.5 Other iron oxides

In addition to hematite and magnetite, the dissolution of other iron oxides has been extensively studied. Among these is goethite, which is one of the most stable iron oxides and often an end member of transformations of other iron oxides. Chiarizia and Horwitz (1991) have discussed several new formulations for the dissolution of iron oxides and concluded that introducing reducing agents, which lower the Fe^{3+}/Fe^{2+} ratio, will accelerate the dissolution. In addition to reducing solution conditions, acidity, solution potential, and the presence of complexing agents have been argued to be significant factors when dissolving iron oxides. The authors suggested that an ideal dissolving agent for Fe(III) oxides would have to be a strong acid, of which the anion would act as a ligand for Fe(III) and even reduce Fe^{3+} to Fe^{2+}. The dissolution of goethite, FeOOH, was done, in their case, with HCl, HNO_3, H_2SO_4, with several organic acids, including oxalic, citric, and ascorbic acid as well as several phosphonic acids (HEDPA, VDPA, DHEDPA). Different reducing agents, e.g. sodium dithionite, ascorbic acid, and sodium formaldehydesulfoxylate (SFS) were considered to study if the combination of a strong acid and a reducing agent would yield improvement in the dissolution kinetics. An improvement in the dissolution kinetics was observed in sulphuric, oxalic, and diphosphonic acids with ascorbic acid, sodium dithionite, and SFS. The diphosphonic acids in particular seemed to benefit from the introduction of the reductant into the system.

Houben (2003) has showed that the goethite and deposits in wells could be effectively dissolved with sodium dithionite and oxalic acid, whereas citric acid and NaOH were less efficient. Here, several models were able to describe the dissolution data so no further elucidation of the actual kinetics could be given.

The photochemical dissolution of goethite in acid/oxalate solutions was investigated by Cornell and Schindler (1987). The authors concluded that both protons and oxalate ions participate in the dissolution process. The maximum rate was observed at pH 2.6, which is approximately the same as reported for other iron oxides in the presence of oxalate ions. The mechanism of dissolution was argued to consist of two consequent steps: (1) adsoption of oxalate on the solid surface to form a complex with Fe(III) and the subsequent release of Fe^{3+} into solution, and (2) reductive dissolution through ferrous oxalate. The latter was found to account for most of the dissolution. Interestingly, whereas several authors have reported not to have seen an increase in pH during the dissolution of iron oxides, here the authors present results showing significant proton consumption during the dissolution.

4 FILTRATION

Filtration is a widely used process that includes depth filtration, pressure and vacuum filtration, and gravity and centrifugal filtration. Here, only the phenomena and equipment related to the filtration of mineral concentrates are considered.

Both pressure and vacuum filters are used in the dewatering of mineral concentrates. The principal difference between pressure and vacuum filters is the way the driving force for filtration is generated. In pressure filtration, overpressure within the filtration chamber is generated with the help of e.g. a diaphragm, a piston, or external devices, e.g. a feed pump. Consequently, solids are deposited onto the filter medium and filtrate flows through into the filtrate channels. Pressure filters often operate in batch mode because continuous cake discharge is more difficult to achieve (Tarleton and Wakeman, 2007).

As the scope of this thesis does not include pressure filtration, it is not discussed further. The following Chapter focuses on briefly introducing the fundamentals of vacuum filtration in order to familiarise the reader with the dewatering process to which this thesis is related. In depth discussion of filtration fundamentals will not be taken on in this thesis nor will any equations related to cake formation be presented as no actual filtration tests or any analyses of filtration data were included here.

4.1 Fundamentals of vacuum filtration

The cake formation in vacuum filtration is based on generating suction within the filtrate channels. The most commonly used filter media for vacuum filters are filter cloths and coated media, e.g. the ceramic filter medium. Although several types of vacuum filters, ranging from belt filters to drums, exist, only the specifics of rotary vacuum disc filters are included here.

Rotary vacuum disc filters are used for the filtration of relatively free filtering suspensions on a large scale, such as the dewatering of mineral concentrates. The operation of the rotary vacuum disc filter resembles that of a drum filter: the filter medium is submerged in the slurry basin where, under the influence of the vacuum, the cake forms onto the medium. Once the sector comes out of the basin, the pores are emptied as the cake is deliquored for a predetermined time which is essentially limited by the rotation speed of the disc. The cake can be discharged by a back-pulse of air or by scraping, after which the cycle begins again. Whereas the use of a cloth filter medium requires heavy duty vacuum pumps, due to vacuum losses through the cloth during cake deliquoring, the ceramic filter medium, when wetted, does not allow air to pass through which can result in a significant decrease of the specific energy consumption (Sparks, 2012). The filtrate obtained through the ceramic filter medium is also typically clearer, i.e. containing less solid matter, than that obtained with a cloth. As pointed out by Tarleton and Wakeman (2007), the replacement of a disc can be expensive and thus the time-in-operation of an individual disc should significantly exceed the time in operation of a corresponding filter cloth, to make the selection of the ceramic filter medium economically viable. The regeneration of the filter medium, only rarely discussed in detail in existing text books, becomes a critical factor when the time in operation of a filter medium needs to be increased.

The applicability and performance of vacuum filtration is commonly established at the laboratory scale or with relatively small pilot scale equipment. The effect of slurry characteristics, e.g. particle size distribution and solids concentration, on cake formation, and possibly cake dewatering and washing, are determined often with extensive test work. Although data from test work and proper design are implemented, long term performance of the filter medium can rarely be estimated based solely on small scale tests. A filter cloth has significantly shorter lifetime than the ceramic filter medium and it is possible that blinding of a cloth could be seen at the pilot scale, as suggested by Thompson (1993). However, pilot trials are still too short to establish slow blinding effects that may take place over years of operation.

Additional details of the ceramic disc filters, especially regarding the regeneration of the filter medium, are given later in Chapter 4.4. In essence, the regeneration of the filter medium is based on a combination of backwashing, ultrasonic cleaning, and chemical regeneration. The optimum combination of these three methods is commonly application specific.

A note regarding the terminology used in this thesis should be given at this stage: washing, in the general literature on filtration, usually refers to the washing of the filter cake, where a solute is removed from the structures of the cake. From here on, washing refers to the chemical washing, or the regeneration, of the filter medium, unless otherwise stated.

4.2 Blinding of the filter medium

The selection of the filter medium is always critical because it "-- is that critical component which determines whether or not a filter will perform adequately." (Tarleton and Wakeman, 2007, p. 78). The term adequate could be further discussed, but as the criteria of assessment include the permeability of the used filter medium and the ultimate goal is usually to separate the particles from the liquid with minimum consumption of energy, the authors must have also implicitly considered the regeneration of the filter medium. Furthermore, the cost of replacing the filter medium and the tendency for blinding were seen as important factors in determining the overall suitability of a filter medium for a certain process. Although considered important, data acquisition methods for the determination of blinding tendency have not been given, which might suggest that those methods do not really exist or are still in the development stage and not considered standard methods.

In addition to covering the principle phenomena of industrial cake filtration, Wakeman and Tarleton (2005) have described some of the aspects of membrane filtration. Although a fundamental difference exists between cake and membrane filtration, phenomena familiar in membrane filtration could be expected to be observed when using a ceramic micromembrane as the filter medium in cake filtration. The particle size, the particle size distribution, and the membrane pore size all play a role in the deposition of particles on and into the filter medium. In addition, the pH of the suspension as well as membrane characteristics are key factors.

Rushton *et al.* (2000) only covered the cleaning process of cloths briefly, but stated a few key facts regarding the washing of any filter medium: (1) the cleaning fluids are dependent on the particular system and can include water, acids, alkalis, and other types of chemicals, (2) many cleaning fluids have been patented, and (3) the pH of the wash water (or indeed the wash chemical in general) needs to be considered. Although many combinations of chemicals have been patented as cleaning fluids, one must wonder how many of those have been a result of extensive research, instead of a trial and error type approach. The pH of the "solvent" must always be taken into account as poor management of process chemistry can result in decreased washing efficiency and even, in the case of formation of undesired precipitates, further blinding the filter medium.

Blinding of the filter medium is a commonly accepted phenomenon in the field of both solid-liquid separation and membrane separation but more published research exists within the latter. Both the terms blinding and fouling are, from hereon, used to indicate the accumulation of extraneous compounds onto the filter medium thus causing the pores to become unavailable for liquid to flow through. The author feels that blinding describes a more general phenomenon whereas fouling is often used for blinding by biological components.

The filter medium can most certainly be assumed to interact with the filtered suspension, and although studies on the effects of filter media blinding in cake filtration are less numerous than those regarding the actual filtration, Weigert and Ripperger (1997) pointed out that the performance of a new and that of a used filter medium is not the same, and that a decline in performance is often observed during use. Although the decline in performance is commonly acknowledged in cake filtration, little attention has been paid to what are the actual mechanisms, which result in the observed decline. Research on blinding and scaling of the filter medium has been more extensive in the field of crossflow membrane filtration but the characteristics of the filtered material differ significantly between dead-end cake filtration and crossflow membrane filtration. The most significant difference is the solids content of the feed. Filter media blinding, here, is determined as the phenomena causing the blocking of

channels through which the liquid would normally flow. Consequently, a loss in filtration capacity and increased cake moisture can be observed.

The mechanisms of filter media blinding are often those enabling cake filtration in the first place. The blocking filtration laws were first introduced by Hermans and Bredee (1936) and further developed by Hermia (1982). These blocking laws describe four different mechanisms of blocking of the filter media by solid particles (Fig. 1):

a. Cake filtration. Particles accumulate onto the surface of the filter medium. Formation of the cake is mainly through bridging of particles.

b. Intermediate blocking. Particles block part of the surface and the pores. Other particles are deposited on top of already deposited particles, and do not participate in the blocking of the surface.

c. Complete blocking. All particles participate in the blocking of the surface of the medium, and a monolayer is assumedly formed.

d. Standard blocking. When particles are significantly smaller than the pores of the medium, the particles will deposit within the pores.

The blocking filtration models are, however, not based on actual observations of the interactions between the filter medium and the slurry particles. The laws have been derived from pressure filtration data and do not directly describe the role of the filter medium in the process. Rushton and Griffiths (1987) have actually suggested that the deposition models might not describe the real physical processes. The blocking filtration laws and their mathematical interpretations have been used by Hwang *et al.* (2007) to describe the particle fouling in microfiltration and by Blankert *et al.* (2006) to identify the fouling mechanism and fouling potential of the feed in dead-end filtration. Both these studies used the filtration data instead of directly studying the interactions between the filter medium and the particles.

Bridging between particles, similar to the cake filtration mechanism, leads to the formation of a filter cake (Wakeman, 2007). Although the filter medium is commonly considered inert and not interacting with the slurry particles, interaction of the skin layer of the cake and the filter medium is likely because adhesion between particles and the filter media, and possible crystallisation of solutes during cake drying (Rushton *et al.*, 2000) increase the probability of blinding of the filter media.

To the best knowledge of the author, no investigations on the long-term scaling effects of filter media of any kind have been published. Several studies do, however, focus on the initial stages of cake filtration in describing pore blocking to prevent particle bleeding into the filtrate and in determining the tendency of different filter media to have blocked pores (Lu *et al.*, 1997) but the interaction between the filter medium and the slurry particles in the early stages of filtration does not necessarily describe the long-term interactions. Differentiation between the mechanisms of blinding, and the consequent significance of those mechanisms on large scale filter performance have attracted little attention. Particle blockage, as a blinding mechanism, has been extensively studied but in-situ crystallisation of solutes has hardly been considered.

As already mentioned, the problem with the use of the blocking models is that they provide a merely theoretical approach to blinding through the indirect use of filtration data. Thus, the true mechanisms of blinding might not be those suggested by this theory at all.

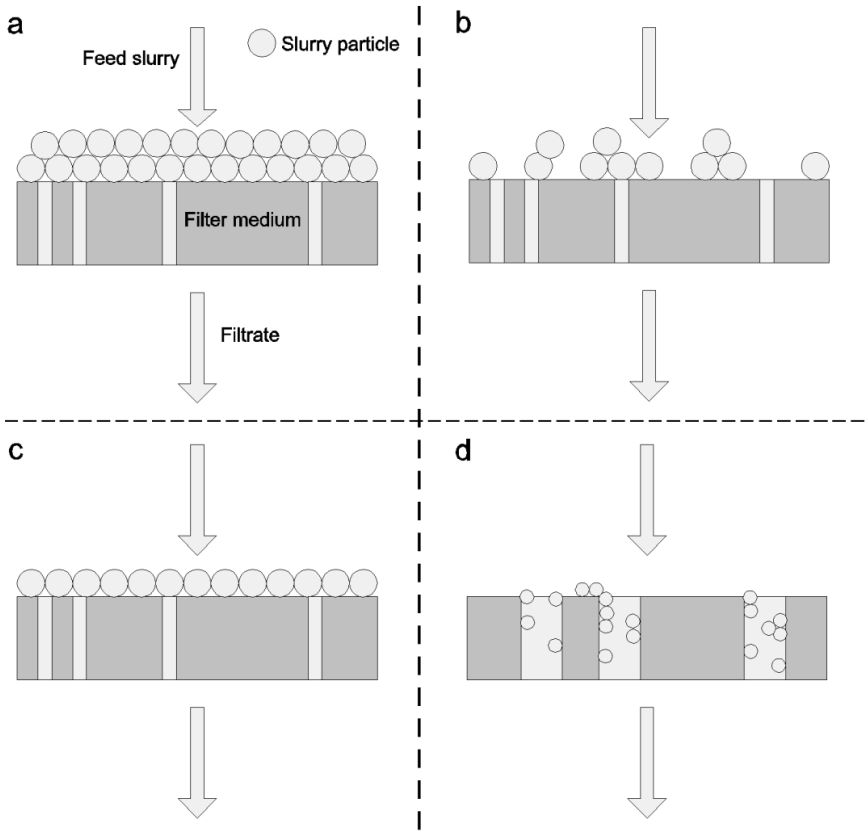

Fig. 1. Blocking mechanisms of the filter medium: (a) cake filtration, (b) intermediate blocking, (c) complete blocking, and (d) standard blocking.

Blinding of the filter medium has an immediate effect on filtration: the filter medium resistance is increased, leading to a decreased filtrate rate, and sufficient cake discharge becomes more difficult (Weigert and Ripperger, 1997). In addition, higher cake moisture content is observed to accompany blinding of the filter medium.

Whereas in the field of cross flow membrane filtration, fouling by extraneous compounds, e.g. salts, has been extensively studied, published literature on possible scaling of the filter medium in solid liquid separation is scarce. Some of the studies performed in cross flow filtration can, however, provide useful insights.

Studies on the effects of ultrasound on ceramic membranes have shown that the membrane can suffer from pitting if the source of the ultrasound is placed too close to the membrane surface. Chen *et al.* (2006a) showed that decreasing the distance between the membrane and the ultrasonic probe can significantly increase membrane permeability after fouling, but once the membrane is placed within the cavitation zone of the probe, damage to the membrane can be expected. The significance of different mechanisms acting to clean the filter medium depends on the distance of the membrane surface from the ultrasonic device, e.g. outside the cavitation zone, the main mechanisms are acoustic streaming and turbulence generated by the collapse of the cavitation bubbles. Chen *et al.* (2006b) also showed that the use of ultrasound significantly reduced the formation of a cake layer in the cross flow membrane filtration of colloidal silica. The frequency of the ultrasound in both these studies was 20 kHz. Kallioinen and Mänttäri (2011) have provided an extensive review of the effects of ultrasound

on various membranes. In most cases, the ultrasonic treatment has an effect on the membrane itself, in addition to increasing the permeate flux as a result of foulant removal. Several other authors (Lamminen *et al.*, 2004; Shu *et al.*, 2007) have also shown that the ultrasound does indeed enhance the cleaning of ceramic membranes significantly.

Yamamura *et al.* (2007) have shown that both oxalic acid and sodium hypochlorite could be used to clean a polyethylene membrane after fouling by mainly iron, manganese, calcium, and organics originating from wastewater. The regeneration efficiency of NaOH and HCl was not as good as that of oxalic acid and hypochlorite. Oxalic acid and HCl were found to remove Fe efficiently in this case.

4.3 Analysis of blinding

Blinding of the filter medium manifests itself as a decrease in the filtrate flux and, in cake filtration, an increase in the moisture content of the cake or the failure to produce any cake. These are obviously not direct observations but based on the effects which the blinding of the filter medium causes. Several different techniques can be used to analyse blinding, although the author is not aware of any existing standard techniques. The selection of the tool for analysing blinding often depends on the availability of analysis equipment and of the nature of the blinding.

Direct analysis methods for blinding include e.g. SEM imaging coupled with elemental analysis used e.g. by Huuhilo (2005) and Väisänen (2004). Väisänen also employed FTIR and AFM techniques and gas adsorption based porosity measurements to characterise both clean and fouled polymeric membranes. In addition, both of the authors used several indirect measurement techniques, indicating a change in a particular property of the filter medium as a result of blinding. These techniques included measurements of ISO brightness, contact angle, flux, and streaming potential.

Järvinen (2005) did not study the blinding of the filter medium but used several analytical techniques to characterise filter cloths. These techniques included the measurements of air permeability, according to SFS 3192, and pore size. Although measuring the air permeability of a cloth is a standard technique for characterising cloths, even those used for liquid filtration, it does not describe the performance of the filter medium for the intended separation since the fluid flowing through is not air. The pore size was measured using capillary flow porometry, which is discussed in more detail later in Chapter 5. Both of these techniques could also be used to investigate blinding and consequent effects of regeneration on the filter medium.

An extensive review on the techniques used to study fouling in membrane bioreactors has been given by Drews (2010). The identification of fouling compounds makes use of chromatography, Fourier transform infrared spectroscopy (FTIR), imaging techniques, photometric methods, and the measurement of total organic carbon (TOC). These techniques are obviously targeted to identify organic compounds and would most likely not be suitable for the study of inorganics. The actual performance of the filter medium is then determined through lab-scale tests and possibly empirically derived correlations. The author has produced an excellent criticism of current methods of investigating fouling and pointed out that solution properties are always critical and cannot, necessarily, be properly matched to real processes at the laboratory scale. Another review of existing analytical techniques used for the characterisation of membrane surfaces has been given by Kallioinen and Nyström (2008). Those methods include the previously mentioned IR method and imaging techniques but also include charge based methods and a more extensive description of microscopy techniques. The techniques used to analyse the chemical composition of the membrane surface here seem quite sophisticated to be used in applications of mineral processing. Interestingly, neither of the reviews listed X-ray diffraction (XRD) as a possible analytical technique for the characterisation of chemical composition of the surface under study although, with current advances in instrument technology, XRD could very well be used to analyse both the membrane and foulants.

The number of existing research papers on membrane scaling, i.e. blinding of the membrane by inorganic compounds, is vast and there would be no point in going through all of them individually. Commonly, however, one trend is observed in all these studies: stimulant solutions are used and e.g. microscopic techniques can be employed because the chemistry of the scaling compounds has been controlled by the absence of impurities or other solution components. This makes the interpretation of the results more straightforward, of course, but leaves the reader to wonder if the results are applicable to real processes.

4.4 The ceramic filter medium

Ceramic disc filters are designed for high-tonnage applications where low and even cake moisture content is desired. Utilising the capillary action phenomenon, on which the technology is based, has enabled the use of smaller vacuum pumps and, consequently, yielded significant energy savings. The filter medium has key significance in the technology: the filter medium, when wetted, does not allow air to pass through, which further decreases the necessary vacuum level. Whereas the traditional cloth filter medium has been shown to suffer from wear and penetration of particles into its structure (Huuhilo, 2005), the ceramic filter medium exhibits high resistance to mechanical wear and is also chemically more stable than cloths. These attributes allow for chemical regeneration of the filter medium with acids, whereas a cloth would have to be discarded, after being blinded by particles, and replaced several times during a year's operation.

The most common laboratory test procedure to evaluate the applicability of ceramic discs filters is to use a vacuum filter leaf described by Rushton *et al.* (2000). In addition to the test procedure being sensitive to human error (Savolainen *et al.*, 2011), most long-term, or even short term, blinding effects cannot be seen with this method.

The filter medium is periodically regenerated with the use of one or more of three different methods: (1) backwashing, (2) ultrasonic cleaning, and (3) acid washing. Both backwashing and ultrasonic cleaning are commonly used techniques for the treatment of ceramic membranes (Chen *et al.*, 2006a; Lamminen *et al.*, 2004, Sondhi and Bhave, 2001). The frequency of the ultrasound used for ceramic disc filters in iron ore applications can be either 20 or 27 kHz.

Puranen *et al.* (2008) showed that the combination of different regeneration techniques can be used to regenerate the filter medium, but the authors have not reported any scale growth during their pilot scale tests. As discussed earlier, even pilot scale experimentation can be insufficient to investigate long-term scale growth. In addition, Mänttäri *et al.* (1996a, 1996b) showed that flocculants do not affect the performance of the ceramic filter medium in the dewatering of a copper concentrate. Several chemicals are used in the upgrading of iron ore, especially in flotation (Araujo *et al.*, 2005), and although the use of chemicals has been shown to affect the filter cake (Besra *et al.*, 1996; Besra *et al.*, 1998), published research on the effects of chemicals on the filter medium has been scarce.

As ceramic disc filters represent a fairly novel technology, research to understand the phenomena related to full scale processes is still needed. Because the technology provides energy efficiency into the mining industry, further research to understand the role of the filter medium is necessary. The new found knowledge can then be applied to reach an undisputed best available technology status for the ceramic capillary disc filters in the dewatering of mineral concentrates.

5 ANALYTICAL TECHNIQUES

As analytical techniques play an important role in any research in the field of chemical engineering, the basics of all analytical techniques used in this thesis are briefly covered in this section.

Although not used in the studies described in Section 4.3, XRD was employed in this thesis to identify the components blinding the filter medium. Its selection here was based on the inorganic crystalline nature of the studied samples and the need to characterise the samples based on the actual compounds present instead of elements, where several of the analytical techniques described in Section 4.3 would have failed.

5.1 X-ray diffraction

X-ray diffraction (XRD) is often used to identify chemical components based on how the targeted X-ray beam is reflected from the studied compounds. In general, XRD is a technique which requires the studied compounds to be in a crystalline form, because otherwise irregularity of the structure of the material might make it impossible to identify the compound. A crystalline material has a regular atom arrangement and, when irradiated with X-rays, the planes of the crystals reflect the X-rays. Several reflected beams result from several crystal planes and if the beams are not in phase, diffraction is not observed. The conditions needed for diffraction are determined by Bragg's law (Eq. (17))

$$n\lambda = 2d\sin\theta \tag{17}$$

where n is the order of diffraction, λ is the wavelength of the x-ray beam, d is the distance between the crystal planes, and θ is the diffraction angle. For each substance, diffraction can be observed at specific angles, which is used to identify the substance.

The output is called a diffractogram or a diffraction pattern, which describes the intensity of the diffracted beam as a function of the angle between the incident and the diffracted beam (2θ). The diffractogram is then compared against known substances to identify the compound. XRD analysis can be run either based on reflection or transmission, but here only reflection is considered. For a more detailed description of the method the reader is referred to Willard *et al.* (1988) or Robinson (1970).

The XRD equipment essentially consists of an X-ray tube, providing the necessary irradiation of the sample, a goniometer, a detector and several optical components. Commonly copper or cobolt X-ray tubes are used but other tubes, depending on the analysis, can be used. The detector can be either, for example, a simple scintillation counter or a more sophisticated pixeled detector. The diffractometer is commonly set up in the Bragg-Brentano geometry where the diffracted angle is always double the incident beam. Depending on the geometry, the sample is either stationary or the sample stage moves. In the Theta/Theta mode, where the sample is stationary, the X-ray tube and the detector move to cover the desired angular range.

X-ray diffraction is a non-destructive technique and is thus suitable for the study of several crystalline solid materials. The analysis does not require extensive preparatory work, e.g. coating, and enables the use of solid samples for further experimental work. Iron oxides do, however, exhibit fluorescence when copper X-ray tubes are used as the radiation source. The induced fluorescence can be observed as an increased background signal in the diffractogram. The effect of fluorescence can be reduced by using a different X-ray tube or by installing slits which does, however, reduce the intensity of the signal.

5.2 Scanning electron microscopy

Scanning electron microscopy (SEM) is a useful imaging technique to investigate any solids or surfaces. SEM can also be coupled with an energy dispersive X-ray spectrometer (EDS) to yield elementary data of the studied sample. The basic principle of the SEM is simple. An electron beam, coming from an electron gun, is used to irradiate the sample. The primary electrons of the beam hit

the sample and, as a result of interactions between the electrons and the sample's atomic structure, the electrons are backscattered (elastic scattering) or result in the emission of secondary electrons (inelastic scattering). Also electromagnetic radiation is emitted. The details of elastic and inelastic scattering have been well described by Goldstein *et al.* (1981).

One of the three, or a combination of them, can then be detected depending on the mode and availability of detectors on the equipment. The SEM image analysis can be performed based on the previously mentioned secondary electrons (SE) or backscattered electrons (BSE). SE mode commonly requires a lower acceleration voltage than the BSE mode as more secondary than backscattered electrons are generated with the same acceleration voltage. The acceleration voltage can vary from below 1 keV to roughly 60 keV. In addition to image analysis, the SEM coupled with EDS can be used to identify the elementary composition of the sample based on the electromagnetic radiation the sample emits when bombarded with electrons, i.e. the characteristic X-rays. An electron, when hitting an atom, can eject one of the inner shell electrons (K, L, or M) which then leaves the atom in an excited state. The excitation is discharged as X-rays when an electron is moved from one shell to another (according to the principle of minimum energy). These X-rays are characteristic to each substance and can then be used to identify the studied elements.

As the interaction volume, i.e. the volume of the sample in which the electrons interact with the solid material, is dependent on the atomic number and the density of the studied sample as well as beam characteristics, it is difficult to determine the depth from which data is collected during the analysis, especially for complex samples.

Although the basic underlying principle is simple, the equipment consists of a complex array of magnetic lenses and apertures to produce the magnification of the image through focusing of the electron beam: the smaller the raster that the beam is focused on, the larger the magnification. In addition to the magnetic lenses, the electron gun is one of the crucial components of the SEM. The emission of the electron beam can be generated by several different components of which one of the most common is the tungsten cathode. The electrons from the tungsten cathode are generated through thermionic emission, where, at high temperatures, some of the electrons receive enough energy to detach from the cathode. The SEM analyses need to be performed in a vacuum chamber as electrons coming in contact with other atoms or molecules very quickly lose their energy and data could not be collected at the detectors.

Although the SEM is a powerful imaging tool, the samples can require significant preparatory work before analysis. The physical size of the sample needs to be appropriate to fit into the sample chamber, and sometimes sample size reduction is necessary. In addition, the acquisition of proper images may require the use of coatings not to have the surface build a charge as it is bombarded with electrons. Furthermore, the data provided by the EDS analysis yields only elements making the identification of compounds difficult if the samples consist of several substances.

5.3 Inductively coupled plasma optical emission spectroscopy

The inductively coupled plasma optical emission spectroscopy (ICP-OES) is a solution analytical tool which yields elemental data. The technique is very similar to other spectroscopic methods where the sample needs to be atomised and excited. Here those are done in an argon plasma. Once the atoms have been excited, changes in the atomic structure take place to accommodate for the free space at lower energy levels. These changes are seen as emitted energy.

The argon plasma is produced in a torch where an induction coil produces a magnetic field which essentially provides enough energy for previously introduced seed electrons to ionise the argon atoms. With further ionisation of argon atoms, a flame-shaped plasma is finally formed and once ignited is almost self-sustaining. The temperature within the measuring area is roughly 6000 – 8000 °C.

The sample is introduced into the system through a capillary tube. Nebulation is used to produce an aerosol which is then introduced into the flame together with argon gas. Desolvation, molecular dissociation, and excitation of the atoms take place in the plasma. Discharge of the excitation is detected as an emission in the visible or ultraviolet regions. The detector is commonly a photoelectric transducer made of a semiconducting material and is pixeled so that each pixel serves as an individual measuring point. The calibration of the spectrometer is often done with two standards: low and high concentrations. The observed emission is then compared to the correlation given by the calibration. A more detailed description of the components in ICP-OES has been given by Willard *et al.* (1988).

The major advantages of the ICP-OES over atomic absorption spectroscopy, discussed in the next chapter, are the much broader analyte concentration range and the possibility of analysing several elements at a time. The ICP-OES is, however, much more sensitive to matrix interference and is significantly more expensive, due to the high consumption of argon, than other atomic spectroscopy methods.

5.4 Atomic absorption spectroscopy

Atomic absorption spectroscopy (AAS) is also a solution analytical tool, along with ICP-OES. Unlike the latter, AAS is based on measuring the absorption of radiation by a specific species. The atomisation of the species in the solution is done in a flame (flame atomic absorption spectroscopy, FAAS), or in some cases in an electric furnace. Here only the flame method is considered.

Before an absorbance can be obtained, the sample needs to be delivered to the flame and atomisation needs to take place. The sample is commonly delivered through a capillary and then a nebulizer where the liquid is broken into small droplets to produce an aerosol. The aerosol is atomised in the flame. The flame is made up of a fuel (e.g. acetylene) and an oxidant (e.g. air or nitrous oxide) and a correct ratio of the two must be used for each element to produce the desired temperature, in the range 1700 – 3200 °C. In the flame, the sample solution undergoes desolvation, vaporisation, and atomisation resulting in the break-up of the metal salt to produce excited atoms. To have absorbance of light, the sample needs to be irradiated once in the flame. Hollow cathode lamps, specific to each element, are used as the radiation source. The detection of the absorbance is based on the difference between the intensity of the incoming radiation and the radiation which has passed through the flame. The concentration of the solute is determined by comparing the observed absorbance to those of set calibration solutions, the concentrations of which are substance specific.

Different oxidation states cannot be identified through analysis using AAS and the technique is mostly intended for the analysis of metals. The technique is also sensitive to certain chemical interference, caused by the anions in the solutions, which, to be removed, require additional sample preparation. In contrast to ICP-OES, FAAS cannot be used to analyse several elements at a time, as each element requires its own hollow cathode lamp. FAAS can, however, be used to analyse much lower concentrations of metal species in comparison to ICP-OES.

For a more detailed description of the technique the reader is referred to Willard *et al.* (1988), Harris and Kratochvil (1981), or Robinson (1970). In addition, Skoog *et al.* (1988) give a short and comprehensive of flame methods in atomic spectroscopy.

5.5 Capillary flow porometry

Capillary flow porometry is a measuring technique to estimate the pore size distribution of a porous material. The technique is based on applying pressure in a displacing fluid (e.g. air) to a previously wetted porous medium, and measuring the consequent flow of the gas through the sample. This has been described by Johnston (1995) through the principles of the bubble point test and the distribution

of flow in a porous material. The calculation of the pore size corresponding to a known pressure is based on the Young-Laplace law (Eq. (18))

$$p = \frac{4\mu_{l/g}\cos\theta}{D} \tag{18}$$

where p is the pressure, $\mu_{l/g}$ is the surface tension of the wetting liquid, θ is the wetting angle, and D is the pore diameter. Commonly, a low surface tension, low vapour pressure, wetting liquid with a very low wetting angle (close to 0) is used resulting in cosθ being equal to 1. Sometimes a correction factor is used to account for nonideality of the sample, as Eq. (18) only applies to pores with smooth walls and a cylindrical shape. The use of such correction factors should, however, be somehow justified instead of being arbitrary.

The determination of the pore size distribution is based on the flow curves, i.e. the dry curve and the wet curve. The dry curve is measured with a dry sample, after which the sample is wetted with the wetting liquid, and the wet curve is measured. The cumulative flow percentage is calculated as the division of the wet flow rate with the dry flow rate. The differential flow percentage is the difference between two consecutive cumulative flows. The pore size distribution can be presented based on either the cumulative or the differential flow percentage. This calculation procedure yields the pore size distribution based on fluid flow. With additional calculations, the technique can also yield a number distribution, but to obtain the number distribution the operator should have knowledge of the average tortuosity of the sample pores.

Capillary flow porometry also yields the bubble point pressure and the corresponding bubble point diameter of the analysed material. The bubble point pressure is the pressure under which the largest pores of the material are emptied of the wetting liquid and gas starts to flow through the sample. This is commonly referred to as the bubble point pressure, but sometimes instruments use the pressure at which a user defined flow (e.g. 20, 50, or 100 ml/min) is measured. As the pressure is increased, an increasing number of pores are blown empty, until all the pores have been emptied and the flow through the sample corresponds to that of a dry sample.

Regarding the terms used to describe the flow through a dry filter medium: Johnston (1995) argued that the true dry flow curve can never be obtained if a wetting liquid of low enough vapour pressure is used. The correct term according Johnston (1995) would be the “damp” curve, but here we use the term dry curve. Another question raised by the author is the interactions between the wetting fluid and the solids. If dissolution of solids from the surface, or from within the filter medium, takes place, the properties of the liquid can change markedly. Thus, the operator should always be aware of the chemical composition of the filter medium under investigation.

Capillary flow porometry has been described and used for several research problems regarding the characterisation of pore size distributions of numerous materials. A description of the applicability of capillary flow porometry in assessing the pore size distributions of thin porous composite sheets have been given by Jena and Gupta (2001) whereas nanofibrous membranes have been characterised by the same technique by Li *et al.* (2006) and polymeric membranes by Agarwal *et al.* (2012).

II EXPERIMENTAL WORK

The experimental work here comprised of laboratory methods to study the dissolution of free particles and the regeneration of the ceramic filter medium. In addition, characterisation techniques to study the filter media samples were employed and are also described in this section. Experimental design was employed where appropriate.

6 EXPERIMENTAL METHODS

The experimental work could, essentially, be divided in three sections:

(1) Dissolution of free particles of iron oxides and iron ore

(2) Characterisation of long-term scaling effects of ceramic filter media used in the dewatering of iron ore

(3) Dissolution of particles and scales from the surface of the filter media.

The three parts were, to some extent, overlapping. The analysis of long-term scaling effects was done during 2010 and the dissolution experiments with the filter medium were finished in 2012. The dissolution experiments with the powders required the most experimental work and were on going for most of the duration of this research from 2008 to 2012.

6.1 Dissolution of free particles

Dissolution of free particles was done with magnetite and hematite. Whereas only synthetic hematite was selected for the kinetic experiments, thermodynamic experiments were done with both synthetic and industrial magnetite. Most published studies on the dissolution of iron oxides are done with synthetic materials prepared in the laboratory. Here the synthetic materials were chosen to account for pure powders but the study of an industrial powder was seen as necessary, too, as the industrial concentrate is not purely iron oxide but contains several other components which could affect the dissolution process.

6.1.1 Experimental design

The need for data is much more extensive in statistical modelling than it is in phenomena-based modelling as commonly more variables are considered for statistical models. The need for large quantities of data is generated especially when purely linear models cannot be expected to describe the behaviour of the system and nonlinear terms are required for the model to perform sufficiently.

Experimental design techniques were only used in the planning of the experiments for magnetite dissolution because the aim here was to generate a statistical model describing the dissolution and the effect of temperature and acid concentration on the concentration of dissolved Fe. Experiments were conducted at 15, 35, and 50 °C. Concentrations of the dissolving chemical varied between the different acids and were initially selected on the basis of weight percentage and then converted into molarities. Three two dimensional full factorial designs (Fig. 2) were generated and the experiments were conducted in randomised order.

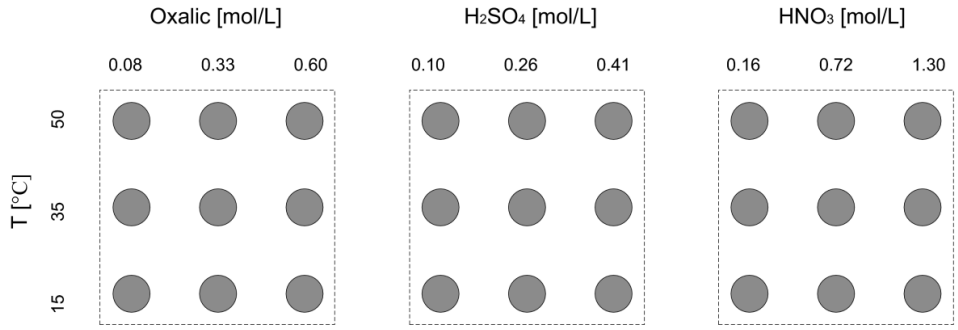

Fig. 2. The experimental design for dissolution experiments in oxalic, sulphuric, and nitric acids.

The pH of the initial acid solutions was measured to indicate the effective hydrogen ion concentration, which, later on, would be used for the comparison of the different dissolving agents. For further reference, 0.10 mol/L sulphuric acid and 0.72 mol/L nitric acid seemed to have similar pH, indicating roughly the same effective hydrogen ion concentration. The dissolution mechanism for oxalic acid was not assumed to be protonation, unlike for the two other acids, thus making comparison based on the hydrogen ion concentration less valid. Detailed information on the pH of the acid solutions can be found in Paper I.

The experiments done with hematite were used to confirm the applicability of previously proposed kinetic models presented in Table I. Because the aim was not to generate a statistical model, design of experiments was not applied for the design of the kinetic experiments and the number of experiments was significantly lower. In short, the kinetic experiments were done only with oxalic acid at two different temperatures, 35 and 50°C, at a constant acid concentration of 0.60 mol/L.

6.1.2 Materials

Oxalic, sulphuric, and nitric acid solutions were prepared with ultrapure water using pro analysis grade reagents: 99 wt-% solid oxalic acid dihydrate from BDH Prolabo (Leuven, Belgium), 96-98 wt-% sulphuric acid from Merck, and 65 wt-% nitric acid from Merck, respectively. For calculation purposes 97 wt-% was selected as the nominal concentration for the sulphuric acid solutions.

6.1.2.1 Magnetite

Dissolution experiments for magnetite were done using two different solid powders. A synthetic magnetite powder was acquired from Alfa Aesar (Karlsruhe, Germany). The purity of the solid was 99 %, as provided by the supplier. A natural magnetite sample was received from a magnetite concentration plant.

The chemical composition of both samples was determined by X-ray diffraction (XRD) using a Bruker D8 Advance diffractometer. The data were collected between 5 and 70°2Θ with a step size of 0.02°2Θ and a scanning speed of 0.02°2Θ. The diffractograms can be found in Fig. 1 in Paper I.

The spectral data showed no impurities in the synthetic sample and only minor peaks, which were not enough to identify the actual phases, were seen in the spectral data for the industrial sample. The impurities were thus determined with the use of a JEOL JSM-5800 scanning electron microscope

coupled with an energy dispersive X-ray spectrometer (SEM-EDS). The most significant impurities were found to be magnesium (Mg), silicon (Si), calcium (Ca), aluminium (Al), and titanium (Ti).

Particle size distributions of the samples were determined by laser diffraction using a Beckman Coulter LS 13320 diffractometer with a separately created optical model for magnetite where the real refractive index was 2.42 (Beckman Coulter, 2003). The mean particle size (d_{50}) for the synthetic and industrial magnetite were 2.14 and 60.71 μm, respectively. Because of the multimodal particle size distribution of the industrial magnetite, the mean particle size alone does not really describe the powder. The d_{10}, i.e. the particle size below which 10 vol-% of the particles are, for the industrial magnetite was 6.05 μm. The particle size distribution can be found in Paper I, in Fig. 7.

6.1.2.2 Hematite

A hematite powder from Alfa Aesar was also used for the kinetic experiments. The purity of the solid powder was 97 %. The chemical composition was again verified by XRD and SEM-EDS. The spectral data showed no other phases than hematite and no impurities were found with the EDS. Particle size distribution were determined for the hematite sample, as previously for the magnetite samples with the exception that a separate optical model was used for hematite. Here the real and imaginary refractive indexes were 3.0 and 0.01, respectively (Beckman Coulter, 2003). The particle size distribution can be found in Paper II, in Fig. 1.

An increasing background was observed in the XRD data. This increase is typical to iron oxides as they exhibit fluorescence under Cu radiation, which results in the observed phenomenon in the data.

No impurities were observed in the XRD data. In addition, elemental composition was again determined with the JEOL SEM-EDS and showed 65 wt-% Fe. The theoretical Fe quantity for pure hematite is 69.9 wt-%. No impurities were found in the EDS data. The particle size distribution was found to be bimodal with a mean particle size for the powder being roughly 2 μm.

6.1.3 Methods

Two types of dissolution experiments were conducted: thermodynamic and kinetic experiments. Thermodynamic experiments require excess quantities of solids to be introduced into the system for the system to reach an equilibrium state where the solubility of the solid can be determined. The quantity of solids in the thermodynamic experiments was roughly 40 g for each experiment with the volume of the liquid being 1 L. Kinetic experiments can be conducted with a known quantity of solids and the dissolution can proceed until all solids have been dissolved.

Both the thermodynamic and kinetic experiments were done with the same reactor setup which has been described in Papers I and II. The only difference was that pH was monitored during the kinetic studies, but not during the thermodynamic experiments.

Here, mixing with a pitched blade turbine was selected to eliminate any mass transfer limitations caused by insufficient mixing. In several previous studies, discussed in Chapter 3, mixing was induced by shaking or the mixing conditions were not reported at all, and the author here feels that the true mechanism of dissolution cannot be accounted for if limiting mass transfer is not excluded. The effect of stirrer speed was investigated and reported in Paper II. Details of the stirrer speeds used and the rationale for their selection have been presented in Papers I and II.

6.2 Characterisation of the filter medium

To validate the research question, investigations were needed to verify that iron oxide particle adhesion indeed occurs during the dewatering of iron ores. The most natural route seemed to be to

acquire samples from an industrial scale dewatering process for further characterisation as any laboratory experiments, e.g. leaf test filtrations, would most likely not produce the same results due to flow conditions, slurry chemistry and time effects.

6.2.1 Materials

Ceramic filter media used in the dewatering of magnetite and hematite concentrates was obtained from Outotec (Filters) Oy. The magnetite dewatering process here was the source for the sample of industrial magnetite for the particle dissolution experiments described in Section 6.1. Detailed information on the installation date and the ultrasonic frequency used in the washing were available for the magnetite samples but not for the hematite samples. A large filter element, illustrated in Fig. 2 of Publication V, with a filtration area of 0.25 m^2, yielded 45 cylindrical laboratory samples with a diameter of 46 mm and height of 30 mm (Fig. 3). The laboratory samples were drawn from the large filter elements by using a diamond drill and were dried at 60 °C after drilling.

Fig. 3. Cylindrical laboratory samples of the ceramic filter elements used for hematite concentrate dewatering.

Instead of analysing all the samples, samples from the corners and from the centre of the element were analysed. Seven different filter elements, adding up to 33 samples, from the magnetite dewatering process were analysed. The corresponding number for the filter elements and the samples from the hematite dewatering process were 3 and 11, respectively.

All of the filter elements from the magnetite dewatering process were manufactured in the United States and data of the installation date and the ultrasonic frequency used in the regeneration in the full scale process were available (Table II). The ceramic material manufactured in the United States has been reported to have a mean pore diameter of 1.7 μm and an initial permeability of 5500 L/m^2h at 1.0 bar. In addition, the concentrate sample, described in Section 6.1.2.1, was obtained from the same dewatering process as the samples of the filter medium.

Table II The numbering, location of the samples on the large filter element, the installation date, and the ultrasonic frequency used in the regeneration in the full scale installation for the magnetite samples. All the elements were removed from the dewatering process in May, 2008.

No.	Location[1]	Inst.date[2]	US [kHz]	No.	Location[1]	Inst.date[2]	US [kHz]	No.	Location[1]	Inst.date[2]	US [kHz]
1	UL	< 2003	20	12	UL	07/2004	27	23	UL	2005	27
2	UR	< 2003	20	13	C	07/2004	27	24	UR	2005	27
3	C	< 2003	20	14	C	07/2004	27	25	C	2005	27
4	C	< 2003	20	15	LR	07/2004	27	26	C	2005	27
5	LL	< 2003	20	16	C	2005	27	27	LL	2005	27
6	LR	< 2003	20	17	LR	2005	27	28	LR	2005	27
7	UR	04/2003	27	18	UL	2005	27	29	UL	06/2004	20
8	C	04/2003	27	19	UL	07/2004	20	30	UR	06/2004	20
9	LL	04/2003	27	20	UR	07/2004	20	31	C	06/2004	20
10	LR	04/2003	27	21	LR	07/2004	20	32	LL	06/2004	20
11	UL	04/2003	27	22	LR	07/2004	20	33	LR	06/2004	20

[1] UL = upper left, UR = upper right, C = center, LL = lower left, LR = lower right
[2] Exact dates were not available on the installation of all the elements

Samples from two different manufacturers, located in China and in the United States, were analysed from the hematite dewatering process (Table III). Only one suitable laboratory sample could be acquired from the Chinese element and, in addition, the sample had to be drawn from fragments instead of a complete large element. Two different filter elements from the manufacturer in the United States were available for analysis. The filter elements were removed from the dewatering process after significant loss of permeability.

Table III The manufacturer and the location of the samples on the large filter element from the hematite dewatering process.

No.	Manufacturer	Loc.[1]	No.	Manufacturer	Loc.[1]
1	China	C	7	United States	UR
2	United States	UL	8	United States	C
3	United States	UR	9	United States	LR
4	United States	C	10	United States	C
5	United States	C	11	United States	UL
6	United States	C			

[1] UL = upper left corner, UR = upper right corner, LR = lower right corner, C = centre

6.2.2 Methods

Characterisation of the samples of the filter medium was mainly done by applying XRD and SEM. Details of the test conditions are given in Paper V. Here, XRD was chosen because of the complex chemical nature of the filter medium used in a large scale process. In addition to the filter medium and the slurry particles, extraneous compounds were expected to be found and by simply employing an EDS analysis would have left the investigator with uncertainty over the chemical nature of the samples. SEM was then used to identify the extent of particle adhesion and scaling.

Principal component analysis (PCA) was used as a tool to identify trends in the XRD data. This technique represents a statistical method which analyses possible grouping in the data set. The analysis was done on the raw XRD data, where an individual spectrum consisted of 4894 data points. Two data preprocessing techniques were used: (1) autoscaling and (2) centering. Autoscaling incorporates mean-centering of each data point followed by division by the standard deviation (Eq. (19))

$$x_a = \frac{x_i - \mathrm{A}}{\sigma} \tag{19}$$

where x_a is the autoscaled value, x_i is the initial value, A is the mean in the dataset, and σ is the standard deviation in the data set. Centering, in turn, does not include the division but only subtracts a single value from all the data points (Eq. (20)).

$$x_c = x_i - \mathrm{B} \tag{20}$$

where x_c is the centred value and B is the constant subtracted from all the data points. The two data pre-processing techniques were chosen to investigate whether the mathematical treatment of the data would yield significant differences but the ultimate goal was to discover if any of the process variables were significant enough to account for grouping of the data.

6.3 Dissolution of particles and scales

6.3.1 Materials

For experiments to dissolve the particles and scales, samples were selected to have only slurry particles or scales to accurately describe the dissolution of only one compound. Methods to determine the characteristics of the samples were introduced in Section 6.2.

Even when the samples were selected to exhibit uniform chemical composition, the extent of particle adhesion or the thickness of the calcium scale layers were mostly not equal in all the samples. This inherent difference in the studied samples was expected to show as minor discrepancies in the trends in the data.

6.3.2 Methods

The regeneration experiments were conducted in glass vessels where the ceramic samples were suspended. Details of the setup of the regeneration experiments have been given in Papers V and VII. The setup differed slightly in the volume of the regeneration solution used. The volume of the solution and the quantity of the solid substance to be dissolved determine the S/L ratio, which can affect the

kinetics of dissolution. As Papers V and VII study the dissolution of two completely different solid compounds, it is not necessary to have comparable dissolution conditions.

The water permeability, denoted here with *H*, was measured by applying water flow through the samples at a known pressure. The permeability was measured for 200 s at 1 s intervals and averaged to yield a single value for permeability. The permeability, as could be seen from the units presented in Paper VII, is not the Darcy permeability but rather a flux describing the volume of flow per unit area and time. This unit is more commonly used in the industry and can be converted into the Darcy permeability by a simple equation.

The pore size distributions during the washing of the Fe particles were measured with a PMI Advanced Capillary Flow Porometer (Fig. 4), the operating principle of which was described earlier in Section 5.4. Analysis with the capillary flow porometer requires an estimation of suitable input parameters. Several of those parameters affect the accuracy of the data and the duration of the analysis. Possibly the most important parameters affecting the accuracy of the data are the pressure and flow increments and the parameters related to the detection of the bubble point. The pressure (preginc) and flow (V2incr) increments essentially determine the number of data points in a given pressure range. The detection of the bubble point is based on an *F/Pt* factor, where *F* is the bubble flow, *P* is pressure, and *t* is time. The bubble flow is the flow rate at which gas is fed into the chamber at the beginning of the test. At pressures below the bubble point, the pressure in the chamber increases linearly with time as gas is fed into the chamber. During this time, the F/PT factor remains constant. As the bubble point pressure is reached, gas starts to flow through the sample and a change in the F/PT factor is observed. Additional details on the operating parameters used for the samples studied here have been given in Paper VII.

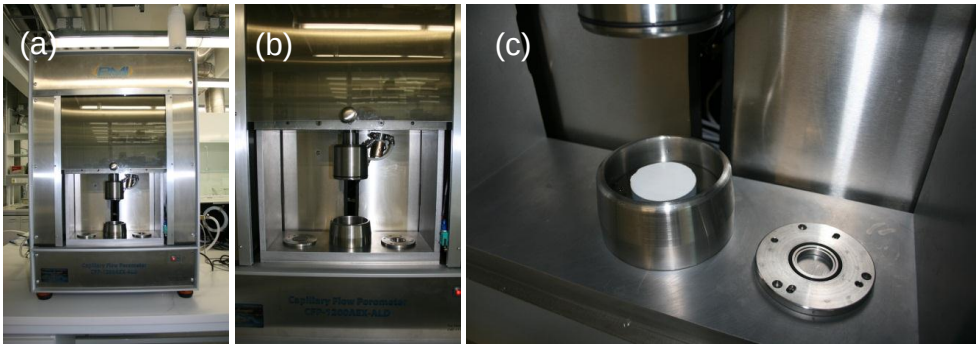

Fig. 4. (a) The PMI Capillary Flow Porometer, (b) the piston, and (c) the sample chamber.

Adapter plates were used during the analysis to eliminate any insulation problems originating from the ceramic samples being exactly the same size in diameter as the default sample chamber configuration.

The pore size distributions were not determined in Paper V as the equipment was not available during the execution of those experiments. The permeabilities can, however, be used as an indication of the changes in the pore size distributions.

III RESULTS & DISCUSSION

The following results are presented in Papers I – VII with some additional data not found in those publications. Chapter 7 has been divided to first discuss the dissolution of free particles, after which chemical characteristics of the ceramic filter medium are introduced to validate the assumption of the presence of iron oxides on the samples. Finally, the dissolution of those iron oxide particles from the surface is discussed in detail. Chapter 8 is used to identify any correlation between the dissolution of free particles and adhered particles.

7 DISSOLUTION OF PARTICLES AND SCALES

The results for the dissolution of free particles of magnetite and hematite will be presented in this section. In addition, the results for the characterisation of the filter media with the dissolution of the identified extraneous compounds will be discussed here.

7.1 Dissolution of free particles

The dissolution of free particles was studied from both kinetic and thermodynamic points of view. Thermodynamic data on the dissolution of iron oxides is scarce and the comparison of different dissolving agents is challenging, based on only kinetic studies, which have varying conditions. Kinetic studies are usually not continued so that they reach equilibrium, which is the only state of a system at which data can be compared.

7.1.1 Magnetite

Thermodynamic experiments of magnetite dissolution with oxalic acid, presented in Paper I, showed that temperature had no effect on the solubility of magnetite when dissolution was done at 35 and 50 °C. At 15 °C lower solubility was, however, observed. Increasing the acid concentration did increase the solubility of magnetite; increasing the acid concentration increases the availability of ligands participating in the reaction, which could explain the effect. Equilibrium was reached much faster in the dissolution of the synthetic magnetite powder. This observation could be explained by (1) the difference in particle size distributions of the two powders or (2) by the effect of the impurities present in the industrial powder. Whereas the lower solubility observed for industrial magnetite is most likely explained by the impurities competing for the ligands, a conclusion cannot be drawn for the faster kinetics of the synthetic powder system. Previous studies (e.g. Lee *et al.*, 2006; Houben, 2003) have suggested that the reaction rate coefficient would be affected by the surface area of the solid, which could support the assumption of the particle size distributions affecting the rate of dissolution.

As shown in the data presented in Paper I, the dissolution of magnetite in H_2SO_4 and HNO_3 did not reach equilibrium in 360 min. Some indications of steady state were observed in sulphuric acid, but no deviations from linearity were observed in nitric acid, i.e. the change in the concentration of dissolved Fe per time still exhibited linear behaviour. Although the comparison of the three different acids could not be directly made, some tentative conclusions could be drawn based on the observed kinetics of dissolution. The previously suggested mechanisms for oxalic acid, H_2SO_4, and HNO_3 are supported here in terms of the order in which these different reagents are effective in dissolving iron oxides. According to the studies presented in Chapter 3, oxalic acid acts through complex formation and reduction and is the fastest. HNO_3 is purely protonation and is thus the slowest. H_2SO_4 lies somewhere between these two as the dissolution mechanism involves both protonation and the adsorption of the anions onto the surface of the oxide to enhance dissolution. The same arrangement was also observed in the experiments presented in this thesis.

The development of empirical models to describe the solubility of magnetite in oxalic acid has been described in Paper VI. As the results of the paper show, the solubility of the synthetic magnetite powder could be explained with a linear model including an interaction term (Eq. (21)) whereas the solubility of the industrial powder required the use of a full quadratic model (Eq. (22)).

$$c_{Fe,eq} = -2.4 \cdot 10^3 \frac{mg}{L} + 63.4 \frac{mg}{L \cdot °C} \cdot T + 3.1 \cdot 10^4 \frac{mg}{mol} \cdot c_{acid} + 96.2 \frac{mg}{°C \cdot mol} \cdot T \cdot c_{acid} \quad (21)$$

$$c_{Fe,eq} = -1.7 \cdot 10^3 \frac{mg}{L} + 230.2 \frac{mg}{L \cdot °C} \cdot T + 1.0 \cdot 10^4 \frac{mg}{mol} \cdot c_{acid} + 377.4 \frac{mg}{°C \cdot mol} \cdot T \cdot c_{acid} - 3.5 \frac{mg}{L \cdot °C^2} \cdot T^2 - 1.8 \cdot 10^4 \frac{mg}{mol} \cdot c_{acid}^2 \quad (22)$$

The p-values reported in Paper VI showed that both the variables were significant in describing the solubility. Although not reported in Paper VI, models were also generated for H_2SO_4 and HNO_3 but those models did not describe solubility because equilibrium was not reached. The models could only account for the concentration of dissolved Fe after 6 h of dissolution at those predetermined conditions described in Section 6.1.1. Consequently, the models could not be used for any comparison as the mechanisms of dissolution are not the same for the three acids and the kinetics of dissolution of each of those mechanisms essentially determine the state at which the system is after 6 h. Whereas a linear model was able to describe the concentration of dissolved Fe of synthetic magnetite in H_2SO_4, linear models failed in all other systems.

7.1.2 Hematite

Both thermodynamic and kinetic experiments were conducted in 0.6 mol/L oxalic acid. The thermodynamic experiments were carried on for 400 h to reach equilibrium. At 50°C the solubility of hematite was obtained in roughly 150 h whereas roughly 400 hours was needed at 35 °C.

The data for the equilibrium experiments in 35 and 50 °C showed that the solubility of hematite in 0.6 mol/L oxalic acid was ultimately not dependent on temperature: the same solubility, roughly 24000 mg/L, was achieved in both temperatures. The same observation was made when dissolving magnetite in 0.6 mol/L oxalic acid. Temperature had no effect on solubility when dissolving the solids at 35 and 50 °C. The dissolution curves have been presented in Paper II.

The behaviour of pH was essentially the same in all the experiments: a fast initial decrease followed by a sigmoidal increase to reach a steady state. The different stages in the pH curve were difficult to link to specific parts of the reaction mechanism. It was, however, interesting to observe a change in pH when several previous studies have reported no observed change in pH.

The dissolution data showed that complete dissolution of the 12 g of hematite was achieved in roughly 60 h. Although first inspection of the dissolution curve indicated deceleratory behaviour, further investigations into the first 30 h of dissolution revealed the curve to be sigmoidal. Consequently, kinetic experiments of hematite dissolution revealed the reaction to proceed through the autocatalytic solid-state reduction route and support the reaction mechanism suggested by Lee *et al.* (2007).

Of the 12 tested models, presented in Paper II, the Kabai equation and the first order nucleation performed the best, based on the correlation coefficients, R^2. In addition, the shrinking core model

gave good correlation. The final selection was essentially made based on the shape of the dissolution curve which was found to exhibit sigmoidal behaviour. Although the reaction mechanism of Lee *et al.* (2007) was supported by the observed sigmoidal behaviour of the dissolution curve, the choice of the kinetic model in this case was different. The shrinking core model (Eq. (7) in Table I) was previously suggested by Lee *et al.* (2007) but the results here, where 12 different kinetic models were compared, supported the selection of the Kabai equation (Eq. (11) in Table I). In fact, Lee *et al.* (2007) did not report testing other kinetic models at all during their data analysis making it difficult to estimate whether the difference between these two studies is in the actual data or in the reasoning for selecting of the kinetic model. The results, however, verified that existing research cannot necessarily be used as such to describe the systems studied here and that discrepancy between individual studies exists.

7.2 Characterisation of the filter medium

The initial hypothesis was that iron oxide particles would be found to adhere to the surface of the filter medium and thus blind the pores of the filter medium at least partially. Precipitates were also expected to be found as most filter media, regardless of the type, used in a large scale processes exhibit amounts of extraneous compounds.

7.2.1 Magnetite dewatering

As reported in Paper V, the XRD data showed essentially three types of samples from the magnetite dewatering process: (1) aluminium oxide and magnetite, (2) aluminium oxide and calcium oxalate, and (3) calcium oxalate.

The hematite dewatering process yielded similar results to the magnetite dewatering process, as could be seen from the results of Paper IV. Samples with alumina and magnetite were most common but some samples were also found to contain different calcium compounds, e.g. gypsum and calcium carbonate. The peaks were, however, quite small indicating that the quantity of the calcium compounds was minimal.

The SEM investigations revealed that two types of media blocking mechanisms played a role in decreasing the performance of the ceramic filter media in the dewatering of hematite and magnetite concentrates. Both (1) particle blockage, resulting from slurry particle adhesion onto the surface of the filter media, and (2) scaling were observed in both iron ore dewatering processes. Scaling was, however, more extensive in the magnetite dewatering process and particle blockage, in turn, was the dominant mechanism of filter media blinding in the hematite dewatering process. This difference could be explained by differences in the particle size distributions of the two concentrates. The hematite concentrate had a more significant fine particle fraction than the magnetite concentrate.

Particles had randomly adhered onto the surface of the filter medium. The size of the particles varied from several millimetres to roughly one micrometer. Some samples showed scale forming separate patches on the sample surface. However, scale had essentially covered the entire surface of the filter medium in most samples. Although a specific crystal shape could not be identified, due to the vast growth, the crystals exhibited a slightly rectangular shape characteristic to calcium oxalate monohydrate. Details of the characteristics of the calcium oxalate scale have been given in Paper III.

Holes in the scale layer were observed at random sites. At those sites, permeability was restored, as indicated by the accumulated magnetite particles. The holes were assumed to be caused by the ultrasound, as ultrasound has been reported to cause pitting of ceramic membranes through microjets and shock waves (Chen *et al.*, 2006). Otherwise, the scale layer seemed impermeable and no slurry particles were observed.

PCA was used to identify trends and group the XRD data, and, consequently, investigate if any of the operating parameters had an effect on the observed long-term phenomena. The most significant factor

determining the formation of the scale seemed to be the location of the sample on the large element, i.e. local variations. These local variations could be explained by differences in flow conditions. The flowrate of the filtrate has been shown to reach a maximum at the filtrate channel outlet and decrease towards the outer corners of the element. Based on the observations here, the permeability of the filter elements should regularly be measured from the corners of the industrial filter elements to detect any signs of scale accumulation.

7.2.2 Hematite dewatering

Particle adhesion was also observed in the filter medium used in the dewatering of the hematite concentrate. Particle adhesion was found more significant in the hematite than in the magnetite dewatering process, whereas almost no scaling was observed in the hematite process.

The alumina used in the manufacture of the Chinese elements seemed to exhibit a larger grain size than the alumina of the filter elements manufactured in the United States. If the grain size is larger, the pores between the grains should then also be larger and possibility of particle penetration increases, but this could not be confirmed since pores were difficult to detect on the used surface.

Calcium was observed to precipitate as gypsum and calcium carbonate in the hematite dewatering process but, surprisingly, calcium oxalate was not observed in any of the samples. Regeneration of the ceramic filter medium is done in the same way in the hematite dewatering process as it is done in the magnetite dewatering process. No clear reason for this distinct difference between the two very similar dewatering processes could be found. Possible underlying causes are differences in process chemistry (e.g. the use of pH modifiers), in the quality of process water (Ca content of raw and recirculated water), and in the quality of the concentrate.

The scale did not exhibit any clear morphology or particle size, as indicated by the SEM images in Paper IV. The extent of coverage of the surface was found to be insignificant when compared to the magnetite dewatering process. This type of scaling can, consequently, be considered marginal and would essentially not affect the permeability of the filter medium.

7.3 Dissolution of particles and scales from the surface of the filter medium

The focus of this thesis was to investigate the dissolution of iron oxide, i.e. slurry, particles for which the results are presented and discussed in this section. An interesting scaling phenomenon was also identified in the dewatering of iron ore and the results for the dissolution of that scale have also been included here.

7.3.1 Dissolution of Fe_3O_4 particles

The dissolution of iron oxide particles with oxalic acid has been described in detail in Paper VII. Some additional data is, however, included here, as all the data was not presented in the paper. The experimental conditions were chosen to mimic those used for the free particle dissolution experiments, i.e. the same temperatures and acid concentration were used for the regeneration experiments. The regeneration was estimated based on the concentration of dissolved Fe in the mother liquour, on the water permeability of the ceramic samples, and on the changes in the pore size distribution of the ceramic media.

The data for the dissolution of Fe_3O_4 during regeneration showed an interesting trend. Roughly similar concentrations of dissolved Fe for all data points would have suggested the complete dissolution of all surface adhered particles. This was not, however, observed but rather the dissolution curves were grouped according to temperature. Roughly similar concentrations of dissolved Fe were obtained for all the acid concentrations.

Several empirical regression models were generated to describe the equilibrium concentration of dissolved Fe, but estimation of the validity of the models was difficult because of variation in the data due to inherent differences in the samples. Consequently, the models are not presented here as no explicit criteria for selection can be used. All of the generated models did, however, show one common feature: temperature was found as the only significant factor influencing the solubility of the surface adhered Fe_3O_4 particles.

Similar changes in the pore size distribution were seen at all the studied temperatures. A decrease in the fraction of smaller pores was observed as a result of the regeneration whereas the fraction of the largest pores remained roughly constant. As also concluded in Paper VII, the bubble point might not be the best indicator of the condition of the filter medium as the fraction of larger pores might not even increase during the regeneration. Instead, changes are seen in the growth of fraction of pores of roughly median size which then corresponds to the increase in liquid permeability.

Images obtained with the SEM after 12 h of regeneration revealed that some small particles were still left on the filter medium. The quantity of those particles was so small, that even if they did dissolve, the extent of dissolution of the Fe oxide may not be measurable.

The concentration of dissolved Fe showed that a steady state is reached even when the solubility limit for magnetite, determined previously in Paper I and described in Section 7.1.1., has not yet been reached. This observation suggests that the regeneration of the ceramic filter medium would not be only kinetically controlled but also affected by some form of equilibrium. In equilibrium, at higher temperatures and acid concentrations, increased quantities of dissolved Fe can be obtained as the state of the systems is not limited by quantity of the solids available to dissolve. For free particles, this seems intuitive, but the quantity of magnetite on the surface of the filter medium is so low, that supposedly complete dissolution in the course of time should take place and not exhibit the observed dependency on the conditions of dissolution. This is, however, not the case.

As also reported in Paper VII, the permeability and the pore size distribution of the filter medium continued to change even after the dissolution of Fe_3O_4 from the surface had ceased. This observation was extremely interesting, as it could point towards two things: (1) the surface of the filter medium itself was dissolved during regeneration or (2) changes due to regeneration were taking place inside the filter medium instead of on the surface. The latter suggestion is based on the fact, that only the dissolution of surface compounds would be seen in the bulk phase as there is virtually no way for the liquid inside the pores to flow outwards in the conditions in which the regeneration was done. Diffusion from within the pores into the bulk solution is possible but the quantity of dissolved Fe would presumably be so low that it would not be observed as an increase in the bulk phase concentration anyways. The first was ruled out by measuring the quantities of dissolved Al in the solutions, which showed that the filter medium had not dissolved during the regeneration. If the filter medium did dissolved, dissolution from the surface would most likely be favoured over dissolution within the pore structure as the surface is readily available, without the need for diffusion, for the dissolving chemical. Therefore regeneration did most likely dissolve something within the pores and, as a result, increased permeability and changes in the pore size distribution were seen. The dissolved species was probably pushed out of the filter medium during the water permeability measurement. Unfortunately, no analytical tools to identify such small concentrations of dissolved metals are available and only these indirect observations can be used to speculate the causes for the observed increase in permeability and changes in the pore structure. Even the capillary flow porometry measurements cannot distinguish between the changes on the surface and in the inner structure of the filter medium.

Currently, ultrasound is used to enhance the regeneration of the ceramic filter medium in iron ore applications. Ultrasound was not considered here for two reasons: (1) introduction of another variable, i.e. sonification, into the studied system would most likely have made it more difficult to interpret the basic underlying phenomena of the acid regeneration, and (2) the pitting reported in previous studies of ceramic membranes would have required an additional test series in order to determine the

optimum distance of the sonification device from the membrane surface so as not to increase the permeability of the filter medium because of damage to the membrane layer. The use of ultrasound would supposedly have increased the rate of reaction (Grénman *et al.*, 2007) but no evidence exists that ultrasound would increase solubility.

7.3.2 Dissolution of calcium oxalate

The removal of the calcium oxalate scale has been discussed in Paper V. As could be seen from the results, the calcium oxalate scale was successfully dissolved with HCl and HNO_3. The highest quantities of dissolved Ca, after 120 min of dissolution, were observed with 2.0 mol/L HCl and HNO_3. The lowest concentration of dissolved Ca was obtained with KOH. H_2SO_4 performed the poorest out of the studied acids but it did dissolve significantly more calcium than KOH.

The higher the acid concentration, the faster was the recovery of the permeability of the filter medium. Two of the studied chemicals, 0.5 mol/L HCl and 2 mol/L HNO_3 gave the most favourable results, as an increase of more than 1500 and 2500 L/(m^2 bar) were observed after 120 min with HCl and HNO_3, respectively. The highest concentration of HCl did not yield the highest increase in permeability, although the highest concentration of dissolved Ca was observed with that acid concentration. Similar discrepancies were observed in the data for the other acids, too. These discrepancies could be explained by varying thickness of the scale layer. The scale layer is most likely not of equal thickness in all the studied samples. Where a thicker layer is found, more calcium needs to be dissolved before an increase in permeability could be observed.

Extending the time for washing, from 120 min to 360 min, resulted in significant improvements in permeability. After 46 h of regeneration, the permeability of the filter element was completely restored. Regarding applicability, chemical regeneration of three hours or more seems unfeasible in industrial practise but a significant increase in performance can be obtained by leaching the scale for extended periods of time. Furthermore, the washing would not have to be so lengthy if it was periodically employed to reverse the precipitation of the scale. This, however, has not been experimentally verified at an industrial scale. The samples studied here were in use for several years and, presumably, such drastic decrease in performance would not be observed if the elements were periodically treated to prevent the long-term accumulation of the scale. The most effective means of scaling management would, however, be to determine the cause of the scaling as the scale growth was only observed in the magnetite and not in the hematite dewatering process.

Again, the removal of this scale could benefit from the use of ultrasound but the effects of sonification were not investigated here for the same reasons as in the case of particle dissolution.

Although the dissolution of this scale is an interesting case and additional research into the causes of the formation of the precipitate could prove useful, this thesis was not focused on the dissolution of extraneous scales from the surface of the filter medium and thus the results are not discussed further.

8 ESTIMATING THE REGENERATION EFFICIENCY AND CAPACITY

The ultimate goal of this thesis was to determine whether free particle dissolution can be used to estimate the regeneration efficiency or capacity of a specific chemical or not. Here, the terms regeneration efficiency and regeneration capacity are separated as follows. Here, regeneration efficiency is used to describe how fast the regeneration of the filter medium takes place when washed with a specific chemical or how much extraneous matter can be dissolved during a certain period of time. Regeneration capacity, in turn, attempts to describe how much of the initial capacity of the filter medium can be restored with that specific chemical. In some ways, regeneration efficiency and regeneration capacity correspond to kinetic (rate) and thermodynamic (equilibrium) aspects of dissolution, respectively

The dependency of free particle dissolution on temperature and on the acid concentration of the solution, presented in Section 7.1, and the observations made for the dissolution of particles from the surface of the filter medium, presented in Section 7.3, exhibited only one similarity: increasing the temperature increased the dissolved Fe concentration. According to these results, a false assumption would be made in thinking that increasing the concentration of oxalic acid would increase the solubility of surface adhered iron oxide particles.

The actual regeneration process is typically much shorter than that presented here and 1 h could be considered a maximum from an operational perspective. In the light of this operational concern, simple linear regression could be used to describe the regeneration efficiency in this case. Lines were fitted only with the first hour of regeneration yielding coefficients of determination from 0.90 to 0.99. The slope of the lines indicated the regeneration efficiency in different temperatures. Here, the slopes were 2.9, 4.0, and 15.5 for 15, 35, and 50°C, respectively. As could be seen, the regeneration efficiency was increased with increasing temperature. As could be seen from the data presented in Paper VII and also indicated by the linear regression in Section 7.3, the regeneration capacity in light of the removed Fe_3O_4, was also increased with increasing temperature. However, neither the regeneration efficiency nor the capacity seemed to be conclusively dependent on the acid concentration.

The regeneration capacity could also be evaluated based on the increase in permeability. In this case, it should be evaluated in this way as the regeneration was shown to exceed well beyond the dissolution of Fe_3O_4 particles. Although the grouping according to temperature was not as strong in the case of permeability as it was in the case of dissolved Fe, slight grouping could still be seen in the data. Slightly lower permeabilities were obtained at lower temperatures indicating that the capacity for permeability restoration was also dependent on temperature. Grouping according to the acid concentration could not be seen in the data suggesting that the acid concentration is not a factor in the permeability restoration capacity. The initial stages of regeneration were, however, much more inconclusive, thus making it difficult to say if temperature or acid concentration had an effect on the permeability regeneration efficiency.

9 CONCLUSIONS

During this thesis, two distinct areas of research were covered: (1) the dissolution of free magnetite and hematite particles and (2) the interaction of slurry components with the ceramic filter medium. These two were then brought together in the study of the chemical regeneration of the ceramic filter medium to investigate the underlying phenomenon of the acid based performance restoration. New information was generated for use in the dissolution of iron oxides and in the filtration of iron ore concentrates. This study incorporated the use of versatile analytical techniques to characterise several of the components in both liquid and solid phases, the use of both laboratory scale experiments and samples from a full scale process, and a range of different data processing techniques.

Agreement on the dissolution of iron oxides, especially in oxalic acid, is still yet to be achieved in the scientific community. The dissolution studies performed during this thesis offer both new data on the thermodynamic solubility of magnetite in oxalic acid, which in general is scarce, as well as evidence on the applicability of another kinetic model to the dissolution of hematite in oxalic acid.

The most significant result of this thesis is, however, the revelation that the dissolution of surface adhered particles does not follow the same laws as the dissolution of free particles. The regeneration capacity and regeneration efficiency of oxalic acid could thus be estimated purely based on temperature and the concentration of the acid could be left out of the considerations.

The regeneration process itself was found to be divided in two. Initially, surface adhered particles were dissolved, resulting in increased bulk concentration of dissolved Fe. Even after the dissolution of surface particles had terminated, the regeneration of the filter medium continued indicating that additional “cleaning” was taking place within the structures of the filter medium. During regeneration the solvent had most likely penetrated the surface of the medium and as the quantity of dissolved components within the medium is extremely small, dissolution within the pores could take place.

In order to develop the regeneration of any filter media in the future, understanding the parameters involved in the regeneration and the consequent effect to the filter medium are crucial. Whereas the study of ideal systems, e.g. in this case the dissolution of synthetic powders, is important to derive new theories and account for basic phenomena, the study of real systems cannot be overlooked as they can diverge significantly from ideality, as was shown in the case of dissolving industrial magnetite and the consequent regeneration of the filter medium used for the dewatering of that same concentrate.

REFERENCES

Agarwal, C., Pandey, A.K., Das, S., Sharma, M.K., Pattyn, D., Ares, P., and Goswami, A., 2012. Neck-size distributions of through-pores in polymer membranes. *Journal of Membrane Science*, 415 – 416, 608 – 615.

Araujo, A.C., Viana, P.R.M., and Peres, A.E.C., 2005. Reagents in iron ores flotation. *Minerals Engineering*, 18, 219 – 224.

Banwart, S., Davies, S., and Stumm, W., 1989. The role of oxalate in accelerating the reductive dissolution of hematite (α-Fe2O3) by ascorbate. *Colloids and Surfaces*, 39, 303 – 309.

Beckman Coulter, 2003. *LS 13320 laser diffraction particle size analyzer instrument manual*. Miami: Beckman Coulter.

Besra, L., Singh, B.P., Reddy, P.S.R., and Sengupta, D.K., 1998. Influence of surfactants on filter cake parameters during vacuum filtration of flocculated iron ore sludge. *Powder Technology*, 96, 240 – 247.

Besra, L., Singh, B.P., Reddy, P.S.R., Sengupta, D.K., and Bhoumik, S.K., 1996. Effect of flocculant on settling and filtration of iron-ore sludge. *Minerals and Metallurgical Processing*, 31, 170 – 173.

Blankert, B., Betlem, B.H.L., and Roffel, B., 2006. Dynamic optimization of a dead-end filtration trajectory: Blocking filtration laws. *Journal of Membrane Science*, 285, 90 – 95.

Blesa, M., Borghi, E.B., Maroto, A-J.G., and Regazzoni, A.E., 1984. Adsorption of EDTA and iron-EDTA complexes on magnetite and the mechanism of dissolution of magnetite by EDTA. *Journal of Colloid and Interface Science*, 98, 295 – 205.

Blesa, M., Marinovich, H.A., Baumgartner, E.C., and Maroto, A.J.G., 1987. Mechanism of dissolution of magnetite by oxalic acid – ferrous ion solutions. *Inorganic Chemistry*, 26, 3713 – 3717.

Borghi, E.B., Morando, P.J., and Blesa, M.A., 1991. Dissolution of magnetite by mercapto carboxylic acids. *Langmuir*, 7, 1652 – 1659.

Brown, W.E., Dollimore, D., and Galwey, A.K., 1980. Reactions in the solid state, in: Bamford, C.H., Tipper, C.F.H. (Eds.), *Comprehensive chemical kinetics*. Elsevier: Amsterdam, 41 – 109.

Bruyere, V.I.E., and Blesa, M.A., 1985. Acidic and reductive dissolution of magnetite in aqueous sulphuric acid. *Journal of Electroanalytical Chemistry*, 182, 141 – 156.

Chang, H.-C. and Matijevic, E., 1983. Interactions of metal oxides with chelating agents IV. Dissolution of hematite. *Journal of Colloid and Interface Science*, 92, 479 – 488.

Chen, D., Weavers, L.drewsdrewsK., and Walker, H.W., 2006a. Ultrasonic control of ceramic membrane fouling by particles: effect of ultrasonic factors. *Ultrasonics Sonochemistry*, 13, 379 – 387.

Chen, D., Weavers, L.K., and Walker, H.W., 2006b. Ultrasonic control ceramic membrane fouling: effect of particle characteristics. *Water Research*, 40, 840 – 850.

Chiarizia, R. and Horwitz, E.P., 1991. New formulations for iron oxides dissolution. *Hydrometallurgy*, 27, 339 – 360.

Cornell, R.M. and Giovanoli, R., 1993. Acid dissolution of hematites of different morphologies. *Clay Minerals*, 28, 223 – 232.

Cornell, R.M. and Schindler, P.W., 1987. Photochemical dissolution of goethite in acid/oxalate solution. *Clays and Clay Mineral*, 35, 347 – 352.

Cornell, R.M. and Schwertmann, U., 2003. *The Iron Oxides.* 2nd Ed. Weinheim: Wiley-VCH.

Drews, A., 2010. Membrane fouling in membrane bioreactors – Characterisation, contradictions, causes and cures. *Journal of Membrane Science*, 363, 1 – 28.

Ginstling, A.M. and Brounshtein, B.I., 1950. O Diffuzionnoi Kinetike Reaktsii V Sfericheskikh Chastitsakh. *Journal of Applied Chemistry of the USSR* (English Transl.), 23, 1327 – 1329.

Goldstein, J.I., Newbury, D.E., Echlin, P., Joy, D.C., Fiori, C., and Lifshin, E., 1981. *Scanning Electron Microscopy and X-Ray Microanalysis*. New York: Plenum Press.

Gonzalez, E., Ballesteros, M.C., and Rueda, E.H., 2002. Reductive dissolution kinetics of Al-substituted goethites. *Clays and Clay Minerals*, 50, 470 – 477.

Gorichev, I.G. and Kipriyanov, N.A., 1984. Regular kinetic features of the dissolution of metal oxides in acidic media. *Russian Chemical Reviews*, 53, 1039 – 1061.

Grénman, H., Murzina, E., Rönnholm, M., Eränen, K., Mikkola, J.-P., Lahtinen, M., Salmi, T., and Murzin, D. Y., 2007. Enhancement of solid dissolution by ultrasound. *Chemical Engineering and Processing*, 46, 862 – 869.

Harris, W.E., and Kratochvil, B., 1981. An introduction to chemical analysis. Philadelphia: Saunders College Publishing.

Hermans, P.H., and Bredee, H.L., 1936. Principles of the mathematical treatment of constant-pressure filtration. *Journal of the Society of Chemical Industry*, 55, 1 – 4.

Hermia, J., 1982. Constant pressure blocking filtration laws – application to power-law non-newtonian fluids. *Transactions of the Institute of Chemical Engineering*, 60, 183 – 187.

Hixson, A.W. and Crowell, J.H., 1931. Dependence of reaction velocity upon surface and agitation (I) theoretical consideration. *Industrial & Engineering Chemistry*, 23, 923 – 931.

Houben, G.J., 2003. Iron oxide incrustations in wells. Part 2: chemical dissolution and modeling. *Applied Geochemistry*, 18, 941 – 954.

Huuhilo, T., 2005. *Fouling, prevention of fouling, and cleaning in filtration*. Doctoral thesis. Lappeenranta University of Technology. ISBN 952-214-123-2.

Hwang, K.-J., Liao, C.-Y., and Tung, K.-L., 2007. Analysis of particle fouling during microfiltration by use of blocking models. *Journal of Membrane Science*, 287, 287 – 293.

Jander, W., 1927. Reaktionen in festen Zustand bei hoheren Temperaturen. *Zeitschrift für anorganische und allgemeine Chemie,* 163, 1 – 30.

Jena, A., and Gupta, K., 2001. An innovative technique for pore structure analysis of fuel cell and battery components using flow porometry. *Journal of Power Sources*, 96, 214 – 219.

Johnston, P.R., 1995. *A survey of test methods in fluid filtration*. Houston: Gulf Publishing Company.

Järvinen, K., 2005. *Development of filter media treatments for liquid filtration*. Doctoral thesis. Lappeenranta University of Technology. ISBN 952-241-137-2.

Kabai, J., 1973. Determination of specific activation energies of metal oxides and metal oxide hydrates by measurement of the rate of dissolution. *Acta Chimica Academiae Scientiarum Hungaricae*, 78, 57 – 73.

Kallioinen, M. and Mänttäri, M., 2011. Influence of ultrasonic treatment on various membrane materials. *Separation Science & Technology*, 46, 1388 – 1395.

Kallioinen, M. and Nyström, M., 2008. Membrane surface characterisation. In: Li, N.N., Winston Ho, W.S., Fane, A.G. and Matsuura, T. (eds.) *Advanced Membrane Technology and Applications*. New Jersey: John Wiley & Sons. 841 – 878.

Lamminen, M.O., Walker, H.W., Weavers, L.K., 2004. Mechanisms and factors influencing the ultrasonic cleaning of particle-fouled ceramic membranes. *Journal of Membrane Science*, 237, 213 – 223.

Lee, S.O., Tran, T., Jung, B.H., Kim, S.J., and Kim, M.J., 2007. Dissolution of iron oxide using oxalic acid. *Hydrometallurgy*, 87, 91 – 99.

Lee, S.O., Tran, T., Park, Y.Y, Kim, S.J., and Kim, M.J., 2006. Study on the kinetics of iron oxide leaching by oxalic acid. *International Journal of Mineral Processing*, 80, 144 – 152.

Levenspiel, O., 1999. *Chemical reaction engineering*. 3rd Ed. New Jersey: John Wiley & Sons, Inc.

Li, D., Frey, M.W., and Joo, Y.L., 2006. Characterization of nanofibrous membranes with capillary flow porometry. *Journal of Membrane Science*, 286, 104 – 114.

Lu, W.-M., Tung, K.-L., and Hwang, K.-J., 1997. Effect of woven structure on transient characteristics of cake filtration. *Chemical Engineering Science*, 52, 1743 – 1756.

Mampel, K.L., 1940. *Zeitumsatzformeln für heterogene Reaktionen an Phasengrenzen fester Körper*. Becker & Erler: Leipzig.

Mandal, S.K., and Banerjee, P.C., 2004. Iron leaching from China clay with oxalic acid: effect of different physico-chemical parameters. *International Journal of Mineral Processing*, 74, 263 – 270.

Mänttäri, M., Nyström, M., and Ekberg, B., 1996a. Influence of flocculants on the performance of a ceramic capillary filter. *Filtration & Separation*, 33, 75 – 80.

Mänttäri, M., Nyström, M., and Ekberg, B., 1996b. Influence of flocculants on the filtration of copper concentrates with a ceramic capillary filter. *Minerals Engineering*, 9, 419 – 428.

Panias, D., Taxiarchou, M., Paspaliaris, I., and Kontopoulos, A., 1996. Mechanism of dissolution of iron oxides in aqueous oxalic acid solutions. *Hydrometallurgy*, 42, 257 – 265.

Puranen, J., Häkkinen, A., Kallas, J., Ekberg, B., 2008. Comparison of regeneration methods for ceramic filter media. *Proceedings of the 10th World Filtration Congress*, Leipzig, Germany, 14 – 18 April.

Robinson, J.W., 1970. *Undergraduate Instrumental Analysis*. 2nd Ed. New York: Marcel Dekker, Inc.

Rueda, E.H., Ballesteros, M.C., Grassi, R.L., Blesa, M.A., 1992. Dithionite as a dissolving reagent for goethite in the presence of EDTA and citrate. Application to soil analysis. *Clays and Clay Minerals*, 40, 575 – 585.

Rushton, A., and Griffiths, P.V.R., 1987. Filter media. In: Matteson, M.J. and Orr, C. (eds.) *Filtration Principles and Practices*. 2nd Ed. New York: Marcel Dekker, Inc. 163 – 200.

Rushton, A., Ward, A.S., and Holdich, R.G., 2000. *Solid-liquid filtration and separation technology*. 2nd Ed. Wiley-VCH: Weinheim.

Savolainen, M., Huhtanen, M., Häkkinen, A., Ekberg, B., Hindström, R., and Kallas, J., 2011. Development of testing procedure for ceramic disc filters. *Minerals Engineering*, 24, 876 – 885.

Shu, L., Xing, W., and Xu, N., 2007. Effect of ultrasound on the treatment of emulsification wastewater by ceramic membranes. *Chinese Journal of Chemical Engineering*, 15, 855 – 860.

Sidhu, P.S., Gilkes, R.J., Cornell, R.M., Posner, A.M., Quirk, J.P., 1981. Dissolution of iron oxides and oxyhydroxides in hydrochloric and perchloric acids. *Clays and Clay Minerals*, 29, 269 – 276.

Siffert, C. and Sulzberger, B., 1991. Light-induced dissolution of hematite in the presence of oxalate: a case study. *Langmuir*, 7, 1627 – 1634.

Skoog, D.A., West, D.M., and Holler, R.J., 1988. *Fundamentals of Analytical Chemistry*. 5th Ed. New York: Saunders College Publishing.

Sondhi, R., and Bhave, R., 2001. Role of backpulsing in fouling minimisation in crossflow filtration with ceramic membranes. *Journal of Membrane Science*, 186, 41 – 52.

Sparks, T., 2012. *Solid-Liquid Filtration: A user's guide to minimizing costs and environmental impact, maximizing quality and productivity*. New York: Elsevier.

Stefanova, A., and Aromaa, J., 2012. *Alkaline leaching of iron and steelmaking dust*. Research report. Aalto University. ISBN 978-952-60-4462-0.

Stumm, W., and Furrer, G., 1987. The dissolution of oxides and aluminium silicates; examples of surface-coordination-controlled kinetics. In: Stumm, W. (ed.) *Aquatic Surface Chemistry*. New York: John Wiley & Sons. 197 – 219.

Sun, Z.X., Su, F.W., Forstling, W., Samskog, P.O. (1998), Surface characteristics of magnetite in aqueous suspension, *Journal of Colloid and Interface Science*, 197, 151 – 159.

Sweeton, F.H. and Baes, C.F., 1970. The solubility of magnetite and hydrolysis of ferrous ion in aqueous solutions at elevated temperatures. *The Journal of Chemical Thermodynamics*, 2, 479 – 500.

Tarleton, S., and Wakeman, R., 2007. *Solid/Liquid Separation: Equipment selection and Process Design*. Oxford: Elsevier.

Taxiarchou, M., Panias, D., Douni, I., Paspaliaris, I., and Kontopoulos, A., 1997a. Dissolution of hematite in acidic oxalate solutions. Hydrometallurgy, 44, 287 – 299.

Taxiarchou, M., Panias, D., Douni, I., Paspaliaris, I., and Kontopoulos, A., 1997b. Removal of iron from silica sand by leaching with oxalic acid. *Hydrometallurgy*, 46, 215 – 227.

Thompson, W.K., 1993. Continuous vacuum filtration: small scale tests versus full scale performance. *Filtration & Separation*, 30, 735 – 738.

Väisänen, P., 2004. *Characterisation of clean and fouled polymeric membrane materials*. Doctoral thesis. Lappeenranta University of Technology. ISBN: 951-764-889-8.

Wakeman, R., 2007. The influence of particle properties on filtration. *Separation and Purification Technology*, 58, 234 – 341.

Wakeman, R. and Tarleton, S., 2005. *Solid/liquid separation: principles of industrial filtration*.1st Ed. Oxford: Elsevier.

Weigert, T., and Ripperger, S., 1997. Effect of filter fabric blinding on cake filtration. *Filtration & Separation*, 34, 507 – 510.

Wells, M.A., Fitzpatrick, R.W., and Gilkes, R.J., 2006. Thermal and mineral properties of Al-, Cr-, Mn-, Ni- and Ti-substituted goethite. *Clays and Clay Minerals*, 54, 176 – 194.

Wells, M.A., Gilkes, R.J., and Fitzpatrick, R.W., 2001. Properties and acid dissolution of metal-substituted hematites. *Clays and Clay Minerals*, 49, 60 – 72.

Willard, H.H., Merritt, L.L., Dean, J.A., Settle, F.A., 1988. *Instrumental Methods of Analysis.* 7th Ed. Belmont: Wadsworth Publishing Company.

Yamamura, H., Chae, S., Kimura, K., Watanabe, Y., 2007. Transition in fouling mechanism in microfiltration of surface water. *Water Research*, 41, 3812 – 3822.

Article I

Salmimies, R., Mannila, M., Kallas, J., and Häkkinen, A.*, 2011. Acidic dissolution of magnetite: experimental study on the effects of acid concentration and temperature, *Clays and Clay Minerals*, 59, 136 – 146.

Clays and Clay Minerals, Vol. 59, No. 2, 136–146, 2011.

ACIDIC DISSOLUTION OF MAGNETITE: EXPERIMENTAL STUDY ON THE EFFECTS OF ACID CONCENTRATION AND TEMPERATURE

RIINA SALMIMIES*, MARJU MANNILA, JUHA KALLAS, AND ANTTI HÄKKINEN

LUT Chemistry, Lappeenranta University of Technology, P.O. Box 20, FI-53851 Lappeenranta, Finland

Abstract—Magnetite (Fe_3O_4) is a key economically valuable component in iron ore and is extracted by dissolution processes, but among the Fe (oxyhydr)oxides its solubility behavior is one of the least understood. The objective of this study was to improve understanding of magnetite dissolution mechanisms leading to thermodynamic equilibrium by comparing the dissolution of two solid samples, one synthetic and one industrial, using oxalic, sulfuric, and nitric acids at varying concentrations and temperatures. Of the three solid-liquid systems investigated, only the system consisting of magnetite and oxalic acid reached an equilibrium state within the duration of an individual experiment (6 h). In this system, increasing the acid concentration resulted in a significant increase in the equilibrium concentration of dissolved Fe. When dissolving synthetic and industrial magnetite, increasing the temperature not only increased the rate of reaction but also affected the concentration of dissolved Fe. Significant effects were observed when increasing the temperature from 15 to 35ºC, but only slight differences were seen on further increases in temperature. Observations regarding the equilibrium state of the sulfuric and nitric acid systems could not be made because equilibrium was not reached. The most important individual observation regarding the equilibrium state of the nitric- and sulfuric-acid systems seems to be that in future studies a much longer reaction time is necessary, due to slow kinetics of the dissolution mechanism. A proton-based mechanism has been hypothesized as the one governing the dissolution of magnetite by these two acids, but only the dissolution of the industrial sample yielded results that were similar for these two acids and consistent with that hypothesis.

Key Words—Dissolution, Iron Ore, Magnetite, Oxalic Acid, Nitric Acid, Sulfuric Acid, Particle Size, Temperature.

INTRODUCTION

Iron ore is one of the most widely mined minerals in the world, as indicated in a report of the British Geological Survey (2009). Iron oxides, key components in iron ore, are used in many areas of technology and are of interest to researchers in fields ranging from biology to mining and engineering.

Magnetite (Fe_3O_4) is one of the multifunctional oxides. Due to the stable nature of magnetite compared to its precursors, as characterized by a high standard free energy of formation ΔG_f^0 (Hemingway, 1990), its chemical dissolution requires a complete understanding of both the kinetics and thermodynamics of the dissolution process.

Although several dissolution models explaining the mechanisms for magnetite dissolution exist, as described by Brown *et al.* (1980), most of them pertain to complete dissolution of the solid compound, *i.e.* kinetics, rather than the reaching of an equilibrium state in the liquid phase. Houben (2003), Lee *et al.* (2007), and Reichard *et al.* (2007) studied the kinetics of dissolution of different Fe oxides in acidic or complexing conditions. The removal of Fe, mainly magnetite, from kaolin with oxalic acid was studied by Arslan and Bayat (2009), who found that increasing temperature and pulp density increased the degree of Fe removal. Interestingly, increasing acid concentration was found to yield no increase in Fe removal. The kinetics of acidic dissolution of other Fe (oxyhydr)oxides has also been studied (Veglió *et al.*, 1998; Mandal and Banerjee, 2004). Hematite (α-Fe_2O_3) and goethite (α-FeOOH), as the most stable and sparingly soluble Fe oxides, have been studied to a much greater extent than magnetite. References to thermodynamic data for magnetite are rare, and only the study of Sweeton and Baes (1970) on the solubility product of magnetite measured in dilute acid and base media can be found in the literature.

When the particle size decreases, the surface area increases. In theory, this should yield faster kinetics due to the increased exposure of the mineral surfaces, which typically enhances dissolution of even the most poorly soluble solids. In particular, compounds with large surface free energies, such as the Fe oxides, should exhibit faster kinetics with decreasing particle size.

Langmuir and Whittemore (1971) derived equations to calculate the solubility products of goethite and hematite according to crystal dimensions, but the equations are only theoretical and no experimental evidence of increased solubility with decreased particle size exists for Fe oxides.

* E-mail address of corresponding author:
riina.salmimies@lut.fi
DOI: 10.1346/CCMN.2011.0590203

A particle-size effect has been discovered for nanoparticles of other solid compounds, especially in the field of pharmaceuticals where many compounds are sparingly soluble. An attempt to predict the dissolution of an active pharmaceutical ingredient by means of particle-size distribution was made by Tinke *et al.* (2005), but they, too, adopted a kinetic approach by calculating the rate constant of dissolution, k, as a function of a single particle diameter, D. As a real solid has a particle-size distribution rather than having just a single particle size, an average rate constant, $\bar{k}$, was calculated. The model was generated using imaginary particle-size distributions and validated using *in vitro* dissolution data and real particle-size distributions measured with a Beckman Coulter LS320 laser-diffraction particle-size analyzer. A good correlation was found between the volume moment mean diameter, $D[4,3]$, and the dissolution rate constant, but for broader size distributions the distribution had to be split into smaller sections to achieve a better fit.

Demirkiran and Künkül (2007) dissolved ulexite, a boron ore, with perchloric acid and found that, even with micro-particles, the rate of dissolution increased with decreasing particle size. An increased dissolution rate was also observed as the perchloric acid concentration increased, as well as with increasing temperature.

A dissolution-enhancing temperature effect was also reported by Raschman and Fedorockova (2004) when dissolving Mg oxide (MgO) with hydrochloric acid. Interestingly, in this case an increase in the acid concentration failed to yield an increase in the dissolution rate. The effect of decreasing particle size was similar to the studies presented previously; a decrease in particle size resulted in an increase in the dissolution rate.

Hydrometallurgical studies (Chiarizia and Horwitz, 1991; Houben, 2003; Lee *et al.*, 2007) often focus on the kinetics of a single dissolution agent and use yield as a measure of performance. However, the mechanisms of dissolution for different dissolution agents, and also the concentration of functional groups in individual studies, can be very different and comparing the absolute performance of a chemical should not be based on kinetic studies alone but rather on mechanisms of dissolution, including the one state comparable for all systems, equilibrium.

Only a few studies exist which consider all three dissolution mechanisms of Fe oxides, *i.e.* protonation, complexation, and reduction (Zinder *et al.*, 1986; Banwart *et al.*, 1989). Although commendable, the studies focus only on kinetics, leaving thermodynamic effects of the three different mechanisms undiscussed.

The objective of the present experimental study was not to investigate the kinetics of dissolution of magnetite, as this has already been covered by several authors, but to investigate the effects of temperature and acid concentration on the equilibrium state of magnetite dissolution. The dissolution experiments were conducted with synthetic and industrial magnetite, using oxalic, nitric, and sulfuric acid at different concentrations and temperatures as the dissolution agents.

MATERIALS AND METHODS

Design of experiments

A full factorial experimental design consisting of 54 experimental points, including the experimental sets for synthetic and industrial magnetite, was generated for data collection. Two variables, temperature and acid concentration, on three levels were considered. Temperature values of 15, 35, and 50ºC were chosen. The values for acid concentration depended on the dissolving acid and were ultimately determined by the pH conditions applicable in industrial processes. Oxalic-acid concentrations of 0.08, 0.33, and 0.60 mol/L (calculated as dihydrate) were chosen. The concentrations for sulfuric acid were 0.10, 0.26, and 0.41 mol/L, and for nitric acid 0.16, 0.72, and 1.30 mol/L. The pH of each solution was measured prior to the dissolution experiments (Table 1).

Experiments covering the set of variables were conducted with all three dissolution agents, dissolving both synthetic and industrial magnetite.

Chemicals

The dissolution experiments were conducted with a synthetic magnetite powder and a natural magnetite sample obtained from an industrial company. The synthetic powder with 97% purity, as reported by the manufacturer, was provided by Alfa Aesar (Karlsruhe, Germany) (Figure 1a).

An energy dispersive X-ray spectroscopy (EDS) analysis of the industrial sample, performed with a JEOL JSM-5800 scanning electron microscope (SEM), revealed that the solid consisted of 68.77 atomic % Fe and 29.25 atomic % O. Magnesium, Si, Ca, Al, and Ti were present as impurities. In addition, X-ray diffraction

Table 1. pH values of oxalic, sulfuric, and nitric acid at chosen concentrations.

	Oxalic acid			Sulfuric acid			Nitric acid		
c_{acid} (mol/L)	0.08	0.33	0.60	0.10	0.26	0.41	0.16	0.72	1.30
pH	1.34	0.95	0.79	1.06	0.70	0.41	1.36	1.01	0.88

(XRD), using a Bruker D8 Advance diffractometer, was also employed to determine the composition of the industrial sample. The XRD data (CuKα radiation) was recorded between 5 and 70º2θ at a step size of 0.02º2θ and a scanning speed of 0.02º2θ s^{-1}. Magnetite was shown to be the primary component of the solid powder (Figure 1b). No other compounds were found in the spectrum, indicating the quantity of impurities to be minimal.

The initial particle-size distributions of the solids were measured using a Coulter LS 13320 laser diffraction particle-size analyzer (Figure 7a,b).

Oxalic acid, sulfuric acid, and nitric acid were chosen as dissolution agents. A solid oxalic acid dihydrate from BDH Prolabo (Leuven, Belgium) with a purity of 99% was used to formulate the oxalic acid solutions. Sulfuric acid and nitric acid from Merck, with purities of 95−97% and 65%, respectively, were used in the preparation of the other two acid solutions. For the sulfuric acid, 96% purity was chosen for calculation purposes. All solutions were prepared in reverse osmosis (RO) water.

Experimental set-up

The dissolution experiments were carried out in a 1 L glass reactor equipped with a thermostat to maintain constant temperature in the reacting mixture. A 4-blade, pitched blade turbine and four baffles were installed according to standard assembly to keep the solids in motion, thus ensuring maximum surface area and eliminating mass transfer as a limiting step.

The liquid was held at constant temperature in the reactor and a blank sample was drawn from the solution adjacent to the mixing shaft with a syringe, after which solids were introduced into the reactor and mixing was commenced. A total reaction time of 360 min, estimated on the basis of previous studies by Cornell and Schindler (1987) and Lee *et al.* (2007), was employed to reach the equilibrium state. Samples were drawn from the mother liquor every 30 min until a reaction time of 120 min was attained, after which samples were taken every 60 min. A syringe equipped with a syringe filter of pore size 0.8 μm was used to draw the samples from the reactor, after which the samples were diluted with RO water ten times to avoid any precipitation caused by changes in the temperature. The dissolved Fe concentration of the mother liquor was analyzed with inductively coupled plasma optical emission spectrometry (ICP-OES) using a ThermoElectron Iris Intrepid II spectrometer.

To estimate the effects of the particle size of the solids on the dissolution process, the particle-size distribution was determined in RO water, incorporating three parallel runs to evaluate the particle-size distribution, before and after the dissolution experiments using a Beckman Coulter LS 13320 laser-diffraction particle-size analyzer. A separate optical model was created for

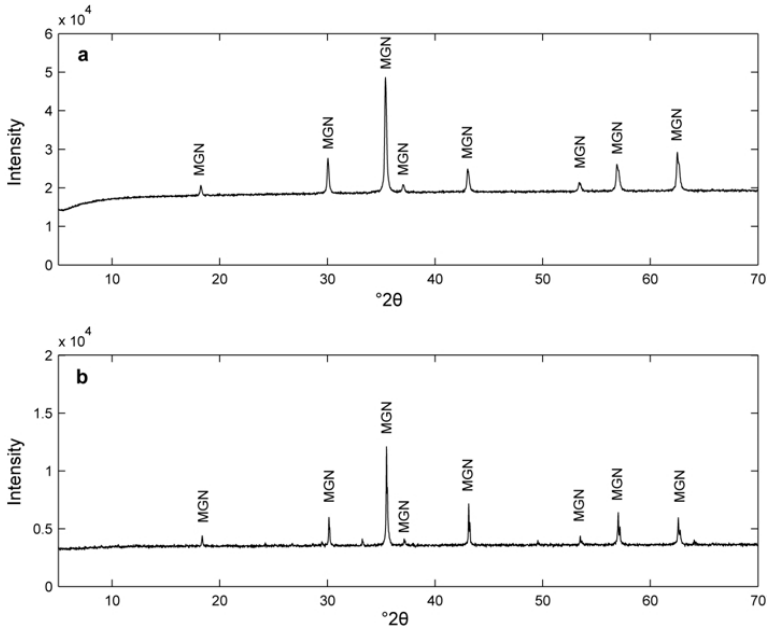

Figure 1. XRD patterns of magnetite powders: (a) synthetic; (b) industrial (MGN – magnetite).

the analysis of the magnetite powders using 2.42 as the real part of the refractive index (*Handbook of Chemistry and Physics*, 1998). The distribution was not determined for all the examined data points but by randomly selecting about half of the points in the experimental design.

RESULTS

Based on the dissolution experiments, the concentration of dissolved Fe increased with time under all conditions investigated but equilibrium was not always achieved.

Oxalic acid

In most cases, equilibrium was reached with oxalic acid after the first 2 h. A clear dependency for the dissolution of synthetic magnetite on temperature and acid concentration was observed (Figure 2a,b). Temperatures of 35 and 50ºC resulted in the same equilibrium concentration of dissolved Fe, but, interestingly, the reaction temperature of 15ºC yielded a much lower equilibrium concentration. As with synthetic magnetite, no significant difference between the reaction temperatures of 35 and 50ºC was observed when dissolving industrial magnetite, and a lower equilibrium concentration of Fe was once again observed at 15ºC (Figure 2c). The temperature effects with oxalic acid were not in line with the other two acids during the initial stages of the dissolution, which may be due to different dissolution mechanisms and different temperature effects. The effect of temperature on equilibrium with nitric and sulfuric acid cannot be discussed as equilibrium was not reached.

The effect of acid concentration on the dissolution of magnetite was clearly seen with oxalic acid. Increased acid concentration yielded increased dissolution of Fe from magnetite. No noticeable difference in kinetics could be observed during the first 60 min when dissolving industrial magnetite and using oxalic acid with concentrations of 0.33 and 0.60 mol/L, indicating that an increase in the acid concentration yields no

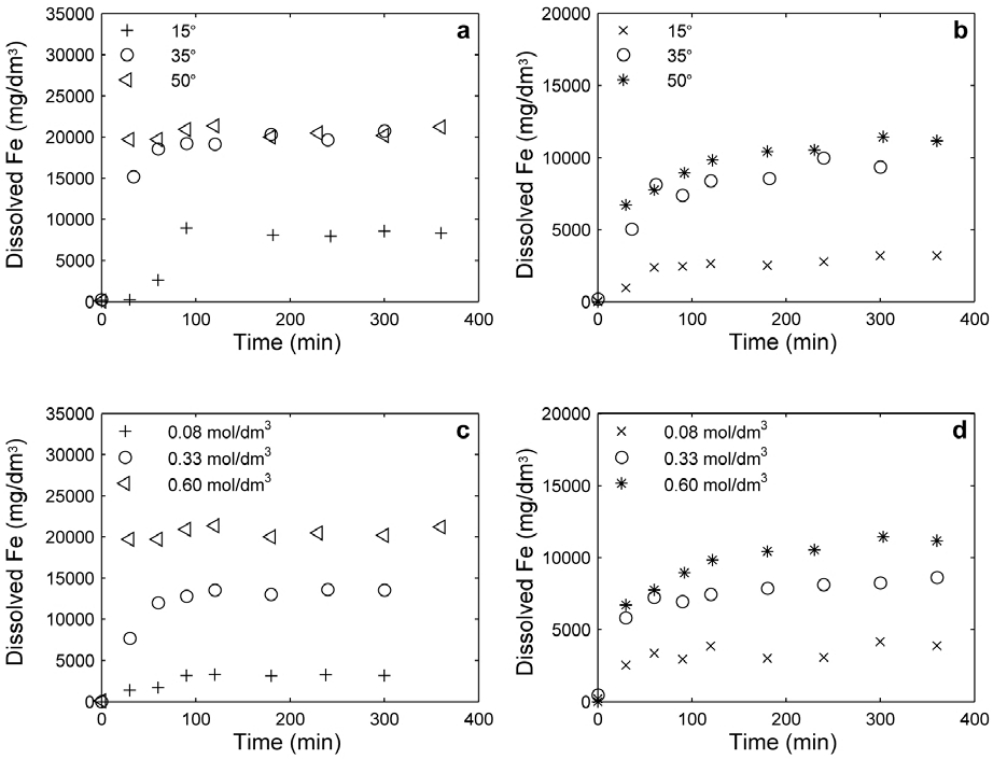

Figure 2. Dissolution of synthetic magnetite with oxalic acid at different (a) temperatures and (c) acid concentrations; and of industrial magnetite at different (b) temperatures and (d) acid concentrations. The concentration of sulfuric acid in (a) and (c) was 0.06 mol/L. The temperature in (c) and (d) was 50ºC.

improvement in kinetics, although it increases the maximum dissolved Fe concentration (Figure 2d). While greater acid concentration yielded slightly faster kinetics with synthetic magnetite, *i.e.* equilibrium was reached more quickly, the opposite was observed for industrial magnetite; the lowest acid concentration yielded the shortest time needed to reach equilibrium.

Sulfuric acid

The dissolution experiments with sulfuric acid yielded kinetic data in addition to the effects of temperature and acid concentration on the equilibrium. Unlike in the case of oxalic acid, 6 h was insufficient to reach an equilibrium state with the sulfuric acid-magnetite system. Some indication that the equilibrium state could be reached by extending the reaction time by a few hours was, however, seen in the data set. The conclusion was based on visual observation of curving of the lines (Figure 3a–c).

When dissolving synthetic magnetite with sulfuric acid, the temperature had a greater effect on the dissolution than the acid concentration. By increasing the temperature from 35 to 50ºC, the dissolution of Fe could be increased twofold (Figure 3a). Acid concentration had only a slight effect on the kinetics in the early stages of dissolution, but as the dissolution proceeded, the effect became more evident (Figure 3c). Interestingly, the greatest acid concentration did not yield the largest quantity of dissolved Fe.

The effect of temperature on the dissolution of industrial magnetite was more straightforward than that of acid concentration. Increasing the temperature led to increased concentration of dissolved Fe (Figure 3b), whereas increasing the acid concentration from 0.26 to 0.41 mol/L yielded almost no difference (Figure 3d). An increase of more than threefold was, however, observed when increasing the acid concentration from 0.10 to 0.26 mol/L. The results for the two greatest acid concentrations could be explained by a limiting acid concentration beyond which no improvement in the dissolution of Fe can be achieved Although the effective hydrogen ion concentrations are directly proportional to the acid concentrations, and are thus not equivalent, the quantities of dissolved iron are similar. A limiting acid

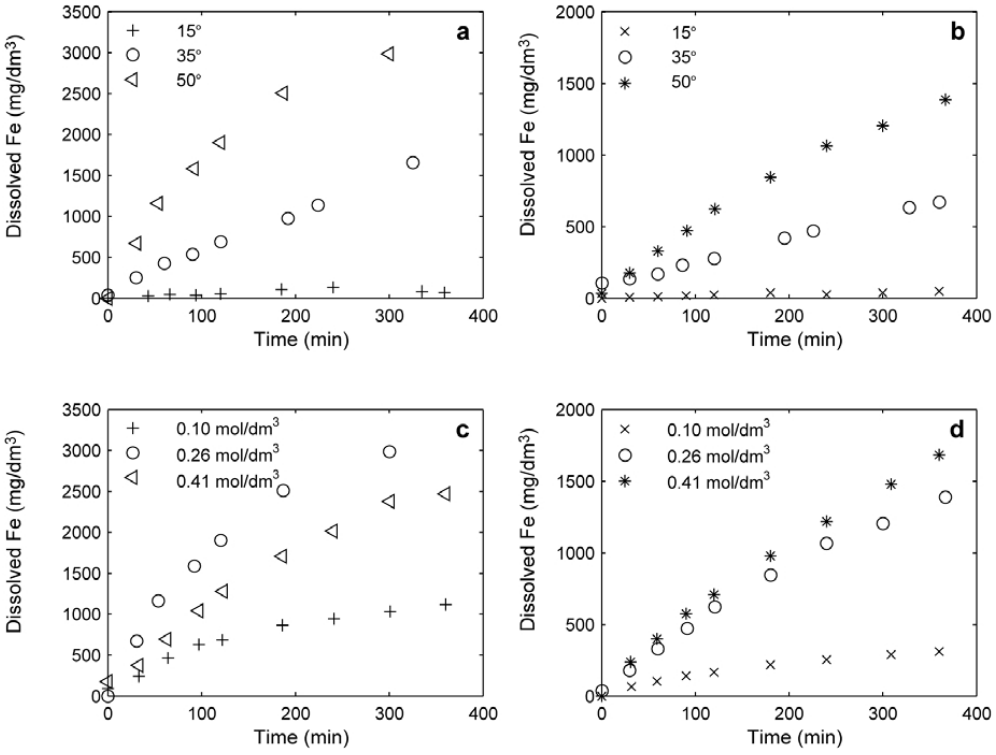

Figure 3. Dissolution of synthetic magnetite with sulfuric acid at different (a) temperatures and (c) acid concentrations, and of industrial magnetite at different (b) temperatures and (d) acid concentrations. The concentration of sulfuric acid in (a) and (b) was 0.26 mol/L. The temperature in (c) and (d) was 50ºC.

concentration in this case means that increasing the effective hydrogen ion concentration results in no enhancement in dissolution. The inhibiting effect of increased anion adsorption could also have played a role here.

Nitric acid

Nitric acid was used as the third dissolution agent, in which case even slower kinetics were observed than with sulfuric acid. The nitric acid system also failed to reach equilibrium within 6 h.

As when dissolving synthetic magnetite with sulfuric acid, the dissolution of synthetic magnetite with nitric acid also exhibited a strong temperature dependency (Figure 4a). Increasing the temperature from 15 to 35ºC increased the slope of the dissolution curve by a factor of more than ten. A more moderate increase, roughly threefold, was observed when further increasing the temperature to 50ºC.

Increasing the acid concentration clearly had an effect on the dissolution of Fe from synthetic magnetite. Increasing the acid concentration from 0.16 to 0.72 mol/L increased the slope more than twofold (Figure 4c). The same effect was observed when increasing the acid concentration from 0.72 to 1.30 mol/L.

The dissolution of industrial magnetite clearly depended on temperature (Figure 4b). Increasing the temperature increased the rate of dissolution and probably influenced the equilibrium concentration of Fe also.

Dissolution of industrial magnetite with nitric acid was similar to dissolution of industrial magnetite with sulfuric acid with respect to the effects of acid concentration. No difference between nitric acid concentrations of 0.72 and 1.30 mol/L was observed (Figure 4d) when dissolving the industrial magnetite. A significant difference was observed, however, between 0.16 and both 0.72 and 1.30 mol/L. As suggested for sulfuric acid, a limiting acid concentration could be the cause, as found also by Raschman and Fedorockova (2004).

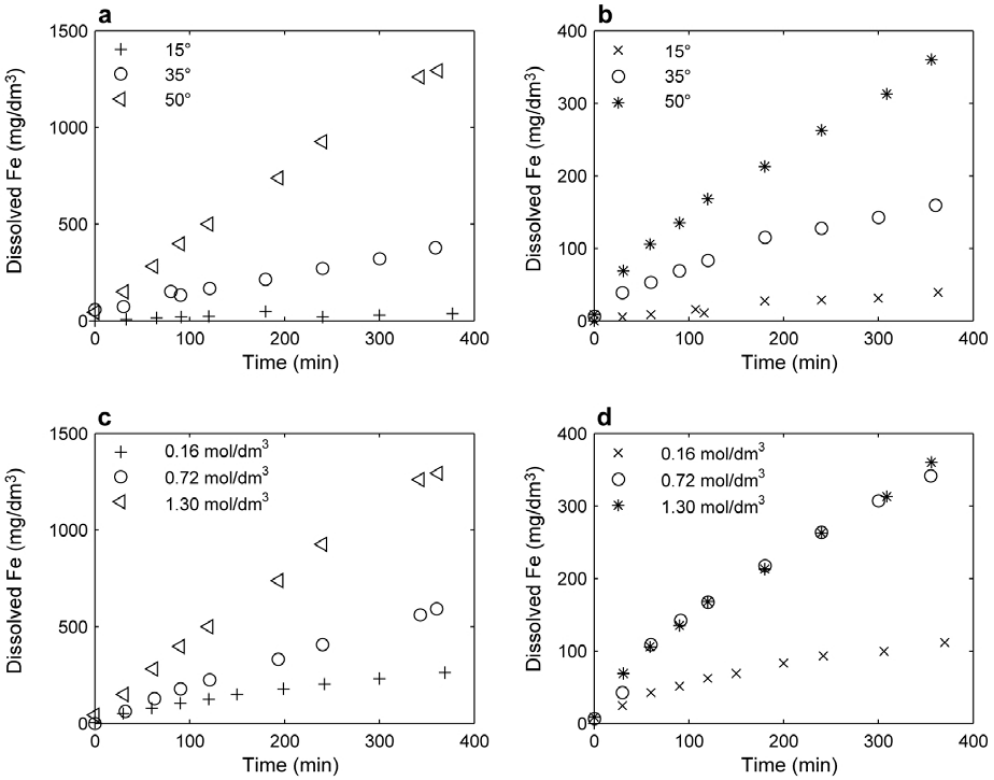

Figure 4. Dissolution of synthetic magnetite with nitric acid at different (a) temperatures and (c) acid concentrations, and of industrial magnetite at different (b) temperatures and (d) acid concentrations. The concentration of nitric acid in (a) and (b) was 1.30 mol/L. The temperature in (b) was 50ºC and the acid concentration in (c) was 0.26 mol/L.

Comparison of the dissolution agents

All three dissolution agents were compared to establish the absolute performance of these chemicals in dissolving Fe from magnetite. As described above, the concentrations of the acids tested were chosen based on what could be applicable in real processes, and were ultimately determined by the pH conditions. Consequently, the minimum and maximum values of the acid concentrations of different dissolution agents are not readily comparable and any such comparison must be viewed with caution.

Nitric-acid dissociates almost completely, yielding an effective hydrogen ion concentration which is the same as the concentration of the actual acid. For oxalic and sulfuric acid, only the first proton represents a strong acid with complete dissociation. The second proton is a weak acid with incomplete dissociation, resulting in a less effective hydrogen ion or functional group concentration than could be calculated from the molecular formula of the acid. When comparing the different acids, pH was used as the basis for comparison instead of absolute acid concentration, as pH is considered to indicate the effective hydrogen ion concentration. Consequently, oxalic (0.33 mol/L, pH = 0.95), sulfuric (0.10 mol/L, pH = 1.06), and nitric (0.72 mol/L, pH = 1.01) acid were used to dissolve both synthetic and industrial magnetite at 50ºC.

Oxalic acid was superior to sulfuric and nitric acid in dissolving Fe from magnetite independent of the type of magnetite (Figure 5a,b). The better performance observed is probably due to the ability of oxalic acid (Zinder *et al.*, 1986) to dissolve Fe oxides by two mechanisms: complex formation and induced reduction (Stumm *et al.* 1985; Cornell and Schindler 1987; Blesa *et al.* 1987; Panias *et al.* 1996).

Sulfuric acid gave concentrations of dissolved Fe approximately twice those of nitric acid when dissolving synthetic magnetite (Figure 5a). When dissolving industrial magnetite, however, almost identical behavior was observed for sulfuric and nitric acids. Bruyere and Blesa (1985) suggested that sulfuric acid dissolves magnetite through protonation. Zinder *et al.* (1986) also suggested protonation as a mechanism of dissolution of hematite and goethite with nitric acid. One could speculate that these two acids act through the same dissolution mechanism, *i.e.* protonation, which would yield the same results for the two acids at the same proton concentration, but the results obtained in the present study fail to support that hypothesis. Although the results for industrial magnetite agree with the suggested mechanism, the results for synthetic magnetite do not. The discrepancy might be due to differences in the adsorption of the anions, as described by Sidhu *et al.* (1981) when comparing the dissolution of several Fe oxides and hydroxides with hydrochloric and perchloric acid, but differing anion adsorption does not explain why a difference is observed when dissolving synthetic but not industrial magnetite.

When dissolving synthetic magnetite, a dissolved Fe concentration of ~14,000 mg/L was reached with oxalic acid, whereas dissolution of industrial magnetite with

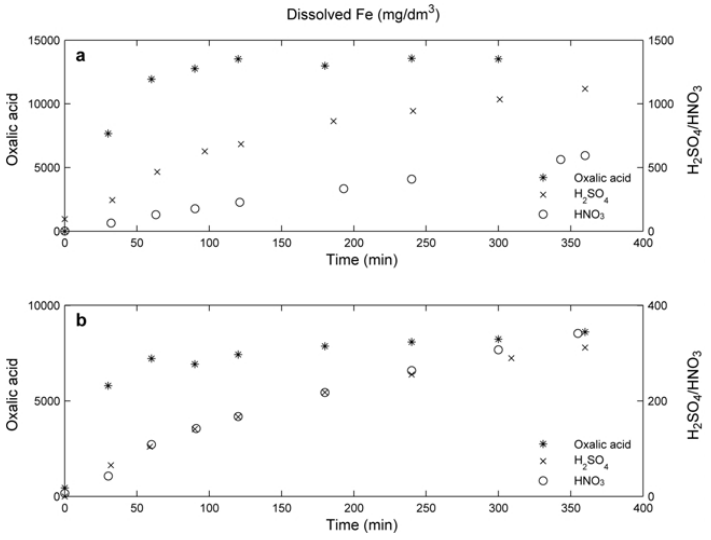

Figure 5. Dissolution of (a) synthetic and (b) industrial magnetite with different acids. The temperature in each experiment was 50ºC. The concentrations of oxalic, sulfuric, and nitric acid were 0.33, 0.10, and 0.72 mol/L, respectively. The corresponding pH values were 0.95, 1.06, and 1.01, respectively.

oxalic acid yielded only 8000 mg/L. A similar decrease was observed with the other two acids, but here the difference could be explained by slower kinetics of dissolution of the industrial sample.

Two possible explanations for the different results for the two magnetite samples appear plausible: differences in particle-size distribution and impurities in the industrial sample. The synthetic magnetite powder had a smaller mean particle size and more fines (Figure 7a), and thus a larger specific surface area. Larger specific surface areas mean, in general, faster dissolution rates, and as discussed above, possibly greater solubility also, although particle size has not yet been shown explicitly to have an effect on the dissolution process of magnetite.

Impurities of other dissolved ions, *e.g.* Mg, Ca, Al, and Si, were reflected in the ICP analysis, indicating the dissolution of something other than Fe from the industrial sample. The impurities were those also found in the initial SEM-EDS analysis of the industrial material. Some traces of Ti were also present in the mother liquor. Dissolution of the impurities exhibited similar behavior to dissolution of Fe from magnetite, *i.e.* in general, greater concentrations of dissolved species were observed with increasing acid concentration and temperature (Figure 6b,c). Calcium and Mg exhibited the greatest concentrations of dissolved impurities in the mother liquor (Figure 6a). Dissolution of Ca was rapid, reaching a maximum in the first 60 min even when dissolving with dilute nitric acid at 15ºC. The concentrations of Ca were, however, not the same for each experiment, suggesting that an equilibrium state was observed rather than the dissolution of all the Ca in the industrial sample. Increasing the temperature greatly increased the dissolution of Mg from industrial magnetite. As was the case for Fe dissolution, increasing the acid concentration from 0.26 to 0.41 mol/L yielded almost the same response for the dissolution of Mg, *i.e.* no significant improvement was observed with increasing acid concentration These impurities can diminish the dissolution capacity of the acid with respect to Fe by forming compounds with the dissolution agent, or even

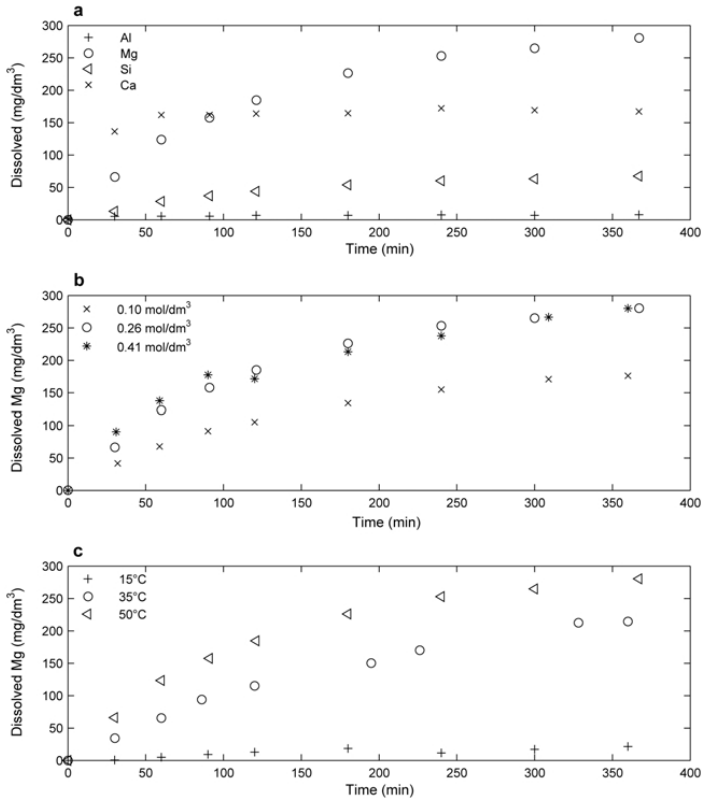

Figure 6. Dissolution of (a) impurities when dissolving industrial magnetite with 0.26 mol/L sulfuric acid at 50ºC, and the effect of (b) temperature and (c) acid concentration on the dissolution of Mg from industrial magnetite. The acid concentration in (b) was 0.26 mol/L and the temperature in (c) was 50ºC.

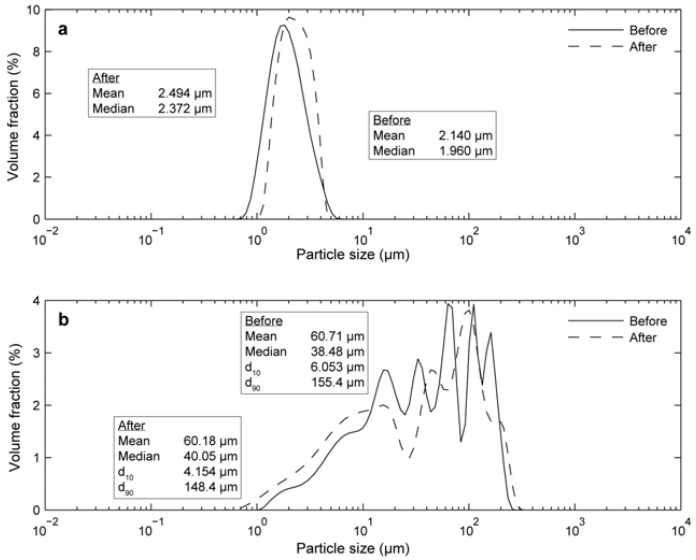

Figure 7. Particle-size distributions before and after dissolution experiments for (a) synthetic magnetite in sulfuric acid at a temperature of 15ºC and acid concentration of 0.41 mol/L, and (b) industrial magnetite in oxalic acid at a temperature of 50ºC and acid concentration of 0.33 mol/L.

inhibiting the dissolution of Fe from the solids. Due to greater dilution factors with oxalic acid (100-fold for ICP-OES), impurities were only observed in samples drawn from the sulfuric and nitric acid dissolutions (no dilution for ICP-OES). Although impurities were not seen in the analysis of the oxalic acid samples, a reasonable assumption would be that the same impurities were present but had just been diluted to a concentration below the detection limit.

No impurities were observed in the samples taken from the mother liquor used to dissolve synthetic magnetite, as would be expected due to the high purity of the synthetic powder.

Particle-size distribution

Particle-size distributions were determined for about half of the experimental points. As with the dissolution data, only a few examples characterizing the major trends in the data are presented here.

The original hypothesis concerning the particle-size distribution before and after the dissolution process was that the mean particle size should decrease and that the distribution itself should move to the left, indicating the dissolution of all particles to some extent. As reported by several authors (Langmuir and Whittemore, 1971; Raschman and Fedorockova, 2004; Demirkiran and Künkül, 2007), smaller particles dissolve faster and may even disappear completely, thereby increasing the fraction of larger particles.

In the present study, smaller particles disappeared, thus increasing the fraction of larger particles and shifting the distribution to the right. This is also seen as an increasing mean particle size (Figure 7a). The results for the industrial sample, with the addition of the d_{10} and d_{90} values, gave a better indication of the changes which took place in the industrial sample as the result of dissolution (Figure 7b).

Due to the coarseness of the industrial sample, settling was a major problem in sampling, and greater deviation with regard to finding a repeating pattern in the particle-size analysis was observed. However, an increase in the fraction of small particles and merging of peaks was observed, indicating different dissolution rates for different particle sizes.

The differences in the mean and median particle sizes before and after the dissolution were small, although obvious changes in the particle-size distribution can be seen quantitatively in the d_{10} and d_{90} values (Figure 7b). The d_{10} value, in particular, suggests an increased fraction of smaller particles. Even the composition of different size fractions could lead to variation resulting in differences in the dissolution. Future work could usefully include dissolution experiments with fractionated industrial material.

CONCLUSIONS

Dissolution experiments with synthetic and industrial magnetite were conducted with oxalic, sulfuric, and nitric acid at different temperatures and acid concentrations in order to compare the effects of different acids on the dissolution mechanism for magnetite.

For each acid, an increase in the dissolution rate was, in general, observed with increased temperature and acid concentration. A few interesting exceptions, *e.g.* a limiting acid concentration with sulfuric and nitric acid, were observed. Equilibrium was reached only when dissolving magnetite with oxalic acid. Temperature affected the equilibrium but only when the temperature was increased from 15 to 30ºC. Further increases in temperature yielded no significant increase in the equilibrium concentration of dissolved Fe independent of the type of magnetite used. Increasing the acid concentration yielded greater solubilities in both synthetic and industrial magnetite. The conclusion concerning sulfuric and nitric acid was that the mechanisms of dissolution are significantly slower than those affecting the dissolution of magnetite with oxalic acid. Protonation has been suggested as the mechanism involved in the dissolution of Fe oxides by sulfuric and nitric acid but, in this study, the results for the two acids differed, indicating that additional factors need to be considered. As equilibrium was not reached, valid comparison based on the dissolution mechanisms could not be made.

Oxalic acid exhibited the best capacity to dissolve Fe from magnetite, followed by sulfuric acid and nitric acid. The differences in dissolved Fe concentration between oxalic acid and the other two acids for both synthetic and industrial magnetite were over tenfold. In dissolving industrial magnetite, sulfuric and nitric acid exhibited similar behaviors, supporting the suggestion of protonation being the dissolution mechanism, but dissolution of synthetic magnetite with sulfuric and nitric acid yielded different results.

In general, synthetic magnetite gave greater concentrations of dissolved Fe in the dissolution experiments than industrial magnetite, as expected. Different particle-size distributions and impurities of the industrial sample are the most likely causes.

Further work on generating models, both empirical and theoretical, needs to be done. In addition, the time required to reach the equilibrium state with sulfuric and nitric acid should be further investigated.

ACKNOWLEDGMENTS

The Graduate School in Chemical Engineering is kindly acknowledged for funding this study.

REFERENCES

Arslan, V. and Bayat, O. (2009) Removal of Fe from kaolin by chemical leaching and bioleaching. *Clays and Clay Minerals*, **57**, 787–794.

Banwart, S., Davies, S., and Stumm, W. (1989) The role of oxalate in accelerating the reductive dissolution of hematite (α-Fe_2O_3) by ascorbate. *Colloids and Surfaces*, **39**, 303–309.

Blesa, M.A., Magaz, G., Salfity, J.A., and Weisz, A.D. (1987) Mechanism of dissolution of magnetite by oxalic acid-ferrous iron solutions. *Inorganic Chemistry*, **26**, 3713–3717.

British Geological Survey (2009) *World Mineral Production 2003–07*. [Online] NERC. Available at: http://www.bgs.ac.uk/mineralsUk/commodity/world/home.html [Accessed 2 November 2009].

Brown, W.E., Dollimore, D., and Galwey, A.K. (1980) Reactions in the solid state, Pp. 41–109 in: *Comprehensive Chemical Kinetics* (C.H. Bamford and C.F. Tipper, editors). Elsevier, Amsterdam.

Bruyere, V.I.E. and Blesa, M.A. (1985) Acidic and reductive dissolution of magnetite in aqueous sulphuric acid. Site-binding model and experimental results. *Journal of Electroanalytical Chemistry*, **182**, 141–156

Chiarizia, R. and Horwitz, E. (1991) New formulations for iron oxides dissolution. *Hydrometallurgy*, **27**, 339–360.

Cornell, R. M. and Schindler, R. W. (1987) Photochemical dissolution of goethite in acid/oxalate solution. *Clays and Clay Minerals*, **35**, 347–352.

Demirkiran, N. and Künkül, A. (2007) Dissolution kinetics of ulexite in perchloric acid solutions. *International Journal of Mineral Processing*, **83**, 76–80.

Handbook of Chemistry and Physics (1998) *Physical and Optical Properties of Minerals*. Pp. 4–140 (W. M. Haynes, editor). CRC Press Inc., Boca Raton, Florida, USA.

Hemingway, B.S. (1990) Thermodynamic properties for bunsenite, NiO, magnetite, Fe_3O_4, and hematite, Fe_2O_3, with comments on selected oxygen buffer reactions. *American Mineralogist*, **75**, 781–790.

Houben, G.J. (2003) Iron oxide incrustations in wells. Part 2: Chemical dissolution and modeling. *Applied Geochemistry*, **18**, 941–954.

Langmuir, D. and Whittemore, D.O. (1971) Variations in the stability of precipitated ferric oxyhydroxides. Pp. 209–234 in: *Nonequilibrium Systems in Natural Water Chemistry* (R.F. Gould, editor). American Chemical Society, Washington D.C.

Lee, S.O., Tran, T., Jung, B.H., Kim, S.J., and Kim, M.J. (2007) Dissolution of iron oxide using oxalic acid. *Hydrometallurgy*, **87**, 91–99.

Mandal, S. and Banerjee, P. (2004) Iron leaching from China clay with oxalic acid: Effect of different physicochemical parameters. *International Journal of Mineral Processing*, **74**, 263–270.

Panias, D., Taxiarchou, M., Paspaliaris, I., and Kontopoulos, A. (1996) Mechanism of dissolution of iron oxides in aqueous oxalic acid solutions. *Hydrometallurgy*, **42**, 257–265

Raschman, P. and Fedorocková, A. (2004) Study of inhibiting effect of acid concentration on the dissolution rate of magnesium oxide during the leaching of dead-burned magnesite. *Hydrometallurgy*, **71**, 403–412.

Reichard, P.U., Kretzschmar, R., and Kraemer, S.M. (2007) Rate laws of steady-state and non-steady-state ligand-controlled dissolution of goethite. *Colloids and Surfaces A: Physicochemical and Engineering Aspects*, **306**, 22–28.

Sidhu, P., Gilkes, R., Cornell, R., Posner, A., and Quirk, J. (1981) Dissolution of iron oxides and oxyhydroxides in hydrochloric and perchloric acids. *Clays and Clay Minerals*, **29**, 269–276.

Stumm, W., Furrer, G., Wieland, E., and Zinder, B. (1985) The effects of complex-forming ligands on the dissolution of oxides and aluminosilicates. Pp. 55–74 in: *The Chemistry of Weathering* (J.I. Drever, editor). D. Reidel, Dordrecht, The Netherlands.

Sweeton, F.H. and Baes, C.F. (1970) The solubility of magnetite and hydrolysis of ferrous ion in aqueous solutions at elevated temperatures. *The Journal of Chemical Thermodynamics*, **2**, 479–500.

Tinke, A.P., Vanhoutte, K., De Maesschalck, R., Verheyen, S., and De Winter, H. (2005) A new approach in the prediction

of the dissolution behavior of suspended particles by means of their particle size distribution. *Journal of Pharmaceutical and Biomedical Analysis*, **39**, 900–907.

Veglió, F., Passariello, B., Barbaro, M., Plescia, P., and Marabini, A. (1998) Drum leaching tests in iron removal from quartz using oxalic acid and sulphuric acid. *International Journal of Mineral Processing*, **54**, 183–200

Zinder, B., Furrer, G., and Stumm, W. (1986) The coordination chemistry of weathering: II. Dissolution of Fe(III) oxides. *Geochimica et Cosmochimica Acta*, **50**, 1861–1869.

(*Received 21 September 2010; revised 21 April 2011; Ms. 491; A.E. J.D. Fabris*)

Article II

Salmimies, R., Mannila, M., Kallas, J., and Häkkinen, A.,* 2012. Acidic dissolution of hematite: kinetic and thermodynamic investigations with oxalic acid, *International Journal of Mineral Processing,* 110 – 111, 121 – 125.

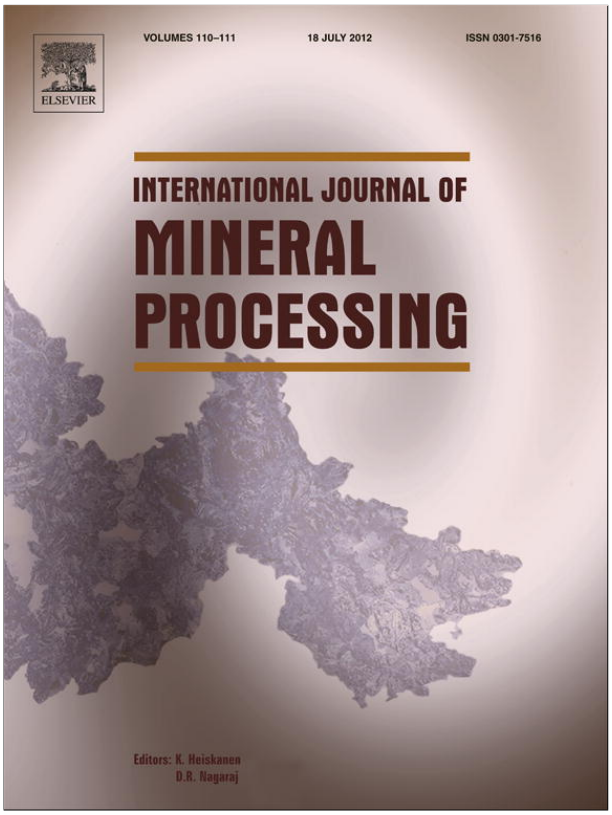

International Journal of Mineral Processing 110–111 (2012) 121–125

Contents lists available at SciVerse ScienceDirect

International Journal of Mineral Processing

journal homepage: www.elsevier.com/locate/ijminpro

Acidic dissolution of hematite: Kinetic and thermodynamic investigations with oxalic acid

Riina Salmimies [a,*], Marju Mannila [a], Juha Kallas [b], Antti Häkkinen [a]

[a] LUT Chemistry, Lappeenranta University of Technology, P.O. Box 20, FI-53851 Lappeenranta, Finland
[b] Laboratory of Inorganic Materials, Tallinn University of Technology, Ehitajate tee 5, EE-19086, Tallinn, Estonia

ARTICLE INFO

Article history:
Received 21 December 2011
Received in revised form 19 March 2012
Accepted 2 April 2012
Available online 10 April 2012

Keywords:
Dissolution
Hematite
Oxalic acid
Kinetic modeling

ABSTRACT

Although extensively studied, consensus on the kinetics or thermodynamics of iron oxide dissolution has not yet been achieved among scientists. The aim of this study was to investigate the applicability of twelve different kinetic models in describing the dissolution of hematite (α-Fe_2O_3). In this study, hematite was dissolved in 0.6 mol/L oxalic acid at 50 °C to obtain kinetic data for modeling. In addition to the kinetic data, thermodynamic data were collected at 35 and 50 °C to discuss the dissolution mechanism. The Kabai equation and the first order rate law were found most suitable in describing the dissolution. The associated reaction rate constants were $2.0 \cdot 10^{-5}$ s^{-1} for both models.

1. Introduction

The dissolution of iron, *Fe*, from hematite has been described through various models. Cornell and Schwertmann (2003) have summarized 12 possible models describing dissolution reactions in general. In addition, a wide range of different experimental conditions have been covered in the dissolution of different Fe oxides. The kinetics of dissolution of hematite in oxalic acid have, however, not been presented by the authors.

Panias et al. (1996) have reviewed existing research and initially suggested a reaction mechanism for the dissolution of Fe oxides in organic acids. The mechanism comprises three processes: (1) adsorption of organic ligands from the solution to the solid Fe oxide surface, (2) non-reductive dissolution, and (3) reductive dissolution consisting of an induction and an autocatalytic period. The suggested mechanism indicates the participation of protons in the dissolution process. Although comprehensive in describing the reactions taking place during Fe oxide dissolution, pH was discussed only as a parameter affecting dissolution and, in this case, no additional experimental work was conducted to further verify the validity of the suggested reaction mechanism. The authors did conclude that non-reductive dissolution is not a viable reaction pathway at low temperatures.

Taxiarchou et al. (1997) investigated the dissolution kinetics of hematite in acidic oxalate solutions. The study indicated that the dissolution of Fe was significantly dependent on temperature and on the pH of the mother liqueur but was not affected by the oxalate concentration. The authors also concluded that increase in the solution acidity decreases the time necessary for the induction period, i.e. the lower the pH the shorter the induction period.

Lee et al. (2006) have studied the kinetics of dissolution of hematite in oxalic acid, too, and found that the dissolution was best described by a diffusion-controlled shrinking core model. The authors also concluded that the dissolution of Fe oxides in oxalic acid was very slow at temperatures of 25–60 °C and that, contrary to Taxiarchou et al. (1997), the dissolution of hematite could be correlated with the oxalate concentration of the mother liqueur. In addition, the authors found that the dissolution of hematite takes place through solid state reduction rather than a combination of non-reductive and reductive dissolution. Interestingly, signs of thermodynamic equilibrium were present in the data, as indicated by the steady state in the concentration of dissolved Fe although less than 40% of the initial Fe was dissolved. The authors reported deviations from linearity in their kinetic modeling but did not discuss the deviations further. The deviations were most likely caused by reaching an equilibrium state within the system. The framework of the study was, however, the dissolution of Fe oxides from clay and silica minerals, and the interpretation of the results and the selection of the suitable kinetic equation could have been based on that framework. In addition, it is unclear whether mixing was used in the studied system or not. Lee et al. (2007) have also suggested that the formation of an Fe oxalate product layer, at pH 1.6–3.2, can inhibit the dissolution of hematite in oxalic acid and that increase in the rate of dissolution can be observed with the addition of magnetite, Fe_3O_4, into the studied system. The addition of magnetite was roughly 10 wt.%. Mandal and Banerjee (2004) also studied the dissolution kinetics of Fe leaching from clay. Rate of dissolution was found to

* Corresponding author. Tel.: +358 40 19 777 95.
E-mail address: riina.salmimies@lut.fi (R. Salmimies).

0301-7516/$ – see front matter © 2012 Elsevier B.V. All rights reserved.
doi:10.1016/j.minpro.2012.04.001

increase with increasing temperature. Mixing was done by shaking, where the shaking speed was not found significant in determining the outcome of the leaching.

Cornell and Schindler (1987) investigated the kinetics of photochemical dissolution of goethite in acidic oxalate solutions and suggested that both protons and oxalate ions participate in the dissolution reaction. The study reported a constantly increasing proton consumption, which could be seen as an increase in pH. To date, there appears to be no other published studies dealing with the behavior of pH in the dissolution of Fe oxides with oxalic acid.

Sidhu et al. (1981) studied the dissolution of several Fe oxides in hydrochloric and perchloric acids and found that the dissolution kinetics of hematite, among other Fe oxides, was described quite well by the cube root law suggesting that the dissolution was proportional to the surface area of the oxide. The mechanism of dissolution is not the same for hydrochloric and oxalic acids, but the authors suggested that complex formation played a role in the dissolution of hematite with hydrochloric acid thus bringing the dissolution processes of the two acids closer together.

Wells et al. (2001) studied the kinetics of acidic dissolution of aluminum substituted hematites in hydrochloric acid and found that the dissolution was well described by the Avrami–Erofe'ev equation, and that the cube root law and the Kabai equation were not applicable in this case.

The effect of temperature and acid concentration on the dissolution of magnetite has been investigated by Salmimies et al. (2011). The study concluded that temperature had no effect on the equilibrium concentration of Fe when dissolving magnetite in oxalic acid.

The objective of this study was to investigate the suitability of different kinetic models, also those discussed earlier in this chapter, in describing the dissolution of hematite in oxalic acid. In addition, thermodynamic data was collected to discuss the mechanisms of dissolution.

2. Materials and methods

2.1. Materials

A solid synthetic hematite powder, provided by Sigma-Aldrich (Schnelldorf, Germany) in 97% purity, was initially characterized with laser diffraction (Beckmann Coulter LS 13320) to obtain a particle size distribution for the powder (Fig. 1). The effects of particle size were not included in this study, although the particle size distribution plays a major role in the dissolution kinetics and possibly also in thermodynamics. The particle size distribution was determined mainly to characterize the used solid material comprehensively. In addition to the particle size measurement, X-ray diffraction (XRD, Bruker D8 Focus) was used to verify the chemical composition of the powder. According to the X-ray analysis, hematite was found to be the only mineralogical phase in the powder. In addition to XRD, scanning electron microscopy coupled with energy-dispersive X-ray spectrometry (SEM-EDS, JEOL JSM-5800) was employed to determine the elemental composition of any impurities. No impurities were found with SEM-EDS.

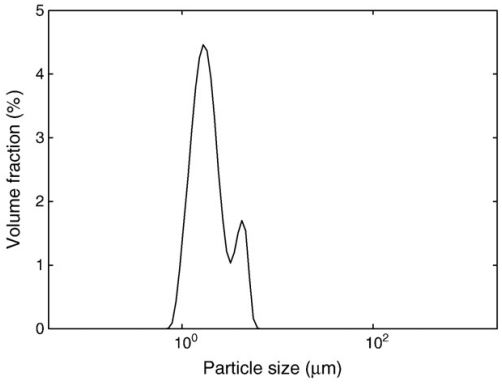

Fig. 1. Particle size distribution of the synthetic hematite powder.

Solutions of 0.6 mol/L oxalic acid were prepared using a solid oxalic acid dihydrate powder from BDH Prolabo (Leuven, Belgium). The purity of the solid powder was 99% with all solutions prepared in ultrapure water. The concentration of the acid was chosen so as to yield comparable results with previous studies conducted with synthetic magnetite (Salmimies et al., 2011).

2.2. Experimental

The dissolution experiments were conducted in a thermostated 1 L glass reactor. A pitched blade turbine and four baffles installed according to standard assembly (Tatterson, 1994) were used to induce sufficient mixing. To ensure that real kinetics would be observed and mass transfer in the bulk phase would not become a limiting factor with the stirred reactor, the effect of the stirrer speed was investigated with three different rotation speeds: 400, 800, and 1000 rpm. All experiments were conducted in 0.6 mol/L oxalic acid at a temperature of 50 °C. Solutions were prepared in ultrapure water and were thermostated in the reactor prior to adding the solids. A blank sample was drawn from the liquid phase by using a syringe, after which the solids were introduced into the reactor and mixing was commenced. Samples of the liquid phase were drawn at regular intervals. Solids were removed with a syringe filter after which the samples were diluted with 10 wt.% nitric acid and analyzed with inductively coupled plasma optical emission spectroscopy (ICP-OES, Thermo Electron Iris Intrepid II XDL) for dissolved Fe. The dilution factor varied between 0 and 300 depending on the experimental conditions. Measuring pH was done continuously from the liquid phase (WTW pH 401i, WTW SenTix 41 electrode). The initial mass of the hematite powder in the kinetic experiment was 12 g making the slurry density in this case 12 g/L.

The equilibrium data were collected in a similar way as the kinetic data but while initializing the experiments solids were added in excess to reach the equilibrium concentration, or solubility, without complete dissolution of the solids. Equilibrium data were collected at 35 and 50 °C. Initial pH in the experiments at 35 and 50 °C was 1.02 and 0.95, respectively.

The experimental error was estimated at roughly 2%. Quantifiable components included sampling and analysis errors.

2.3. Modeling

The models, summarized by Cornell and Schwertmann (2003), tested in this study have been presented in Eqs. (1)–(12).

$$\alpha^2 = kt \tag{1}$$

$$(1-\alpha)\ln(1-\alpha) + \alpha = kt \tag{2}$$

$$\left[1-\left(1-\alpha^{1/3}\right)\right]^2 = kt \tag{3}$$

$$\left(1-\frac{2}{3}\alpha\right)-(1-\alpha)^{2/3} = kt \tag{4}$$

$$-\ln(1-\alpha) = kt \tag{5}$$

$$[-\ln(1-\alpha)]^{1/2} = kt \tag{6}$$

$$[-\ln(1-\alpha)]^{1/3} = kt \tag{7}$$

$$\ln\ln\left(\frac{1}{1-\alpha}\right) = a\ln k + a\ln t \quad (8)$$

$$1-(1-\alpha)^{1/2} = kt \quad (9)$$

$$1-(1-\alpha)^{1/3} = kt \quad (10)$$

$$\alpha^{1/n} = kt \quad (11)$$

$$\ln\alpha = kt \quad (12)$$

where α is the extent of reaction ranging from 0 to 1 (−), k is the reaction rate constant (s^{-1}), t is time (s), and a is an estimated parameter (−). In this study, the extent of reaction was determined as the ratio of concentration of dissolved Fe to concentration of initially added Fe. Complete dissolution was achieved during the kinetic experiment. The actual fitting was done by plotting the left hand side of the equation, from now on denoted as Y, as a function of time, or, for Eq. (8), as a function of logarithmic time.

The physical background of the equations for dissolution, of which a summary is included here, has been extensively reviewed by Brown et al. (1980). Eqs. (1), (2), (3), and (4) all describe diffusion mechanisms, where the diffusion of a reactant or of the reaction product to or from the boundary layer, is the rate determining step. Eq. (1) is generally regarded with reactants occurring in thin sheets. Whereas Eq. (2) describes the dissolution of cylindrical particles, Eqs. (3) and (4) apply for spherical particle. Eq. (5) represents the first order random nucleation process, which is a surface reaction and may take place in final stages of solid phase decomposition. All the equations above are described by deceleratory t–α curves. The two Avrami–Erofe'ev equations (Eqs. (6) and (7)) exhibit sigmoidal t–α curves and have been seen to be valid over a wide range of α. The forms of the equations are similar to that of Eq. (5). The difference originates from the denominator of the exponent. For Eq. (5) the denominator could be considered to be 1 whereas for Eqs. (6) and (7) it is 2 and 3, respectively. The different denominators relate to crystal growth characteristics. An assumption that the reaction is initiated at edges or surface cracks of the solid is incorporated into the Avrami–Erofe'ev treatment. Eq. (8), also known as the Kabai equation, is a modification of the Nernst equation and represents a surface reaction. The equation exhibits sigmoidal t–α curves. Eqs. (9) and (10) consider the reaction to be initiated at all faces of the solid. Eq. (9) can be considered when dissolving cylindrical particles and Eq. (10) applies for cubical and spherical particles. Eqs. (11) and (12) represent the power and the exponential law, respectively, and have acceleratory t–α curves.

Eq. (4) represents the previously mentioned diffusion-controlled shrinking core model whereas Eq. (11), with n = 3, represents the cube root law. The more extensive use of Eq. (11), however, requires knowledge of the order of the reaction.

3. Results

3.1. Stirring speed

Because the formation of an inhibiting product layer has been shown to be possible, the effect of the stirring rate was investigated. With insufficient mixing, the formation of a stagnant product layer is possible and can result in increased mass transfer resistance, possible precipitation of the reaction product, and subsequent inhibition of the dissolution. If sufficient mixing is induced the reaction product is effectively transferred into the bulk phase and does not inhibit the dissolution reaction. The effect of the stirrer speed was investigated by performing the dissolution under 400, 800, and 1000 rpm. At those stirring speeds mixing was found to have no significant effect on the dissolution (Fig. 2) suggesting that no increase in mass transfer resistance took place and, consequently, the formation of an inhibiting product layer was unlikely. A small deviation was found with 400 rpm: the slope of the dissolution curve was slightly smaller than with the other two experiments. Consequently, 800 rpm was chosen for all the following experiments as it was found sufficient enough to eliminate mass transfer in the bulk phase. Furthermore, 800 rpm yielded a more homogeneous mixing and less settling of the particles in the reaction vessel.

3.2. Temperature

Experiments done at 35 and 50 °C yielded roughly the same equilibrium concentration (Fig. 3A), indicating that the temperature had no effect on the equilibrium concentration of dissolved Fe. The equilibrium kinetics were, however, affected by the change in temperature. Whereas equilibrium was reached in roughly 150 h in 50 °C, in 35 °C signs of equilibrium were visible only after 330 h.

3.3. pH

The pH of the system was in most cases below 1.00 which should eliminate the risk of formation of an inhibiting product layer, as the solid Fe oxalate has been shown not to be stable at such low pH. A constant decrease in pH was observed during the kinetic experiment until the system reached equilibrium where pH also reached a steady state. Observing a constantly decreasing pH in this study is contradictory to results of other authors (Cornell and Schindler, 1987) where the consumption of protons has been observed.

In the thermodynamic experiments, a decrease in pH was observed in the early stages of the reaction, after which pH started to increase and reached a constant value at the end of the dissolution. The initial decrease was faster in 50 °C than in 35 °C indicating faster kinetics at elevated temperatures. In both cases, the behavior of the pH was similar (Fig. 3B). To compare the two experiments done at different temperatures, pH values were normalized by dividing all pH values with the initial pH. Normalization eliminated the small difference observed in the initial pH of the two solutions making the data more comparable.

3.4. Kinetic modeling

Complete dissolution was achieved in roughly 80 h (Fig. 4A) in the kinetic experiment which would support the conclusion of previous

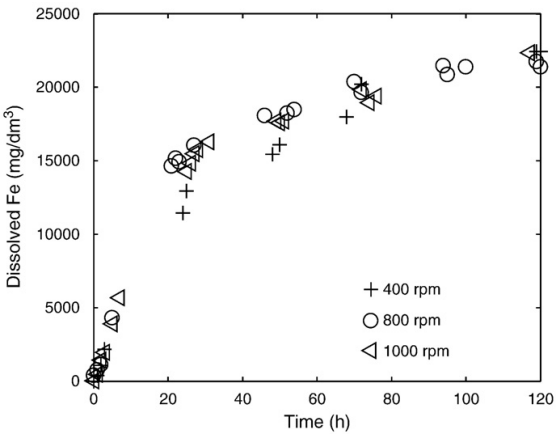

Fig. 2. Concentration of dissolved Fe as a function of time at three different stirring speeds: 400, 800, and 1000 rpm. Concentration of oxalic acid was 0.6 mol/L and the temperature was 50 °C in all experiments.

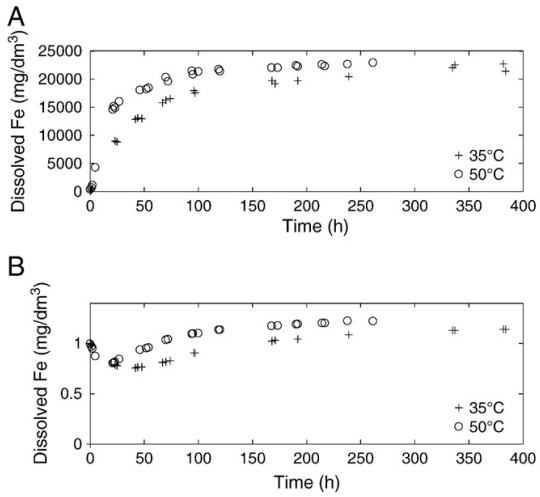

Fig. 3. Thermodynamic studies of hematite dissolution in 0.6 mol/L oxalic acid at 35 and 50 °C. (A) Concentration of dissolved Fe. (B) pH of the solution. The stirring speed was 800 rpm in both experiments.

studies on the slow dissolution rate of hematite at low temperatures. Here the average rate of dissolution was roughly 0.15 g_{Fe2O3}/h. The hematite powder was found to contain no significant impurities, including magnetite, and the dissolution can indeed be assumed to describe that of hematite without any interference from other mineral phases. Although the initial observation was that the t–α curve exhibited a decelerator nature, closer investigation of the early stages of dissolution revealed a slightly sigmoidal shape (Fig. 4B).

The suitability of 12 different kinetic models in describing the complete dissolution of hematite in 0.6 mol/L oxalic acid at 50 °C was evaluated by fitting the models with the data (Fig. 5A–D). The best fit ($R^2 = 0.99$) was achieved with Eq. (8), the Kabai equation. Eq. (5), also referred to as the 1st order nucleation model, yielded a good fit with an R^2 value of 0.95. The Kabai equation exhibits sigmoidal whereas for the 1st order nucleation model the curves are deceleratory. The induction period can be relatively short in comparison to the time needed to reach equilibrium, especially as acidity of the solution is high. When enlarging the initial stages of the dissolution, a sigmoidal trend was indeed observed further supporting the selection of the Kabai equation. In addition to the two equations performing the best, the diffusion-controlled shrinking core model (Eq. (4)) also performed well with an R^2 value of 0.93. Eqs. (3) and (7) were found least suitable based on the R^2 values. Whereas the R^2 value for most of the models varied between 0.71 and 0.89, the corresponding values for Eqs. (3) and (7) were 0.35 and 0.26, respectively. Interestingly, Eq. (3) gave one of the poorest correlations when, in fact, the physical background of that equation is similar to the diffusion-controlled shrinking core Eq. (4) with the exception of the dimensions of the diffusion surface. Both of those equations describe the dissolution of spherical particles. The failure of those equations in describing the dissolution could be found in the relatively small particle size of the particular solids used in this study. As the size of particles is reduced, the surface area available over which diffusion can take place is increased, thus decreasing the significance of diffusion as rate limiting. Similarity in Eqs. (3) and (7) can be found when considering their physical background: both models assume the interface to advance in three dimensions. The third clearly three-dimensional equation, Eq. (10), did not, however, yield a poor correlation. The correlation coefficients and obtained reaction rate constants, *k*, are summarized in Table I. The correlation coefficient and reaction rate constant were not considered for Eqs. (11) and (12) because the data exhibited no linear behavior even after processing and resulted in a negative correlation coefficient. The reaction rate constants for the two best models, namely the 1st order nucleation and the Kabai model, were $2 \cdot 10^{-5}\ s^{-1}$.

4. Conclusions

The research on the dissolution of hematite, and of other Fe oxides, has been extensive over the past decades. The aim of this study was to further investigate the dissolution of hematite with oxalic acid by conducting dissolution experiments in 0.6 mol/L oxalic acid at temperatures of 35 and 50 °C.

With a fine solid powder, a stirring speed of 800 rpm was found to be sufficient enough to eliminate the limiting effect of bulk phase mass transfer which ultimately could lead to the formation of a stagnant product layer. The choice of the stirring speed should, however, always be made based on the settling properties of the solid as well as on the dissolution kinetics. Settling, in this case, was not a major issue, but can become significant in processes where the particle size is larger and the particle size distribution is asymmetrical and irregular.

According to the experiments conducted here, increasing the temperature from 35 to 50 °C had no effect on the equilibrium concentration of Fe when dissolving hematite. Based on the thermodynamic studies, kinetics were, however, affected by the change in temperature. To reach the same concentration of dissolved Fe, the necessary dissolution time was increased with a factor of 2–3 when decreasing the temperature from 50 to 35 °C.

A decrease in pH was observed in the kinetic experiment. However, the behavior of the pH was not as straightforward when conducting thermodynamic experiments. A decrease was observed, similar to the kinetic experiment, but was followed by a steady increase of pH. The increase in pH could indicate the consumption of hydrogen ions in the dissolution process. The initial decrease of the pH lasted roughly 42 and 23 h at temperatures of 35 and 50 °C, respectively. The authors suggest that a change in the dissolution process took place when the change in pH behavior was observed. Although the mechanism of hematite dissolution in oxalic acid has been discussed in the Introduction, linking the changes of pH to certain reaction steps seems difficult. Both the adsorption of ligands and reductive dissolution consume protons which could explain the increase in pH but the decrease of pH was left unexplained. The decrease was continuous

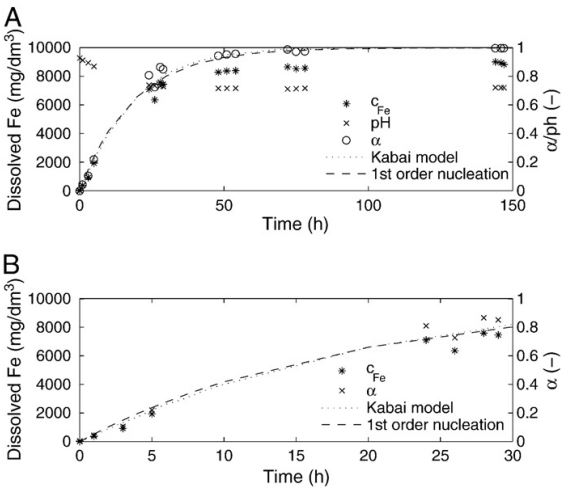

Fig. 4. Concentration and mass of dissolved Fe, pH, and extent of reaction (A) of the whole kinetic dissolution experiment and (B) of the first 30 h of dissolution. Hematite was dissolved in 0.6 mol/L oxalic acid at 50 °C. The stirring speed was 800 rpm.

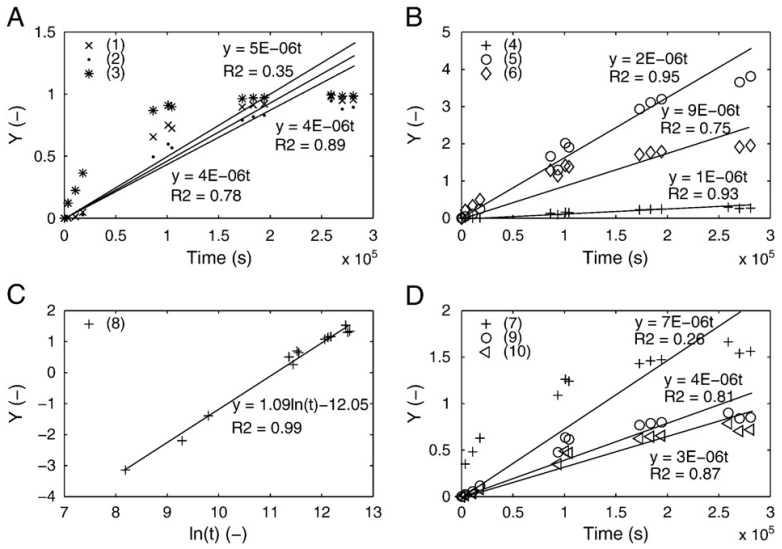

Fig. 5. Fitting of Eqs. (1)–(10) to the experimental data. Correlation coefficients (R^2) were used to evaluate the suitability of the models. Y represents the left hand side of Eqs. (1)–(10). Eqs. (11) and (12) were omitted due to negative correlation between the data and the model.

in the kinetic experiments where both the induction and the autocatalytic periods of reductive dissolution were observed making it unlikely for the change in pH behavior to indicate the shift between the two periods. If the observation indicated a change from one dissolution mechanism to another, e.g. from reductive dissolution to non-reductive dissolution, a more drastic change in the shape of the dissolution curve could be expected. Here, the shape of the dissolution curve was not disturbed despite the change in pH behavior.

In comparing the kinetic models, the best fit was obtained with the Kabai equation. The suitability of the Kabai equation in describing the dissolution process and the identified sigmoidal behavior of the t–α curve further support the suggestion that the dissolution indeed proceeds through solid-state reduction of Fe(III), as both of these characteristics of dissolution can be related to autocatalytic reactions. In addition to the Kabai equation, good results were observed with the 1st order nucleation equation and the diffusion-controlled shrinking core model. Both the Kabai equation and the 1st order nucleation describe surface reactions and thus differ from the diffusion-controlled shrinking core model in their physical background. Based on this study, the reaction rate coefficient appears to be $2 \cdot 10^{-5}\ s^{-1}$. In this study, the cube root law was not able to explain the complete dissolution of hematite. Acquisition of thermodynamic data on the dissolution of hematite is laborious due to the long reaction time needed to reach equilibrium. However, this study goes to show that further research and discussion on the mechanisms of Fe oxide dissolution is still needed.

Table 1
Correlation coefficients (R^2) and reaction rate constants (k) for Eqs. (1)–(10).

Equation no.	R^2, –	k, s^{-1}
1	0.79	$4 \cdot 10^{-6}$
2	0.89	$4 \cdot 10^{-6}$
3	0.35	$5 \cdot 10^{-6}$
4	0.93	$1 \cdot 10^{-6}$
5	0.95	$2 \cdot 10^{-5}$
6	0.75	$9 \cdot 10^{-6}$
7	0.26	$7 \cdot 10^{-6}$
8	0.99	$2 \cdot 10^{-5}$
9	0.80	$4 \cdot 10^{-6}$
10	0.87	$3 \cdot 10^{-6}$

a = 1.09 for Eq. (8).

Acknowledgments

The Graduate School in Chemical Engineering and Outotec (Filters) Oy are kindly acknowledged for their financial support. The authors also wish to thank Mr. Mikko Huhtanen for proof reading and valuable comments.

References

Brown, W.E., Dollimore, D., Galwey, A.K., 1980. Reactions in the solid state. In: Bamford, C.H., Tipper, C.F.H. (Eds.), Comprehensive Chemical Kinetics. Elsevier, Amsterdam, pp. 41–109.
Cornell, R.M., Schindler, P.W., 1987. Photochemical dissolution of goethite in acid/oxalate solution. Clays Clay Miner. 35, 347–352.
Cornell, R.M., Schwertmann, U., 2003. The Iron Oxides. Wiley-VCH GmbH & Co, Weinheim.
Lee, S.O., Tran, T., Park, Y.Y., Kim, S.J., Kim, M.J., 2006. Study on the kinetics of iron oxide leaching by oxalic acid. Int. J. Miner. Process. 80, 144–152.
Lee, S.O., Tran, T., Jung, B.H., Kim, S.J., Kim, M.J., 2007. Dissolution of iron oxide using oxalic acid. Hydrometallurgy 87, 91–99.
Mandal, S.K., Banerjee, P.C., 2004. Iron leaching from China clay with oxalic acid: effect of different physico-chemical parameters. Int. J. Miner. Process. 74, 263–270.
Panias, D., Taxiarchou, M., Paspaliaris, I., Kontopoulos, A., 1996. Mechanisms of dissolution of iron oxides in aqueous oxalic acid solutions. Hydrometallurgy 42, 257–265.
Salmimies, R., Mannila, M., Häkkinen, A., Kallas, J., 2011. Acidic dissolution of magnetite: experimental study on the effects of acid concentration and temperature. Clays Clay Miner. 59, 136–146.
Sidhu, P.S., Gilkes, R.J., Cornell, R.M., Posner, A.M., Quirk, J.P., 1981. Dissolution of iron oxides and oxyhydroxides in hydrochloric and perchloric acids. Clays Clay Miner. 29, 269–276.
Tatterson, G., 1994. Scaleup and Design of Industrial Mixing Processes. McGraw-Hill, Inc., New York.
Taxiarchou, M., Panias, D., Douni, I., Paspaliaris, I., Kontopoulos, A., 1997. Dissolution of hematite in acidic oxalate solutions. Hydrometallurgy 44, 287–299.
Wells, M.A., Gilkes, R.J., Fitzpatrick, R.W., 2001. Properties and acid dissolution of metal-substituted hematites. Clays Clay Miner. 49, 60–72.

Article III

Salmimies, R., Kallas, J., Ekberg, B., Häkkinen, A.*, 2012. Scale growth in the dewatering of iron ore, *International Journal of Mining Engineering and Mineral Processing*, 1, 69 – 72.

Article IV

Salmimies, R., Kallas, J., Ekberg, B., Andreassen, J.-P., Häkkinen, A.,* 2012. Long-term fouling of ceramic filter media used in the dewatering of hematite, *Filtration*, 14, 219 – 222.

FILTRATION

ISSN 1479-0602

the international journal for filtration and separation



The FILTRATION Society

AFS

FILTRATION is the official journal of The Filtration Society and the American Filtration & Separations Society

Volume 12 Number 4

www.filtrationsolutions.co.uk

BACKGROUND

Clean air has been an issue for centuries. In the year 1306 King Edward of England made a proclamation banning the burning of coal, due to the heavy smoke it caused. One of the first examples of air pollution caused by coal burning comes from King Edward's mother (Queen Eleanor). She became so sick from coal fumes that she had to flee from Nottingham Castle. King Edward subsequently imposed a death penalty for burning coal in England. In the USA the first attempt to take control of air pollution was done in Chicago and Cincinnati. In 1881 these cities enacted clean air legalization.

The World Health Organization (WHO) has published a number of guidelines regarding air quality, the latest version is from 2005 and deals with particulate matter (PM), ozone, nitrogen dioxide and sulphur dioxide. PM is measured for different particle sizes where the result is the dust concentration (in μg/m^3). PM is defined for

LONG TERM FOULING OF CERAMIC FILTER MEDIA IN THE DEWATERING OF HEMATITE CONCENTRATE

Riina Salmimies[1] (riina.salmimies@lut.fi), Antti Häkkinen[1], Bjarne Ekberg[2], Juha Kallas[3] and Jens-Petter Andreassen[4]

[1]*LUT Chemistry, Lappeenranta Univ. of Technol., P.O. Box 20, FI-53851 Lappeenranta, Finland.*
[2]*Outotec (Filters) Oy, Urusvuorenkatu 5, FI-20630 Turku, Finland.*
[3]*Laboratory of Inorganic Materials, Tallinn Univ. of Technol., Ehitajate tee 5, EE-19086 Tallinn, Estonia.*
[4]*Dept. Chem. Eng., Norwegian Univ. of Science and Technol., NO-7491 Trondheim, Norway.*

The long-term blinding of a filter medium can affect the performance and lifetime of the medium, but can rarely be observed or quantified in the laboratory. Pilot scale experiments can offer additional information for the design of the washing of the filter medium, however they still don't provide enough time in operation to evaluate the effects of hundreds of dewatering cycles. The long term fouling effects of a ceramic filter medium were investigated in this study by characterising samples taken from an industrial hematite dewatering process. Chemical characterisation was done using X-ray diffraction (XRD) after which scanning electron microscopy (SEM) was employed to identify the shape and size of the foulants on the surface of the filter medium. The study showed that the ceramic filter medium used in the dewatering of hematite concentrate was primarily affected by slurry particle blockage, and to a lesser extent by precipitate formation, after operation at the plant scale. Whether the sample was taken from the centre or from the edges of the filter element did not to play a role in determining the nature or the extent of blinding.

INTRODUCTION

Ceramic capillary action filters are favoured in high-tonnage applications where low and even cake moisture is desired. The use of these filters provides energy efficiency, and has the advantage of being a regenerable filter medium. Whereas traditional cloth filter media must be replaced at regular intervals due to blocking and breakage, ceramic filter media are rigid enough to withstand physical and chemical regeneration. The use of ceramic capillary action filters in the dewatering of ore concentrates is a fairly novel technology and there is much room for scientific research, both regarding the actual filtration stage as well as dewatering and regeneration of the filter medium. The challenges with investigating blinding of the filter medium lie in the fact that the effects are rarely seen at the laboratory scale with short operating periods. Pilot scale experimentation can offer additional information on the efficiency of the regeneration techniques[1], but blinding by crystallisation of solutes can go undetected even at the pilot scale.

Complete blocking and bridging between particles have been described as the mechanisms enabling cake filtration[2]. In addition, crystallisation of solutes during the cake drying process has been suggested to induce additional adhesion between the solids and filter medium[3]. The same mechanisms can, however, also become those blinding the filter medium in long term operation. Nevertheless, long term effects, especially those related to filter media blinding, can rarely be seen at the laboratory scale[4]. A study of the effects of filter cloth blinding on the cake filtration of aluminium hydroxide (0.6 vol %, d_{50} = 13 μm) has shown that deposition of particles occurred both onto the surface of the filter medium as well as into the cloth at weave intersections and between the individual fibres of multifilament yarn[5]. Seven fabric weaves (plain, twilled and satin), both non-calendered and calendered, made of polypropylene, were investigated.

Research concerning the dewatering of a magnetite concentrate suggested that, in addition to blocking by slurry particles, the filter medium is affected by heavy calcium scaling[6]. This scaling was observed more strongly at the edges of the large filter element. Preliminary results on the removal of the calcium scale with acids have also been reported[7]. Dissolution of the scale was best achieved with the use of 2 M nitric acid, although hydrochloric and sulphuric acid also performed well. The liquid permeability of the filter medium could be increased by approximately 2000 L/(m^2 h bar) in a 2 h washing.

In this paper, where particle blockage is discussed, the term refers to particle adhesion onto the surface of the filter medium. The term does not include particle penetration into the structure of the medium as this is seen as unlikely, based on the particle size of the slurry solids and on the pore size of the filter medium.

METHODS

Samples of ceramic filter media used in the dewatering of a hematite concentrate were obtained from an industrial partner. During operation, the filter medium was periodically treated by backwash to remove any particle blockage. When necessary, ultrasound assisted acid cleaning was employed to reverse the effects of iron oxide scaling. Four full sized elements, manufactured by an American supplier, were investigated. In addition, pieces of a fifth element, by a Chinese supplier, were investigated. The studied elements were all used at the same site. The dimensions of the elements were 48.5 x 31.5 x 3.0 cm. Circular samples, with a diameter of 46 mm, were extracted from the corners and from the centre of each filter element using a diamond drill. After drilling, the samples were dried at 50ºC for three days. A total of 11 samples were characterised.

XRD, using a Bruker D8 Advance diffractometer (Karlsruhe, Germany), was employed to characterize the chemical compounds present on the surface of the filter media. The X-ray data were collected with CuKα radiation from between 10 and 90°2Θ at a step length of 0.02°2Θ. SEM, using a Hitachi S-3400N VP-SEM (Delaware, USA), provided additional information on the degree of surface coverage and of the particle size and shape of the different chemical components. The microscope was operated in backscatter mode at low vacuum with a 15 kV voltage. Operating in a low vacuum allowed the samples to be analysed without additional coating.

RESULTS AND DISCUSSION

Qualitative characterisation of the chemical composition of the ceramic samples was done by XRD. Data for a sample taken from the centre and from the corner of a large filter element are shown in Figure 1.

As can be seen from the diffraction data, two major components could be identified in the samples: (1) alumina, Al_2O_3, from the filter media, and (2) hematite, Fe_2O_3, originating from the filtered slurry. In addition to these primary components, the diffraction data also showed minor traces of calcium scaling in all the samples. The high intensity of the alumina peaks was due to the large support structure of the membrane which is assumed to show in the spectral data. Consequently, quantification of the chemical components from the data presented here is questionable. A small difference between the elements of the two manufacturers was observed during the acquisition of the XRD data: a more significant increase in the background was found with the Chinese element. An increasing background is often caused by iron compounds which exhibit fluorescence in X-ray analysis. Consequently, the higher increase in the analysis of the Chinese element could indicate more iron being present in those samples.

The effects of the different chemical species on the filter media, as well as blocking mechanisms, are difficult to determine with compositional data alone. As a result, SEM was used to identify the particulate mechanisms by which the different components were attached onto the surface of the filter medium. SEM images are shown in Figure 2. Figures 2a and 2c demonstrate the significance of particle adhesion. Figures 2b and 2d show how the particles are lodged onto the surface of the medium. The samples had undergone mechanical treatment, i.e. drilling and drying during sample preparation, indicating that the particles indeed sat tightly on the surface. The particle size of the adhered particles varied from approximately 1 to 40 µm.

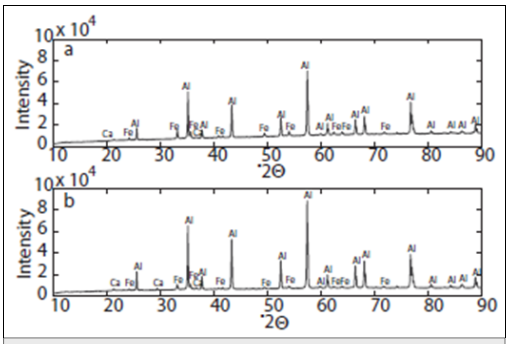

Figure 1: XRD data for ceramic filter media used in the dewatering of iron ore. Data were collected with samples (a) from the centre and (b) from corners of the filter elements. Al is for alumina, Fe for hematite, and Ca for calcium scale.

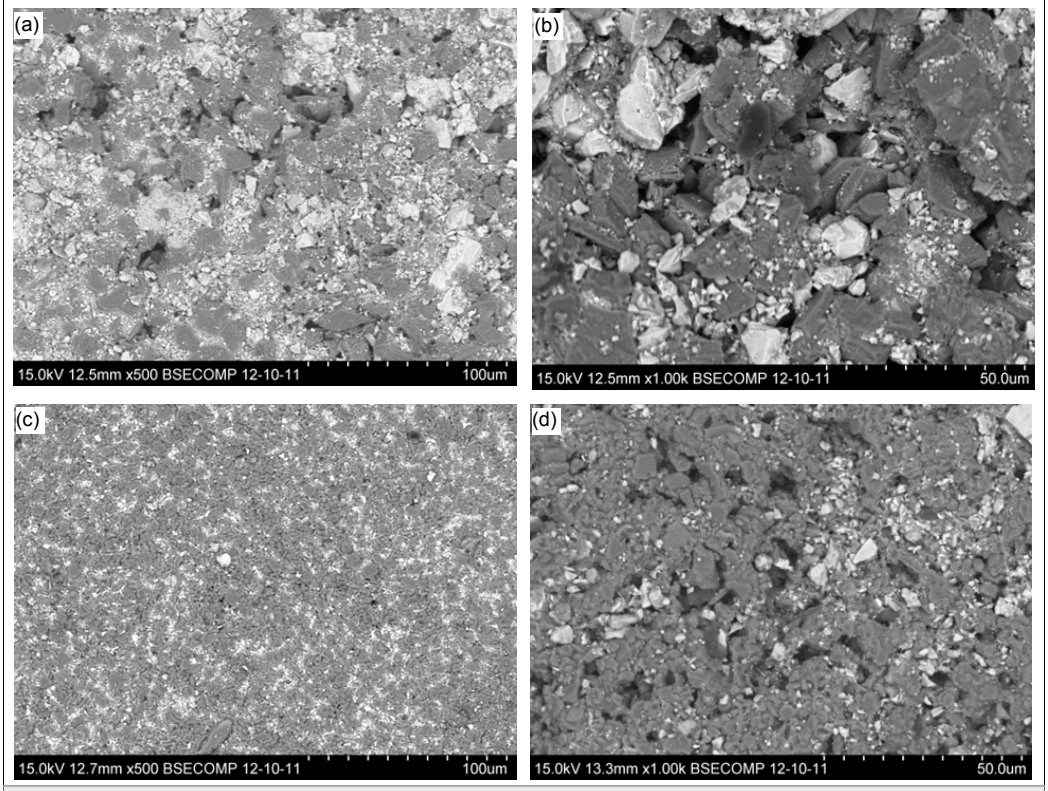

Figure 2: Scanning electron microscope images of (a), (b) the ceramic filter element manufactured in China, and (c), (d) the ceramic filter element manufactured in the United States. The light coloured particles represent hematite and the dark represent alumina.

The filter media were relatively uniformly affected by the adhesion of slurry particles. The centre was affected to the same extent by particle adhesion as the corners. Whereas differences between different locations on a large filter element have been previously observed in magnetite dewatering, no significant differences were observed in the current study. This observation can simply be explained by the lack of heavy calcium scaling in the hematite dewatering process. The surface of the filter medium had not been blinded by extraneous scaling, and thus the whole surface was available for the filtration of concentrate during operation. Consequently, particle adhesion is visible throughout the large element.

Although calcium compounds were shown in several samples in the XRD analysis, precipitate was difficult to locate in the SEM images. Some images of the scale were, however, obtained; one of these images is shown in Figure 3. The scale exhibited an undefined particle shape and size. Characteristics of the precipitate, for further discussion, were, however, difficult to identify with the SEM. The limited observations of the calcium scale did not seem to have any dependence on the location of the sample on the large filter element, i.e. the scale was equally likely to form in the centre of the element as in the corners. SEM images from the two manufacturers' filter elements were compared and the only difference observed was the more amorphous-like nature of the Chinese alumina. More defined alumina particles were observed in the SEM images for the American filter elements. The difference in the two elements might be explained by differences in the casting process of the ceramic elements.

CONCLUSIONS

Particle blockage of the surface, resulting from adhesion of slurry particles onto the surface of the filter media, appeared to act as the primary mechanism leading to deterioration in performance of the ceramic filter medium during dewatering of a hematite concentrate. Interestingly, almost no calcium scaling was observed

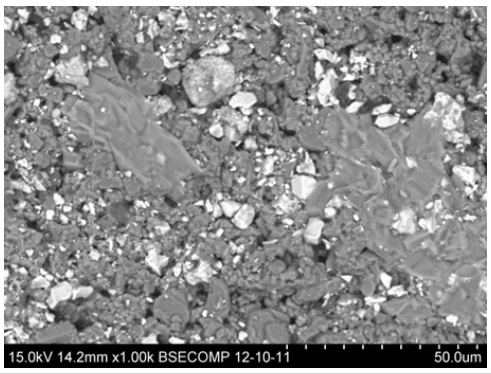

Figure 3: Scanning electron microscope image of scale precipitated onto the surface of the ceramic filter medium in the dewatering of hematite. The light coloured particles represent hematite and the dark represent alumina.

in the samples obtained from a hematite dewatering process. In earlier studies of magnetite dewatering, calcium scaling was found to be even more significant than particle blockage. The observed difference could be due to a number of reasons such as differences in process chemistry or conditions, or varying quality of process water used at different locations.

No significant difference in chemical composition between Chinese and American ceramic filter elements was observed with XRD measurements. Based on the SEM images, the most significant difference between the Chinese and American ceramic material seemed to be the degree of structure of the alumina. Whereas the American element had more well defined, smaller alumina particles covering the surface, the Chinese element seemed to exhibit a less defined alumina phase with particles attached to each other. This observation must, however, be treated with caution as only pieces of a single Chinese filter element were available for study, and more research is needed to verify the findings and discuss the implications of different alumina structures. In theory, larger alumina particles could result in larger pores in the filter medium. Increased pore size, in turn, could mean higher vacuum losses and increased liquid permeability. Furthermore, larger pores could result in increased probability of particles penetrating the structure of the filter medium.

The availability of samples from hematite processes was a major factor limiting a more extensive study of the long term effects. The results of this study, however, contribute to the understanding of filter media lifetime by demonstrating that particle blockage accounts for the majority of long-term deterioration in performance of ceramic filter media during the dewatering of a hematite concentrate.

Both particle adhesion, onto the surface of the filter medium, and process related scaling are effects which are very difficult to determine at the laboratory scale. Investigations of the deterioration in performance of the filter medium in long-term operation must be done in co-operation with process owners to obtain valid data. Research efforts can then be targeted at optimizing the process conditions, thereby increasing the performance of the filter medium. Future developments could include permeability measurements and washing experiments to further quantify the effect of observed phenomena on the performance of the filter medium. Any decrease in permeability, in this case, would most likely be explained by particle adhesion rather than scale formation, as in the case for magnetite dewatering.

ACKNOWLEDGEMENTS

The authors would like to acknowledge The Graduate School in Chemical Engineering and Outotec (Filters) Oy for funding this research, and Dr Julian Tolchard from the Norwegian University of Science and Technology for his valuable assistance with the analytical work.

REFERENCES

1. Puranen J., Häkkinen A., Kallas J. and Ekberg B., 2008. Comparison of regeneration methods for ceramic filter media, *Proc. 10th World Filtration Congress*, pp.165-169, Leipzig, Germany, 14-18 April.
2. Wakeman R.J., 2007. The influence of particle properties on filtration, *Separation and Purification Technology*, **58**, 234-241.
3. Rushton A., Ward A. and Holdich R.G., 2000. *Solid -Liquid Filtration and Separation Technology*, 2nd Edn., pp.151-153, Wiley-VCH, New Jersey.
4. Thompson W., 1993. Continuous vacuum filtration: Small scale tests versus full scale performance, *Filtration & Separation*, **30**, 735-738.
5. Weigert T. and Ripperger S., 1997. Effect of filter fabric blinding on cake filtration, *Filtration & Separation*, **34**, 507-510.
6. Salmimies R., Häkkinen A., Kallas J., Ekberg B., Andreassen J.-P. and Beck R., 2011. Characterisation of long-term scaling effects of ceramic filter media used in the dewatering of iron ore, *Proc. Iron Ore 2011*, pp.521-527, Perth, Australia, 11-13 July.
7. Salmimies R., Häkkinen A., Ekberg B., Kallas J., Andreassen J.-P. and Beck R., 2011. Removal of calcium scales from the surface of a ceramic filter medium, *Proc. Filtech 2011*, Wiesbaden, Germany, 22-24 March.

Article V

Salmimies, R., Häkkinen, A., Kallas, J., Ekberg, B., Andreassen, J.-P., and Beck, R.,* Characterisation of long-term scaling effects of ceramic filter media used in the dewatering of a magnetite concentrate, *International Journal of Mineral Processing* (Accepted for publication)

International Journal of Mineral Processing (Accepted for publication)

The scaling and regeneration of the ceramic filter medium used in the dewatering of a magnetite concentrate

Riina Salmimies[*1], Juha Kallas[2], Bjarne Ekberg[3], Guido Görres[4], Jens-Petter Andreassen[5], Ralf Beck[5], Antti Häkkinen[1]

[1] LUT Chemistry, Lappeenranta University of Technology, P.O. Box 20, FI-53851 Lappeenranta, Finland

[2] Laboratory of Inorganic Materials, Tallinn University of Technology, Ehitajate Tee 5 EE-19086, Estonia

[3] Outotec (Filters) Oy, Urusvuorenkatu 5 FI-20630 Turku, Finland

[4] Outotec Pty Ltd, 40 Kings Park Road, AU-6005, Perth, Australia

[5] Department of Chemical Engineering, Norwegian University of Science and Technology, Sem Sælandsvei 4 NO-7491 Trondheim, Norway

[*] Corresponding author: email riina.salmimies@lut.fi, mob +358 40 19 77 795, fax +358 5 621 2199

International Journal of Mineral Processing (Accepted for publication)

Abstract

The dewatering of iron ore is a high tonnage application in general requiring high energy input. Choosing a ceramic capillary action disc filter can offer decreased specific energy consumption in addition to a fully regenerable filter medium. The aim of this study was to obtain new information on the fouling of the filter medium in an iron ore process to enhance and develop the regeneration process of the medium in the future. X-ray diffraction and scanning electron microscopy were used to characterise the chemical composition and the morphology of the different chemical components, respectively, of the filter media used in the dewatering of magnetite. Two types of media blockages were found to play an important role in an acidic iron ore dewatering process: fouling by slurry particles and by in-situ crystallisation of calcium oxalate, of which the latter originated from the combination of process water and process chemistry. The scale was dissolved with hydrochloric, nitric, and sulphuric acids, and with potassium hydroxide. The best results, i.e. highest quantity of dissolved calcium and increase in permeability of the filter medium, were achieved with 2 mol/L nitric acid.

1 Introduction

Ceramic membranes are commonly associated with crossflow membrane filtration but they have found their purpose in dead-end cake filtration, too. Ceramic capillary action disc filters provide energy efficiency through the use of an air impermeable ($p < 1.0$ bar) alumina membrane. Whereas conventional filter cloths would have to be replaced once irreversibly blinded by the slurry particles or possibly damaged in operation, the ceramic filter media is both chemically and mechanically stable enough to withstand regeneration. Common regeneration methods include ultrasonic treatment, backwashing, and chemical cleaning (Görres and Hindström, 2007). Puranen et al. (2008) have previously shown that the combination of the previously mentioned regeneration methods results in the restoration of the permeability of the filter medium. The authors did not report any scale growth during their pilot scale experiments.

In the dewatering of iron ore the decrease in the filtration capacity is not only due to the particle blockage but also due to the growth of unwanted scales onto the surface of the medium. Rushton et al. (2000) have described the mechanisms of particle adhesion and recrystallisation of solutes as major factors in causing the bonding between the filter medium and the filtered material. The theory, however, considers mainly the mechanisms of the formation of a filter cake, and is not focused on what the mechanisms of filter media blinding are. Hermia (1982) has described four blocking mechanisms, which essentially are filtration mechanisms, but those consider only particle blockage. Lu et al. (1997) have studied the blocking of woven filter cloths with a simulation model, but the aim in their case was to describe the time necessary to reach a state in filtration where no particle bleeding into the filtrate could be observed. The bridging of particles over the pores of the media was, therefore considered as a positive phenomenon. Blocking of membrane pores has also been intensively studied during the last few decades. Among others is the study of Liu and Kim (2007) who set out to compare constant flow rate blocking laws and artificial neural network models. Although the comparison between conventional models and neural networks is interesting and provides relevant information about membrane filtration, the flow conditions and composition of the feed are significantly different when performing dead-end filtration with an iron ore concentrate. Long term effects, especially those related to filter media blockage can rarely be seen in laboratory scale (Thompson, 1993), thus requiring the study of actual processes during long operating periods. No studies, however, were found on the long-term effects of media blockage in iron ore dewatering processes.

Complicated chemistry of industrial processes commonly gives rise to unanticipated precipitation of different chemical compounds. Managing the process chemistry of an ore concentrator can be especially challenging due to impurities in the ore itself and in the process water in addition to the actual chemicals used in the upgrading process. The accumulation of alkali and alkaline earth metals, e.g. calcium, in process water cycles has been shown to cause unwanted precipitation and scaling in process equipment. Calcium oxalate scales, amongst other precipitates, have been shown to form e.g. when water cycles are closed in the pulp and paper industry (Ulmgren, 1997; Ulmgren and

Rådeström, 1997) and in evaporators in the food industry (Doherty, 2006; Yu *et al.*, 2003). Water quality, however, is not the only possible source of metals but ores also commonly have soluble metal components. The dissolution and accumulation of those ore components is, however, quite difficult to study as raw materials have varying composition, processes have unique features, and determining the effects of accumulation would require the study of the whole process chain.

As scaling has previously not been observed in pilot scale experiments with magnetite, the aim of this study was to investigate the effects of longer operating periods, i.e. full scale operation, on the blinding of the ceramic filter medium used in the dewatering of a magnetite concentrate. Samples of ceramic filter elements from an operating plant site were investigated by collecting characterisation data with X-ray diffraction (XRD) and scanning electron microscope coupled with energy dispersive spectrometer (SEM-EDS). The samples were then washed with different acids to establish their regeneration efficiency towards the identified calcium deposit.

2 Methods

2.1 Samples

Ceramic filter elements were acquired from an industrial partner after being used for three to five years in the dewatering process of a magnetite concentrate.

The particle size distribution of the concentrate (Fig. 1) was determined with laser diffraction using a Beckmann Coulter LS13320 particle size analyser. The Mie theory was used to create a separate optical model for the magnetite particles. The real part of the refractive index was 2.42 (Beckman Coulter, 2003). The imaginary refractive index for magnetite could not be obtained from literature. The refractive index of hematite, another iron oxide, was, however, available and was used setting the imaginary part as 0.01 (Beckman Coulter, 2003). XRD analysis of the solid showed magnetite as the only mineralogical phase. Minor impurities ($c < 1.5$ wt%) of calcium (Ca), magnesium (Mg), silicon (Si), and aluminium (Al) were identified with SEM-EDS using a JEOL JSM-5800 microscope.

During the operation time of 3 – 5 years, the filter medium was periodically treated with backwash to remove any particle blockage. In addition, acid cleaning with a combination of nitric (1 wt%) and oxalic acid (4 wt%), assisted with ultrasound, was periodically employed to reverse any effects of iron oxide scaling. Initial permeability of such filter elements is roughly 5500 L/(m^2 h bar). Two-sided filter elements in the size of 48.5 x 31.5 x 2.4 cm with a filtration area of 0.25 m^2 were drilled to yield 45 cylindrical laboratory samples with a diameter of 46 mm. Samples for analysis were chosen from the upper left and right corners, from the lower left and right corners and from the centre of the element (Fig. 2). Altogether, 7 different elements yielding 33 individual samples were characterised. Details of the samples and a CFD model for the full scale filter element can be found elsewhere (Salmimies *et al.*, 2011).

2.2 Identification of blinding components

The filter media was characterised by using XRD and SEM-EDS. A Bruker D8 Advance diffractometer was used for the XRD analysis to study the chemical composition of the samples, after which a Hitachi S3400 VP-SEM was employed to characterise the particles and scales on the surface of the filter medium. The XRD data were collected from 10 to 90°2θ with a step size of 0.016°2θ. Operating the SEM at a low vacuum with the backscatter detector with an acceleration voltage of 15 kV enabled the analysis of the samples without any coating.

2.3 Dissolution experiments

The dissolution of the found scale was done in 1 L solutions using hydrochloric (HCl), nitric (HNO_3), and sulphuric (H_2SO_4) acids. The concentrations of HCl and HNO_3 were 0.5, 1.0, and 2.0 M and the concentrations of H_2SO_4 were 0.25, 0.5, and 1.0 M. The selection of the concentration of the acids

was based on their hydrogen ion concentration, thus making the concentration of H_2SO_4 half of the concentration of HCl and HNO_3. In addition, dissolution of the scale was done with potassium hydroxide (KOH) in concentrations of 0.5, 1.0, and 2.0 M to yield a reference for alkali dissolution in this particular case. The concentrations for KOH were based on the hydroxide ion concentration. All chemicals were pro analysis grade and provided by Merck, and solutions were prepared using ultrapure water generated by reverse osmosis.

All experiments were conducted at 20 °C. The dissolution was monitored by measuring the concentration of dissolved calcium in the liquid phase, using inductively coupled plasma optical emission spectroscopy (ICP-OES) with a Thermo Electron IRIS Intrepid II XDL spectrometer, and the water flux through the filter medium samples. Samples were drawn and flux measurements were done at time 0 min, 60 min, and 120 min. The water flux was measured using ultrapure water with 1 bar pressure over 200 s at 1 s intervals. The data was then averaged to yield the value for flux. The dissolution experiments were continued for 120 min. In addition, experiments with 2 M HCl and HNO_3 were continued until reaching 360 min dissolution time.

3 Results

3.1 Blinding of the filter medium

Two types of samples were identified with XRD: (1) samples consisting only of the filter medium and magnetite (Fig. 3a), and (2) samples with only the calcium scale (Fig. 3b). Of the 33 samples analysed 21 contained calcium oxalate. In addition, other calcium compounds, e.g. calcium sulphate and calcium carbonate, were found in five samples. The presence of the calcium scale was mostly observed in the samples taken from the corners of the full scale filter elements. Samples drawn from the centre exhibited more aluminium oxide and magnetite and only randomly the calcium scale. More detailed statistical analysis of the characterisation data has been presented by Salmimies *et al.* (2011).

The oxalate is not inherent to the concentration process of magnetite nor does it originate from the filter material. Most likely the unanticipated precipitation is caused when the oxalic acid, used for the regeneration of the filter medium, encounters calcium rich liquid, e.g. low quality process water. Further determination of the morphology and extent of surface coverage of different chemical components was taken on with the SEM.

Particle adhesion was found to blind the filter medium to a relatively low extent (Fig. 4a) in comparison to the scaling observed in the studied samples. The magnetite particles were mainly resting on the surface of the filter medium and partially lodged into the pores. Smaller particles seemed to be adhered onto larger ones. As also indicated by the XRD analysis, the surface of the filter medium was still exposed at sites where magnetite particles were also found (Fig. 4b).

Contrary to the magnetite particles, the calcium scale seemed to cover the whole surface of the samples where it was found (Fig. 4c). Signs that the scale had actually grown onto the surface were seen in the SEM images. Pitting of the scale layer was observed randomly, and, based on previous studies with ceramic membranes (Chen *et al.*, 2006a; Chen *et al.*, 2006b). Holes punctured by the ultrasound were especially interesting, as in those the actual growth of the scale was more obvious. Although some indication of crystal shape could be seen in the SEM images, absolute certainty of the platy shape could not be gained due to overlapping growth of the crystals (Fig. 4d).

3.2 Dissolution of the calcium oxalate scale

The water permeability of all scaled samples was essentially zero indicating that the scale had blinded the surface of the samples completely. The dissolution of the scale seemed most successful with HNO_3 and HCl. Highest quantities of dissolved Ca within 120 min of dissolution, roughly 300 mg/L, were achieved with 2 M HNO_3 and 2 M HCl (Fig. 5). Increasing the acid concentration obviously increased the quantity of dissolved Ca. Increasing the time for dissolution resulted in increase in the concentration of dissolved Ca, especially significant for 2 M HNO_3.

The quantity of dissolved calcium demonstrated the effect of different dissolving agents in decomposing the calcium scale, but the differences in process performance between individual samples could only be observed by determining the changes in the water flux through the filter medium after the scale was dissolved. The largest increases in the water flux were observed with 1 M HCl and 2 M HNO_3 (Fig. 6) after dissolving the scale for 120 min. Here an inconsistency was observed with increasing concentration of HCl: a lower concentration resulted in higher increase in the water flux.

Explicit conclusion on whether HNO_3 or HCl would be better cannot be made because the thickness of the scale most likely varied from sample to another. Consequently, better results for experiments where the dissolved layer was thinner may have been observed. Values for change in permeability against However, the concentration of dissolved Ca can be regarded as an indicator on the effectiveness of the different acids. Good dissolving agents, in general, dissolve the scale faster. The concentration of dissolved Ca cannot, however, be used as an indicator of the regeneration efficiency because there the thickness of the scale layer, again, becomes a parameter. The dissolution of the scale was visually observed as a colour change as well as the disappearance of the extraneous layer of deposit on the samples (Fig. 7). As discussed previously, both HNO_3 and HCl did perform well in dissolving the scale.

Potassium hydroxide yielded no significant improvement in the flux and only a few mg/L of calcium were dissolved using the alkali, meaning that higher concentrations of alkali should be used to dissolve the scale. Whereas acids are also more effective in dissolving iron oxides in comparison to alkalis, deciding on an alkali would most likely not produce desired results in the regeneration of the ceramic filter medium used in iron ore dewatering. In addition, high alkali concentrations can result in health, safety, and environmental problems and put strain on equipment material. These risks would also apply with increasing acid concentration, but according to the results here, acids in the range of 0.5 – 2.0 M worked relatively well in dissolving the scale and further increase of the acid concentration might not necessarily be needed. The dissolution of the scale in alkali, on the other hand, seemed minor and significant increase of the alkali concentration to dissolve the scale is likely to be needed.

When considering the total solution volume and the filtration area of the laboratory samples, 150 $L_{solution}/m^2$ was used to dissolve the scale here. This value should, however, not be used for scale up as these laboratory experiments here were nott designed for that purpose. Smaller solution volumes could very well be used, and here the selection of the solution volume was partially restricted by practical aspects, i.e. how to ensure that the whole sample was treated with the solution.

The samples were qualitative characterized to ensure similarity of the samples, and to eliminate any uncertainties originating from different chemical composition of the samples. However, inherent differences in the initial water flux, resulting from the manufacturing process of the ceramic elements, and in the chemical structure of the filter samples are still the most likely causes for any discrepancies in the data presented here. In addition, varying times in operation and even fluctuations in process conditions could have resulted in differences in the samples and in the nature of the precipitated scale. Despite their similar chemical composition, the thickness of the scale layer most likely varied and could not be estimated based on the characterisation data. The thicker the layer, the longer time is needed to dissolve the layer and observe increase in permeability.

4 Conclusions

Ceramic filter media used in the dewatering of iron ore over operating periods of 3-5 years were characterised using XRD and SEM. X-ray analysis revealed the main chemical components in the samples to be aluminium oxide, i.e. the filter material, magnetite originating from the filtered slurry, and a calcium oxalate scale. Whereas the surface coverage of slurry particles was less extensive, the scale, in turn, seemed to blind the whole surface of the filter medium. The identified calcium scale was subsequently removed from the surface of the filter medium with acids to restore the permeability of the medium.

The decline of long term performance of the ceramic filter medium was found to be a result of particle adhesion and, to a larger extent, of calcium scaling. As this type of scaling has, to the best knowledge of the authors, not been reported earlier for iron ore applications, the information can prove useful in the future to specialist working in minerals processing. The results of the characterisation need not be merely ore specific as the components of the calcium scale could be found in several other ore concentration processes and in other industries, too. As the results of the characterisation suggested that the full scale filter elements are affected by scaling more on the peripheral area than at the centre, measurements of permeability from the corners rather than the centre could give earlier indication of a developing scaling problem. The filter elements have a distinct flow profile where the centre has the highest flow velocities which then decrease towards the corners. Increased flow velocities mean increased mixing and less stagnant layers where local concentration gradients can form and result in precipitation. Other factors can, however, also have contributed to the formation of the scale and estimating the underlying cause for the scaling, based on the data presented here, is difficult.

According to these results, the accumulated calcium scale can quite effectively be removed with acids. All the studied acids here performed adequately but HNO_3 seemed to be the best choice. In most cases, the higher the concentration of the acid is, the faster the target value for permeability can be achieved. Alkali leaching, with KOH, does not seem a suitable alternative for the removal of the scale. Commonly, HCl is not favoured due to health, safety, and environmental issues and corrosion risk of equipment material. Odours, the risk of producing chlorine gas, and chloride corrosion of steel during use make HCl a less attractive option than the other two acids studied here.

Increasing the time for dissolution from 120 to 360 min resulted in significant changes in flux restoration with both HNO_3 and HCl. From an operational perspective, two options to carry out such regeneration could be considered: (1) a long wash extending to the previously mentioned six hours could result in a permeability increase of 3000 L/(m^2 h bar) of a filter medium of no significant permeability, or (2) a more frequent shorter wash could be employed when the filter medium has not been so severely affected by the scaling to prevent the loss of permeability in long term operation.

The presence of extraneous alkali and alkaline earth metals combined with process chemistry can cause unwanted precipitation of salts. Thus the management of e.g. process water quality is of high importance, especially if the use of fresh water is to be reduced and water cycles closed. In addition, liberation of metals from the ore itself, due to pH changes and use of chemicals in the concentration, can also increase the risk for unexpected precipitation. With effective control of accumulation of ions in process streams, the high performance of the ceramic filter medium could more easily be maintained and the need for any additional chemical regeneration could be avoided. The study and understanding of long term scaling in an industrial filtration process can ultimately lead to significant cost improvements, in addition to an increased degree of material efficiency.

Acknowledgements

The Graduate School in Chemical Engineering is kindly acknowledged for their financial support. In addition, the authors wish to thank Mr Julian Tolchard at the Norwegian University of Science and Technology for his analytical assistance.

References

Beckmann Coulter, 2003. LS 13 320 Laser Diffraction Particle Size Analyzer Instrument Manual (Beckman Coulter, Inc.: Florida).

Chen, D., Weavers, L.K., and Walker, H.W., 2006a. Ultrasonic control of ceramic membrane fouling by particles: effect of ultrasonic factors, Ultrasonics Sonochemistry, 13, 379 – 387.

Chen, D., Weavers, L.K., and Walker, H.W., 2006b. Ultrasonic control ceramic membrane fouling: effect of particle characteristics, Water Research, 40, 840 – 850.

Doherty, W., 2006. Effect of calcium and magnesium ions on calcium oxalate formation in sugar solutions, Industrial and Engineering Chemistry Research, 45, 642 – 647.

Görres, G., Hindström, R., 2007. Some experiences with modern dewatering technologies in fine iron ore application, Proceedings of Iron Ore 2007, Perth, 283 – 287.

Hermia, J., 1982. Constant pressure blocking filtration laws: application to power-law non-newtonian fluids, Trans. IChemE, 60, pp. 183 – 187.

Liu, Q-F., Kim, S-H., 2007. Evaluation of membrane fouling models based on bench-scale experiments: A comparison between constant flowrate blocking laws and artificial neural network (ANNs) model, Journal of Membrane Science, 310, 393 – 401.

Lu, W-M., Tung, K-L, Hwang, K-J., 1997. Effect of woven structure on transient characteristics of cake filtration, Chemical Engineering Science, 52(11), 1743 – 1756.

Puranen, J., Ekberg, B., Häkkinen, A., Kallas, J., 2008. Comparison of regeneration methods for ceramic filter media, Proceedings of the 10th World Filtration Congress, Leipzig, 165 – 169.

Rushton, A., Ward, A., Holdich, R., 2000. Filter media, in Solid-Liquid Filtration and Separation Technology, 131 – 179 (Wiley-VHC Verlag GmbH: Weinheim).

Salmimies, R., Häkkinen, A., Kallas, J., Ekberg, B., Andreassen, J.-P., Beck, R., 2011. Characterisation of long-term scaling effects of ceramic filter media used in the dewatering of iron ore, Proceedings of Iron Ore 2011, Perth, 521 – 527.

Thompson, W., 1993. Continuous vacuum filtration: small scale tests versus full scale performance, Filtration & Separation, 30, 735 – 738.

Ulmgren, P., 1997. Non-process elements in a bleached kraft pulp mill with high degree of system closure – state of the art, Nordic Pulp & Paper Research Journal, 12, 32 – 42.

Ulmgren, P., Rådeström, R., 1997. Calcium oxalate in bleach plant filtrates, Proceedings of the Minimum Effluent Mills Symposium, San Francisco, 51 – 62.

Yu, H., Sheiksholeslami, R., Doherty, W., 2003. Composite fouling of calcium oxalate and amorphous silica in sugar solutions, Industrial and Engineering Chemistry Research, 42, 904 – 910.

Tables and figures

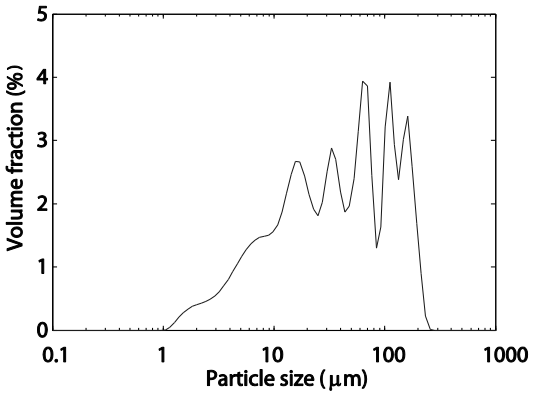

Fig. 1. Particle size distribution of the magnetite concentrate.

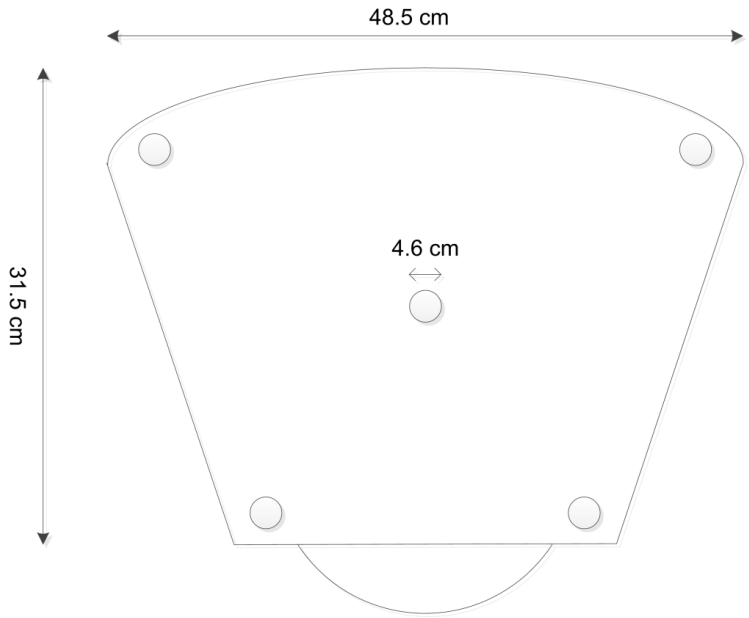

Fig. 2. Schematic of the full scale filter element and the locations from which samples where drawn.

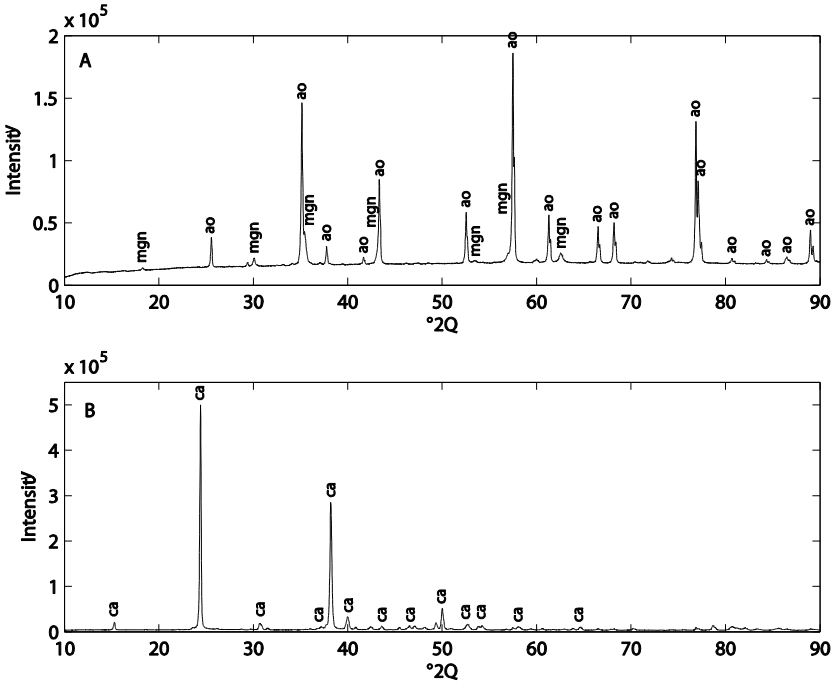

Fig. 3. (a) Spectral data of a sample containing aluminium oxide (ao) and magnetite (mgn), and (b) of a sample containing the calcium scale (ca).

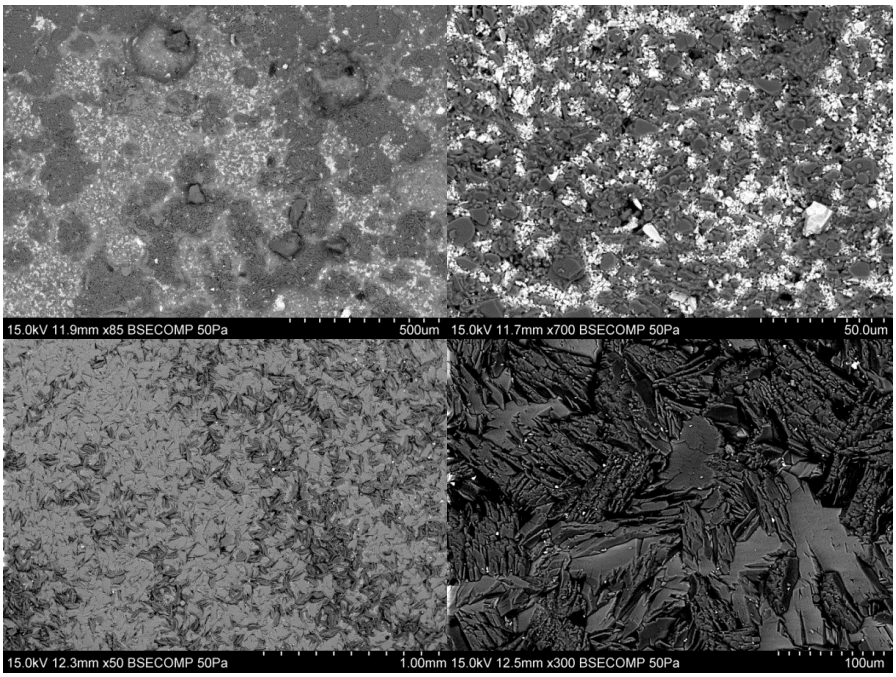

Fig. 4. SEM images of (a) the surface of the ceramic filter medium, (b) the particle adhesion onto the surface of the filter medium, (c) the coverage of the calcium scale and (d) the overlapping scale crystals.

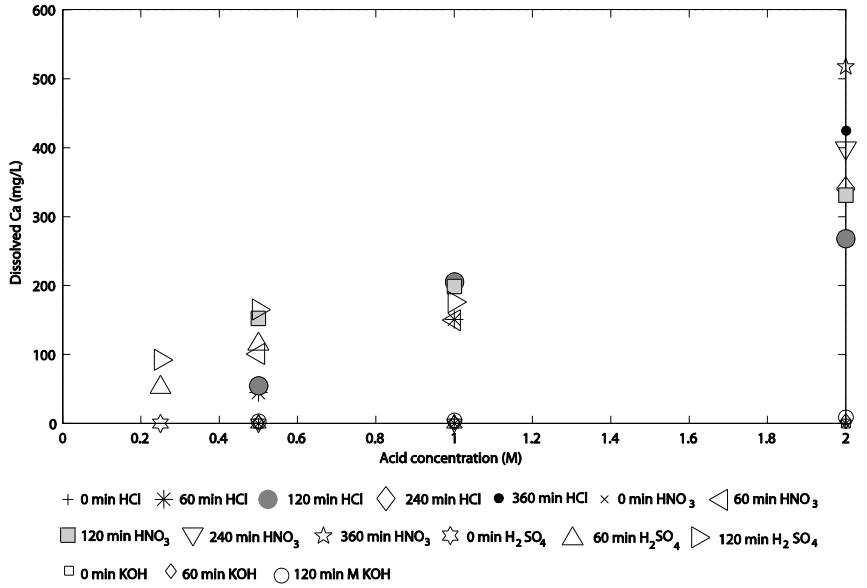

Fig. 5. The concentration of dissolved Ca in the liquid phase when dissolving the calcium oxalate scale with HCl, HNO_3, H_2SO_4 and KOH of different concentrations at 20°C.

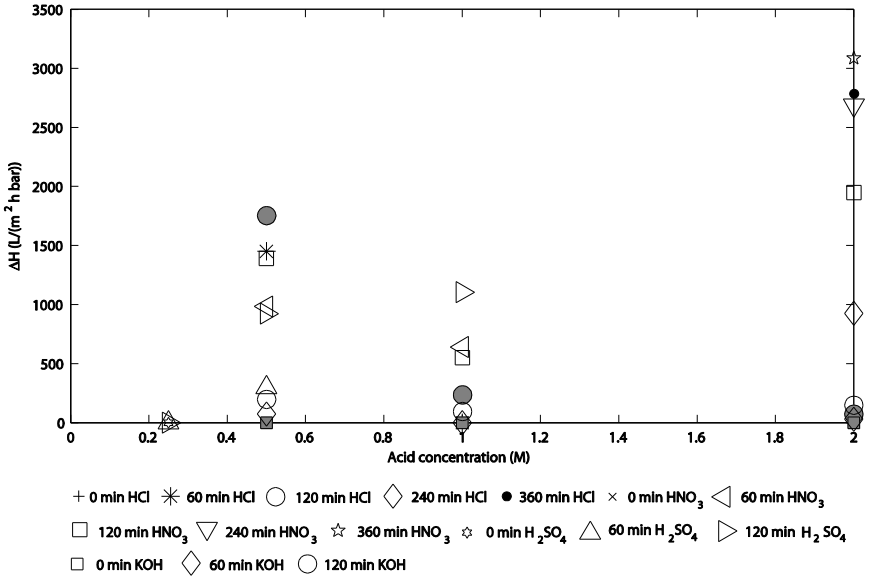

Fig. 6. Increase of permeability when dissolving the scale in (a) HCl, (b) HNO_3, (c) H_2SO_4, and (d) KOH of different concentrations at 20 °C.

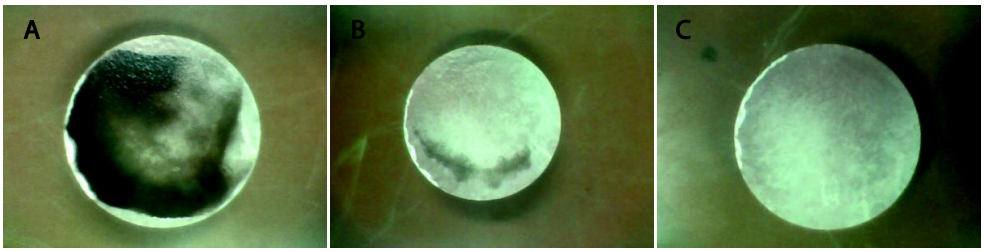

Fig. 7. Dissolution of the scale in 2 mol HNO_3 at 20 °C: (a) 60 min, (b) 120 min, and (c) 360 min. The sample was drawn from the upper left corner of a full scale filter element which had been in use for 3 years in the dewatering process.

Article VI

Salmimies, R., Huhtanen, M., Kallas, J., and Häkkinen, A.,* Empirical modelling to describe the solubility of magnetite in oxalic acid, *Journal of Powder Technology* (Accepted for publication)

Journal of Powder Technology (Accepted for publication)

THE SOLUBILITY OF TWO MAGNETITE POWDERS IN OXALIC ACID – APPLICABILITY OF EMPIRICAL MODELLING

Riina Salmimies*, Mikko Huhtanen, Juha Kallas, and Antti Häkkinen

LUT Chemistry, Lappeenranta University of Technology,

Skinnarilankatu 34, FI-53850 Lappeenranta, Finland

*Corresponding author: e-mail riina.salmimies@lut.fi, mob +358 40 19 77 795, fax +358 5 621 2199

Journal of Powder Technology (Accepted for publication)

Abstract

Phenomena based models can be used in a predictive manner, but statistical modelling methods can also yield interesting findings, and can serve as a tool for analysing the effects of different variables on the overall phenomenon. In addition, the generation of theoretical models can sometimes be limited due to unideality of the studied system. Statistical modelling, in this case Multiple Linear Regression (MLR), was used to describe the effects of temperature and acid concentration on the dissolution of magnetite, Fe_3O_4, with oxalic acid. Whereas a linear model with an interaction term was sufficient in describing the dissolution of synthetic Fe_3O_4, a more complex full quadratic model had to be used to describe the dissolution of industrial Fe_3O_4 in the same conditions.

Keywords: Magnetite, solubility, regression

1 Introduction

Both phenomena based thermodynamic and kinetic models could be utilised in the study of iron oxide dissolution. Sometimes the acquisition of data can, however, be very laborious and complex characteristics of the dissolution phenomenon may be difficult to account for through theory. Experimental modelling methods can provide an additional tool for understanding the behaviour of the system, for example the effects of different variables and the interaction of those variables to account for dissolution. Whereas kinetic studies of dissolution are common amongst metallurgist and soil scientists, equilibrium studies determining solubility are less published. Solubility, however, has key significance in any dissolution system because the difference between the equilibrium concentration and the concentration of the solute in the liquid phase determine the driving force for dissolution. Empirical modelling could also be found useful in describing solubility, as widely accepted theoretical models, e.g. the Debye-Hückel law, do not apply in concentrated solutions.

Statistical modelling methods have been utilised to describe the kinetics of dissolution of iron from kaolin by chemical leaching and bioleaching [1]. In addition, nonlinear regression modelling has been employed in estimating the effects of different parameters, namely sulphuric acid concentration, sucrose concentration, and temperature, on the acidic dissolution of manganiferous ores [2].

The dissolution of other components besides iron has also been described using statistical methods. The use of statistical methods in research of pharmaceuticals has been summarised elsewhere [3]. Especially principal component analysis (PCA) has been popular in analysing the dissolution profiles of different pharmaceuticals [4, 5]. The solubility of calcium oxalate monohydrate has been statistically described as a function of temperature, calcium ion, magnesium ion, oxalic, and nitric acid concentrations of the solution [6]. An adequate correlation (R^2 = 0.90) was achieved with a model comprising a linear and an interaction terms.

Although less used in the field of dissolution of magnetite, Fe_3O_4, statistical modelling methods have been successfully employed on other unit operations in ore beneficiation. Partial least squares (PLS) regression has been used to describe the dewatering process of Fe_3O_4 at LKAB, Sweden [7]. Regression analysis, in turn, has been employed to study the performance of a horizontal belt filter [8]. Several techniques of experimental design were included in the study to determine the significance of operating parameters on the capacity, cake moisture content, and cake purity. In general, both linear and nonlinear models performed well in describing the response of the filtration process. The pelletising process of iron ore has been described with a quadratic model where the median pellet diameter was expressed as a function of the moisture percent of the material, the inclination angle of the pelletiser disc, and the pelletising time [9]. These studies mostly represent optimization cases but do go to show that different systems can be modelled with statistical techniques.

To the best knowledge of the authors, little attention has been paid on equilibrium studies of acidic dissolution of Fe_3O_4 whereas kinetic studies are more common [10, 11, 12]. The solubility of Fe_3O_4 has been investigated in KOH and in HCl solutions at elevated temperatures [13] but is essentially one of the very few published studies on the solubility of Fe_3O_4. In addition, the authors have not found publications reporting the applicability of experimental modelling methods in describing the acidic dissolution of Fe_3O_4 adding to the novelty of this specific approach. Whereas optimization and predictive models are common in experimental design and modelling, the applicability of experimental modelling could go far beyond those. Where discussion on the significance of different parameters, e.g. the oxalate concentration [14, 15, 16], on the dissolution of iron oxides is undertaken, experimental models could provide additional insight to that discussion.

The aim of this study was to investigate the applicability of experimental models, based on empirical data, in describing the effects of temperature and acid concentration on the solubility of Fe_3O_4 in oxalic acid. Oxalic acid especially would be challenging for theoretical models because the dissolution mechanism consists of several steps, including adsorption, complex formation, and even solid state reduction [14, 15, 16]. Experimental models could, however, be used as tools to understand the behaviour of a dissolution system in respect to controllable parameters. Consequently, dissolution behaviour, to some extent, could be explained without physico-chemical considerations.

2 Methods

2.1 Experimental

Two Fe_3O_4 powders were used for the dissolution experiments: a synthetic powder from Alfa Aesar, and an industrial Fe_3O_4 concentrate. The purity of the synthetic sample, according to the supplier, was 97 wt-% and, furthermore, the composition of the powder was verified with X-ray diffraction, using a Bruker D8 Advance diffractormeter, and showed Fe_3O_4 as the only mineralogical phase. The industrial sample was also analysed by XRD and additionally with scanning electron microscopy coupled with energy dispersive X-ray spectrometer, using a JEOL JSM-5800 scanning electron microscope, and indicated 68.77 wt-% iron (Fe) and 29.25 wt-% oxygen (O) with magnesium (Mg), silicon (Si), calcium (Ca), aluminium (Al), and titanium (Ti) as impurities. Oxalic acid ($H_2C_2O_4 \cdot 2H_2O$) in concentrations of 0.08, 0.33, and 0.60 mol/L was used to dissolve Fe_3O_4. The purity of the oxalic acid was 99 %. Values of initial pH were in the range of 0.79 – 1.34. Temperatures were 15, 35, and 50 °C. All solutions were prepared with ultrapure water. Because of lack of prior knowledge on such systems, the dissolution experiments here were conducted according to a 3^2 full factorial design (Table I) [17]. The experiments were conducted in a randomised order to decrease the effect of extraneous time-related factors [18].

A two level design could have also been implemented but would have resulted in only five data points and would have limited the possibility of testing more complex models, for example full quadratic models, because of limited degrees of freedom.

Table I The 2^3 full factorial design and the data used for modelling. Experiments 5, 6, and 7 represent the replicates of the centre point of the full factorial, and experiment 12 is an additional centre point for one of the corners of the experimental plan. The total number of experiments was 24.

No.	T, °C	Oxalic acid c, mol/L	Synthetic c_{Fe}, mg/L	Industrial c_{Fe}, mg/L
1	15	0.08	1942	2576
2	35	0.08	1996	2536
3	50	0.08	3181	4021
4	15	0.33	7523	4014
5	35	0.33	11056	8114
6	35	0.33	11704	7252
7	35	0.33	11673	7825
8	50	0.33	13522	8307
9	15	0.60	18041	3193
10	35	0.60	21001	10215
11	50	0.60	21224	11289
12	25	0.47	16051	7332

The experiments were conducted in a 1 L glass reactor equipped with a heating jacket, baffles, and a stirrer with a pitched blade turbine. Installation of the mixing device was done according to standard assembly [19].The liquid was kept in constant temperature in the reactor and a blank sample was drawn, after which solids were introduced and mixing was commenced. Excess quantity of solids was used to obtain a thermodynamic equilibrium between the solid and the liquid phases. The total reaction time was 360 min. The concentration of Fe in the liquid phase, after the reaction time, was measured with the ThermoElectron IRIS Intrepid II XLD inductively coupled plasma optical emission spectrometer (ICP-OES) and plotted against time. Although data were collected during the dissolution experiments, only the final Fe concentration was considered for modelling. Estimation of the total error of the sampling and analysis procedure, based on quantifiable error sources, indicated an experimental error of 2 %. The error consisted of uncertainty in the weighing of the primary sample, the volumetric dilution to obtain the secondary sample, and the inherent error of the analysis method. Additionally, the experimental error was estimated by repeating individual experimental points.

All the data on the dissolution experiments and a more extensive description of the experimental procedure and the materials (chemical composition and particle size distribution) used in this study have been presented elsewhere [20].

2.2 Modelling

Multiple Regression tools were employed in Matlab to generate the models describing the solubility of Fe as a function of the acid concentration and the temperature. The modelling was based on the equilibrium concentration of Fe (Table I). Kinetic aspects, e.g. pulp density or effects of different particle sizes, were not considered as variables here.

Firstly, linear models (Eq. (1)) with no interaction or quadratic terms were generated to study if fairly simple models would perform well in describing the dissolution. Models were evaluated based on the coefficient of determination, R^2, and the scatter plots of measured and modelled Fe concentrations.

$$Y = \beta_0 + \beta_1 x_1 + \beta_2 x_2 \quad (1)$$

Where linear modelling failed, interaction (Eq. (2)) and quadratic terms (Eq. (3) and (4)) were taken into account. Only the linear models with interaction terms or quadratic models best suited for describing the dissolution phenomena have been included in this paper but both were generated.

$$Y = \beta_0 + \beta_1 x_1 + \beta_2 x_2 + \beta_3 x_1 x_2 \tag{2}$$

$$Y = \beta_0 + \beta_1 x_1 + \beta_2 x_2 + \beta_3 x_1^2 + \beta_2 x_2^2 \tag{3}$$

$$Y = \beta_0 + \beta_1 x_1 + \beta_2 x_2 + \beta_3 x_1 x_2 + \beta_4 x_1^2 + \beta_5 x_2^2 \tag{4}$$

Eq. (4) is from hereon called as the full quadratic model. In general, not all the terms in Eq. (1) – (4) need to be taken into account if a good fit is obtained by excluding some of the terms.

A p-value of 0.05 or less was used to identify the statistical significance of each variable in the models containing only linear terms. A p-value of 0.05, in practice, represents a 5 % chance of an observed correlation being untrue, i.e. not representative the studied phenomenon. The relative errors, in turn, were calculated by dividing the residuals (difference between the observed and modeled values) with the observed values for each data point.

3 Results and Discussion

The models for the three systems described in Chapter 2 are discussed in this Chapter. Linear models, linear models with interaction terms, and quadratic models are introduced, where necessary, to demonstrate the applicability of different statistical models in describing the studied systems.

The maximum number of terms, when two variables are considered, would be six: (1) a constant, (2) – (3) linear terms of both variables, (4) an interaction term, and (5) – (6) quadratic terms of both variables. When applying statistical modelling it is, however, not self-evident that increasing parameters would result in a better model. Including additional terms can, but does not always, result in an increased R^2 value and in such cases the model could be explaining the systematic variance of the experimental data rather than the actual phenomena. In some cases, an additional term might not explain any of the variation left in the data after applying a purely linear model thus rendering no improvement in the model. The addition of parameters of any kind does not automatically mean a better model but can sometimes produce desired results.

3.1 Synthetic Fe_3O_4

The linear regression model, not including an interaction term, for the synthetic Fe3O4 – oxalic acid system was generated using the whole data set for the system (Eq. (5), Figure 1a).

$$c_{Fe,eq} = -3.5 \cdot 10^3 \frac{mg}{L} + 96.2 \frac{mg}{L \cdot °C} \cdot T + 3.4 \cdot 10^4 \frac{mg}{mol} \cdot c_{acid} \tag{5}$$

where

	$c_{Fe,eq}$	concentration of dissolved *Fe* at equilibrium, mg/L
	T	temperature, °C
	c_{acid}	concentration of the acid, mol/L.

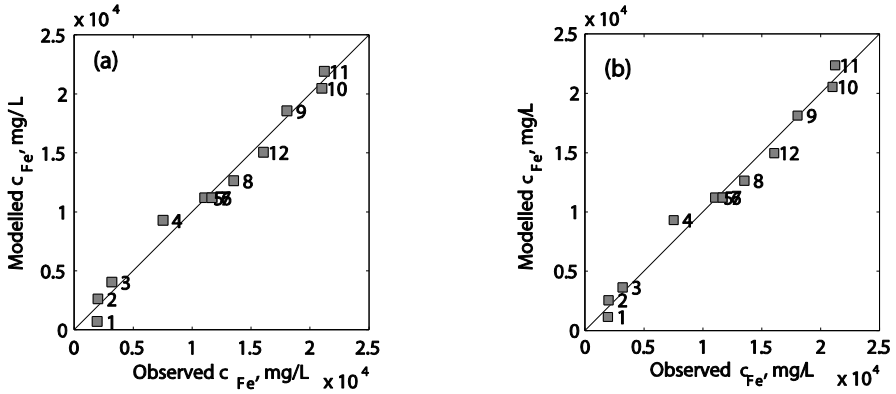

Figure 1. Synthetic Fe_3O_4 – oxalic acid. Scatter plot of the measured Fe concentration against the modeled one (a) for the purely linear model, and (b) for the linear model with the interaction term.

The fit was good having an R^2 value of 0.983. The p-values for the constant and for the two variables were 0.006, 0.002, and 0.000, respectively, meaning that all the terms included in the model were significant.

The model seemed to estimate the solubility better with higher equilibrium concentrations, meaning that the difference between the observed and the predicted values was larger for low values of solubility and smaller for high values. The largest relative errors were observed with data points 1 – 4, from 20 to 64 %. With the exception of data point 1, the predicted solubility was higher than the observed one. Data points 5 – 12 had significantly smaller errors with a maximum error of 6.5 % between the observed and predicted values.

Including the interaction term did not significantly improve the R^2 value (0.984) or the fit in general (Figure 1b), but the residuals for this model (Eq. (6)) were smaller than for the linear model. The difference here was that including the interaction term decreased the errors in the predicted values as compared to the observed ones at those smaller equilibrium concentration which were found challenging for Eq. (5). The errors in data points 1 – 4 were now from 14 to 41 %. The errors in the other data points did not change significantly.

$$c_{Fe,eq} = -2.4 \cdot 10^3 \frac{mg}{L} + 63.4 \frac{mg}{L \cdot °C} \cdot T + 3.1 \cdot 10^4 \frac{mg}{mol} \cdot c_{acid} + 96.2 \frac{mg}{°C \cdot mol} \cdot T \cdot c_{acid} \quad (6)$$

Both the linear model and the model including the interaction term exhibited very similar behaviour: a negative constant and an increased response with increasing variables. The regression coefficients for the variables were, in fact, very alike for the two models, which could be expected as including the interaction term only slightly affected the coefficient of determination, R^2.

3.2 Industrial Fe_3O_4

The linear model (Eq. (7)) describing the industrial Fe_3O_4 – oxalic acid system (Figure 2a) was not successful, as also indicated by R^2 of 0.746.

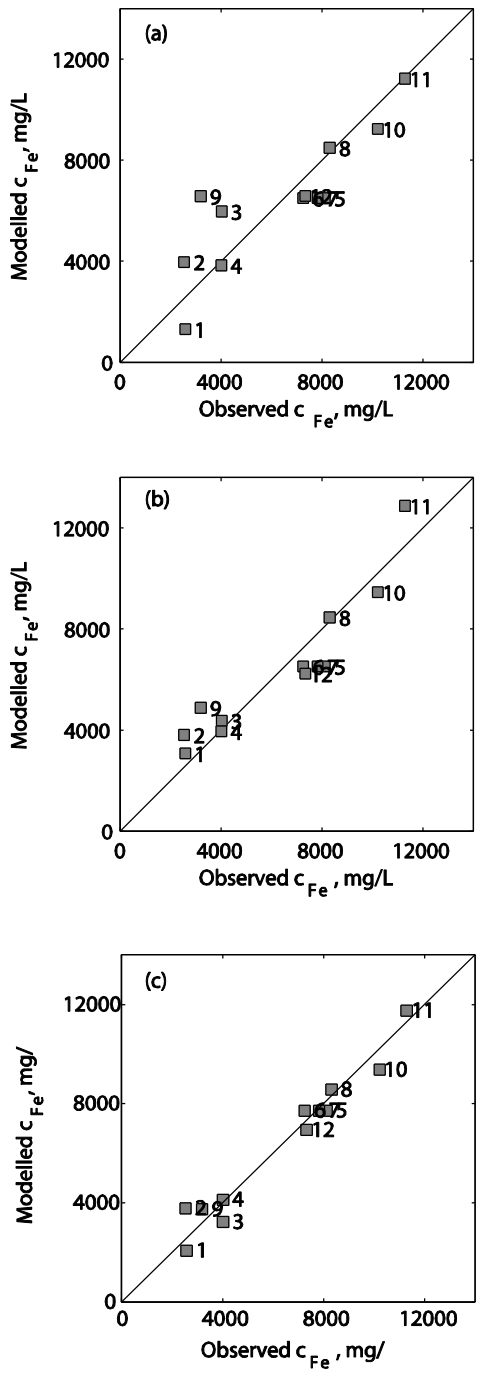

Figure 2. Industrial Fe_3O_4 – oxalic acid. Scatter plot of the measured Fe concentration against the modeled one (a) for the purely linear model, (b) for the linear model including an interaction term, and (c) for the full quadratic model.

Here, the p-values for the terms were 0.385, 0.007, and 0.004.

$$c_{Fe,eq} = -1.5 \cdot 10^3 \frac{mg}{L} + 133.1 \frac{mg}{L \cdot °C} \cdot T + 1.0 \cdot 10^4 \frac{mg}{mol} \cdot c_{acid} \quad (7)$$

The relative errors varied on a wide scale, and an individual observation of a relative error above 100 % made. Such a model would most likely not be suitable for any purpose.

A nonlinear model performed better but was still left with a poor coefficient of determination and a poor fit of the model with the data ($R^2 = 0.860$, Figure 2b).

$$c_{Fe,eq} = 2.7 \cdot 10^3 \frac{mg}{L} + 7.6 \frac{mg}{L \cdot °C} \cdot T - 2.0 \cdot 10^3 \frac{mg}{mol} \cdot c_{acid} + 367.9 \frac{mg}{°C \cdot mol} \cdot T \cdot c_{acid} \quad (8)$$

With the investigation of Eq. (8), one could immediately see that the model was completely different to all the previous ones. The constant was not found negative but the coefficient for acid concentration was, which led to suspect if this model would indeed describe the actual phenomenon at all. Here, the relative errors did, however, decrease. Although for most data points the errors were below 15 %, individual data points exhibited errors of roughly 50 %.

As the introduction of the interaction term did not produce the desired improvement in the modeling, the incorporation of quadratic terms was investigated. The interaction term was not included here. The results were not significantly improved, as the R^2 value was left unchanged (0.860).

Finally, a full quadratic model was generated to improve the fit. A significant improvement was observed in the R^2 value (0.957) as well as in the fit of the model with the experimental data (Eq. (9), Figure 2c).

$$c_{'Fe,eq} = -1.7 \cdot 10^3 \frac{mg}{L} + 230.2 \frac{mg}{L \cdot °C} \cdot T + 1.0 \cdot 10^4 \frac{mg}{mol} \cdot c_{acid} + 377.4 \frac{mg}{°C \cdot mol} \cdot T \cdot c_{acid} - 3.5 \frac{mg}{L \cdot °C^2} \cdot T^2 - 1.8 \cdot 10^4 \frac{mg}{mol} \cdot c_{acid}^2 \quad (9)$$

Here, the relative errors for data points 1 – 3 were the highest and varied from 19 to 49 %. Otherwise, relative errors below 10 % were observed. By excluding the linear terms or even the first quadratic term, R^2 of 0.904 and 0.887, respectively, could have been achieved, and might be considered adequate for rough estimation in an industrial environment. Here, the objective was, however, to describe as accurately as possible the equilibrium concentration of Fe in the mother liqueur in order to make comparison between the two solid powders, and the model was thus rejected.

The centre point of the experimental plan was repeated three times, where all repetitions for the synthetic Fe_3O_4 were found to fit within 4 % of experimental error. The corresponding experimental error was roughly 6 % for the industrial Fe_3O_4. The larger experimental error could have been a result of the inhomogeneous nature of the industrial sample. The particle size distribution and impurities in the sample could have resulted in varying results in the repeated experiments.

3.3 Comparison of the two powders

Essentially, two methods of comparison can be used for regression models: (1) comparison based on regression coefficients, and (2) comparison based on main effects of the models. In this case, mere regression coefficients could not be directly used for the comparison of the different models, because the data were not scaled before applying the numerical methods, and the coefficients were, therefore, affected by the variable ranges. Although scaling the data would have made it possible to evaluate the

significance of each term from the regression coefficients alone, the models would not have been generated with real values of the variables but with scaled values which could make the application of the models more laborious for industrial purposes. Thus, no real added value would have been achieved by scaling the data. Consequently, here the comparison of the different models was done based on the analysis of the main effects.

Main effects of a statistical model are more difficult to compare when interaction terms are taken into the model. With linear models, every variable is represented by only one model term making it easier to estimate the effect of the variable on the response. Interaction terms, as in this case, include several of the variables under investigation which means that when evaluating the magnitude of the effect of a single variable, the effect coming from the interaction term should also be considered. Because of these characteristics of statistical models, it was best to evaluate the effect of single variables using purely linear models where interaction terms did not yield interference in the interpretation.

Main effects (Table II) were calculated for both of the studied variables in the selected variable space. The main effects, in this case, were calculated simply by multiplying the appropriate regression coefficient with the change (ΔT, Δc_{acid}) in the appropriate variable.

Table II R^2 values and main effects of the variables for both oxalic acid – Fe_3O_4 systems with purely linear models.

Eq.	Magnetite	R^2, -	T, mg/L	c_{acid}, mg/L
5	Synthetic	0.983	3367.0	17680.0
8	Industrial	0.860	4658.5	5200.0

In the dissolution of industrial Fe_3O_4, the effect of the acid concentration in the studied variable space was found similar to the dissolution of synthetic Fe_3O_4: increase in the acid concentration increased the concentration of dissolved iron. The effect of the acid concentration in increasing solubility was not as significant as it was in dissolving synthetic Fe_3O_4. The smaller effect of the acid concentration could be explained by the dissolution of impurities from the industrial material: impurities with higher solubility than Fe oxide consumed the acid. Consequently, the apparent increase in acid concentration was not completely directed at the dissolution of iron resulting in a smaller total effect. The dissolution of the impurities has also been discussed elsewhere [20].

4 Conclusions

The applicability of MLR to describe the effects of temperature and acid concentration on the solubility of Fe_3O_4 in oxalic acid was studied by creating linear and nonlinear regression models based on the dissolution data.

The effects of temperature and acid concentration on the dissolution of synthetic Fe_3O_4 in oxalic acid, specifically on the equilibrium concentration of iron in the liquid phase, could be explained by linear models well. The concentration of oxalic acid was found highly significant in the dissolution of Fe_3O_4, and can be explained by the increase of available ligands enabling the dissolution. Consequently, even the statistical models do, to a certain extent, yield relevant tools to identify the significance of different factors. In developing a new dissolution process, these tools could be used to determine the most desirable direction for further experimentation: can we increase recovery most effectively by increasing the temperature or by introducing more chelating agents into the system?

To describe the dissolution of an industrial powder in the same conditions required the application of nonlinear models including interaction and quadratic terms. The dissolution of impurities from the industrial Fe_3O_4 could explain the need for more complex models as the co-occurring dissolution of the impurities might interfere with the dissolution of the Fe_3O_4. The same conclusion might apply also to the observed difference with the two powders regarding the effect of temperature: in the dissolution

of the synthetic powder, increasing the acid concentration played a much greater role than increasing the temperature whereas the effect was roughly the same for increasing either of the variables.

Extrapolation should never be attempted based on purely empirical models. Empirical, and in this case statistical, models only apply in the variable space in which the models were generated. As seen here, the regression models performed poorly in explaining data collected at low temperature and high acid concentration.

Acknowledgements

This study was supported by the Graduate School in Chemical Engineering and by Outotec (Filters) Oy.

References

[1] Volkan, A., and Oktay, B., 2009. Removal of Fe from kaolin by chemical leaching and bioleaching. Clays Clay Miner. 57, 787 – 794.

[2] Beolchini, F., Petrangeli Papini, M., Toro, L., Trifoni, M., and Vegliò, F., 2001. Acid leaching of manganiferous ores by sucrose: Kinetic modelling and related statistical analysis. Miner. Eng. 14, 175 – 184.

[3] O'Hara, T., Dunne, A., Butter, J., and Devane, J., 1998. A review of methods used to compare dissolution profile data. Pharm. Sci. Technol. Today 1, 214 – 223.

[4] Adams, E., De Maesschalk, R., De Spiegeleer, B., Vander Heyden, Y., Smeyers-Verbeke, J., and Massart, D.L., 2001. Evaluation of dissolution profiles using principal component analysis. Int. J. Pharm. 212, 41 – 53.

[5] Maggio, R.M., Castellano, P.M., and Kaufman, T.S., 2009. PCA-CR analysis of dissolution profiles. A chemometric approach to probe the polymorphic form of the active pharmaceutical ingredient in a drug product. Pharm. Nanotechnol. 378, 187 – 193.

[6] Salmimies, R., Louhi-Kultanen, M., Ekberg, B., Häkkinen, A., Kallas, J., and Huhtanen, M., 2008. Fouling of filter media: solubility of oxalate solutions. In: Filtech Exhibitions Germany, 10th World Filtration Congress. Leipzig, Germany, 14-18 April 2008. Meerbusch: Filtech Exhibitions Germany.

[7] Herath, B., Albano, C., Anttila, A., and Flykt, B., 1992. Empirical modelling of a dewatering process using multivariate data analysis. Filtr. Sep. 29, 57 – 65.

[8] Huhtanen, M., Häkkinen, A., Ekberg, B., and Kallas, J., 2011. Experimental study of the influence of process variables on the performance of a horizontal belt filter, Filtr. 11, 118 – 123.

[9] Thella, J. S., and Venugopal, R., 2011. Modeling of iron ore pelletization using $3^{**(k-p)}$ factorial design of experiments and polynomial surface regression methodology. Powder Technol. 211, 53 – 59.

[10] Sidhu, P.S., Gilkes, R.J., Cornell, R.M., Posner, A.M., Quirk, J.P., 1981. Dissolution of iron oxides and oxyhydroxides in hydrochloric and perchloric acids. Clays Clay Miner. 29, 269 – 276.

[11] Bruyere, V.I.E., Blesa, M.A., 1985. Acidic and reductive dissolution of magnetite in aqueous sulfuric acid. J. Electroanaly. Chem. 182, 141 – 156.

[12] Blesa, M.A., Marinovich, H.A., Baumgartner, E.C., Maroto, A.J.G., 1987. Mechanism of dissolution of magnetite by oxalic acid – ferrous ion solutions. Inorg. Chem. 26, 3713 – 3717.

[13] Sweeton, F.H., Baes, C.F., 1970. The solubility of magnetite and hydrolysis of ferrous ion in aqueous solutions at elevated temperatures. J. Chem. Thermodynamics 2, 479 – 500.

[14] Panias, D., Taxiarchou, M., Paspaliaris, I., Kontopoulos, A., 1996. Mechanisms of dissolution of iron oxides in aqueous oxalic acid solutions. Hydrometallurgy 42, 257 – 265.

[15] Taxiarchou, M., Panias, D., Douni, I., Paspaliaris, I., Kontopoulos, A., 1997. Dissolution of hematite in acidic oxalate solutions. Hydrometallurgy 44, 287 – 299.

[16] Lee, S.O., Tran, T, Park, Y.Y., Kim, S.J., Kim, M.J., 2006. Study on the kinetics of iron oxide leaching by oxalic acid. Int. J. Miner. Process. 80, 144 – 152.

[17] Box, G.E.P., Hunter, W.G., Hunter, J.S., 1987. Statistics for experiments. John Wiley & Sons, Inc., New Jersey.

[18] Montgomery, D., 1997. Design and analysis of experiments. John Wiley & Sons, Inc. Toronto.

[19] Tatterson, G., 1994. Scaleup and design of industrial mixing processes. McGraw-Hill, Inc., New York.

[20] Salmimies, R., Mannila, M., Häkkinen, A., and Kallas, J., 2011. Acidic dissolution of magnetite: experimental study on the effects of acid concentration and temperature. Clays Clay Miner. 59, 136 – 146.

Article VII

Salmimies, R., Kinnarinen, T., Kallas, J., Ekberg, B., and Häkkinen, A.,* Oxalic acid regeneration of ceramic filter medium fouled in the dewatering of iron ore, *ISRN Chemical Engineering*, 2012.

International Scholarly Research Network
ISRN Chemical Engineering
Volume 2012, Article ID 921873, 6 pages
doi:10.5402/2012/921873

Research Article

Oxalic Acid Regeneration of Ceramic Filter Medium Used in the Dewatering of Iron Ore

Riina Salmimies,[1] Juha Kallas,[2] Bjarne Ekberg,[3] and Antti Häkkinen[1]

[1] *LUT Chemistry, Lappeenranta University of Technology, Skinnarilankatu 34, 53850 Lappeenranta, Finland*
[2] *Laboratory of Inorganic Materials, Tallinn University of Technology, Ehitajate Tee 5, 19086 Tallinn, Estonia*
[3] *Outotec (Filters) Oy, Urusvuorenkatu 5, 20630 Turku, Finland*

Correspondence should be addressed to Riina Salmimies, riina.salmimies@lut.fi

Received 17 September 2012; Accepted 23 October 2012

Academic Editors: J. Lobato and A. Szymczyk

The regeneration of the ceramic filter medium in the dewatering of iron ore enables the use of the medium for much longer periods in comparison to traditional filter cloths. The regeneration is commonly a combination of several techniques, of which one is the acid washing of the medium. Despite being effective against iron oxides, the phenomena related to the acid washing of the ceramic filter medium with oxalic acid have so far been less extensively published. The aim of this study was to investigate the dissolution of iron oxide particles from the surface of the filter medium and the consequent changes in the performance and in the structure of the medium. The dissolution of the particles was found to exhibit some kind of a steady state dependent on temperature but not so much on the acid concentration. Changes in permeability as well as in pore size were found to take place even after the dissolution of the particles had ceased.

1. Introduction

The final dewatering of a magnetite concentrate can be performed with ceramic capillary action disc filters. During operation, magnetite particles are adhered to the surface of the filter medium causing the decline of filtrate flux. The ceramic filter medium, however, is robust enough to withstand both mechanical and chemical regeneration, and, consequently, the performance of the filter medium can be restored.

The regeneration of the ceramic filter medium in capillary action disc filters incorporates several operations: (1) backwashing, (2) ultrasonic cleaning, and (3) acid regeneration. In iron ore applications, oxalic acid can be used for the regeneration as it has been shown to efficiently dissolve iron oxides [1–9].

Although the regeneration of ceramic membranes fouled by oxide particles has been receiving an increasing attention in cross flow filtration [10–13], published research on the regeneration of the ceramic membrane used for the dewatering of mineral concentrates is scarce. Even the fundamental effects of oxalic acid regeneration, currently used for several ceramic disc filters in iron ore dewatering, on the filter medium are fairly unknown and make it challenging to develop the regeneration process. The further development of the process, however, requires a deeper understanding of the phenomena underlying the acid treatment of the filter medium.

The aim of this study was to provide more insight into the dissolution of particles during the regeneration and into what are the actual changes in the filter medium as a result of the regeneration. The experiments were done with samples from a full scale dewatering process so to have the samples represent a real case where regeneration is needed.

2. Methods

2.1. Regeneration Experiments. Samples for the regeneration were received from a full scale magnetite dewatering process where the filter elements had been in use for 3 to 5 years. The samples of the filter media were characterized with X-ray diffraction and scanning electron microscopy, of which the details and results have been presented elsewhere [14]. Samples for the experiments done here were chosen so

to only have magnetite as an extraneous compound, to eliminate the effect of any other chemical species on the dissolution of magnetite from the surface of the samples.

The ceramic samples were regenerated using oxalic acid at concentrations of 0.08, 0.33, and 0.60 mol/L, corresponding roughly to 1, 4.5, and 7 wt%, respectively. All solutions were prepared from a solid proanalysis grade oxalic acid dihydrate from Merck. Ultrapure water was used to eliminate any impurities. The regeneration was done at three different temperatures: 15, 35, and 50°C. The regeneration was done in 0.6 L beakers where the solutions, 0.5 L in volume, were thermostated to the desired temperatures under magnetic mixing. A blank sample was drawn of each beaker before introducing the ceramic samples into the beakers. During the regeneration samples of the mother liquour were taken at regular intervals until reaching a total regeneration time of 12 h. The extracted sample volume was roughly 3 mL with a total volume of solution removed from the system during the regeneration being roughly 40 mL. This accounts for roughly 8% of the initial total volume of the solution. The samples were drawn with a syringe and filtered with a syringe filter, with a pore size of 0.25 μm, to remove any solid particles. Finally, the samples were diluted three times with 10 vol% HNO_3 to prevent the precipitation of the soluble Fe.

2.2. Dissolution of Fe_3O_4. The Fe concentration of the mother liquour was determined with flame AAS using a Thermo Scientific iCE 3000 AA spectrometer. The calibration standards were 0.5, 1.5, 3.0, and 5.0 mg/L and were prepared in 10 vol% HNO_3 to mimic the matrix of the samples drawn from the beakers. The samples were diluted with 10 vol% HNO_3 to yield an absorbance fit for the calibration range.

In addition to analyzing the concentration of dissolved Fe from the mother liquour, an imaging with a JEOL JSM-5800 scanning electron microscope (SEM) was performed to investigate if any iron oxide particles were still present on the surface of the filter medium. The SEM was operated in backscatter mode with an acceleration voltage of 10 keV. No coating was used.

2.3. Permeability. The water flux was measured with a pressure of 0.5 bar for 200 s with data recorded every 1 s. The data was then averaged to yield a value for the permeability of the sample. The equipment for measuring the permeability consisted of a feed vessel, a pump, a pressure control unit, and housing for the sample (Figure 1).

The permeability, or the water flux in L/(m^2 h bar), was determined every three hours with the exception of determining it at $t = 1$ h and $t = 3$ h at the beginning of the experiments. The circular measuring area was roughly 46 mm; that is, the whole surface of the sample was used in the measurement.

2.4. Pore Size Distribution. The pore size distributions were determined using a PMI Advanced Capillary Flow Porometer. The principle of the porometer is fairly simple: the sample is inserted into a sealed chamber, pressure is increased, and the flow of gas through the sample is measured. Measurements are done with a dry and a wet sample yielding the cumulative flow versus time curves for both to calculate the flow corresponding to each pore diameter. The calculation of the pore diameter is based on (1)

$$p = \frac{4\mu_{l/g}\cos\Theta}{D}, \quad (1)$$

where p is the differential pressure, $\mu_{l/g}$ is the surface tension of the wetting liquid, Θ is the contact angle between the liquid and the solid, and D is the pore diameter (SI units). The wetting liquid is assumed to be an ideal wetting agent with a contact angle of 0° (or 0 rad to be exact) making $\cos\Theta$ equal to 1. Ultrapure water was used as the wetting liquid here. Although ultrapure water may not be an ideal wetting liquid, it was the best choice in this case, as contamination of the samples and of the regeneration system could have been resulted if was used another liquid.

The bubble point pressure is the point at which the largest pores are emptied from the wetting liquid and gas starts to flow through the sample. At pressures below the bubble point, the wet sample does not allow gas to flow through. Whereas visual bubble point detection is common, here the detection of the bubble point is based on an F/PT factor (or more accurately the $F/(\Delta P/\Delta T)$). F stands for the bubble flow, P for pressure, and T for time. The studied sample is inserted into the chamber to which air then starts to flow at a rate set as the bubble flow. At pressures below the bubble point, no flow occurs through the sample and the change in pressure correlates with the change in time. Before reaching the bubble point pressure, the F/PT factor remains constant after which a change, commonly a sharp increase, in the factor is observed at the bubble point pressure.

The pore size distribution is determined as the percentage of flow resulting from each pore diameter. The cumulative percentage is calculated by dividing the wet flow with the dry flow and multiplying by a hundred. The differential percentage is then the difference between two consecutive cumulative values.

The pore size distributions were determined by using a compression pressure of 4 bar and a measuring range from 0.5 to 4 bar. The F/PT factor was 50 and the bubble flow was 27 cm^3/min. The pressure and flow increments were 3 and 0.25 counts, respectively. The F/PT factor and the bubble flow are parameters affecting the detection of the bubble point pressure and the increments are those determining the number of steps at a given pressure range, that is, the number of data points. The circular measuring area had a diameter of roughly 35 mm; that is, the whole surface of the sample was not used in the measurement. The pore size distribution was determined every three hours, like the permeability, after the sample had been dried in an oven over night.

3. Results and Discussion

3.1. Dissolution of Fe_3O_4. The final concentration of dissolved Fe seemed to be temperature dependent as, in the whole data set, the dissolution curves showed slight grouping

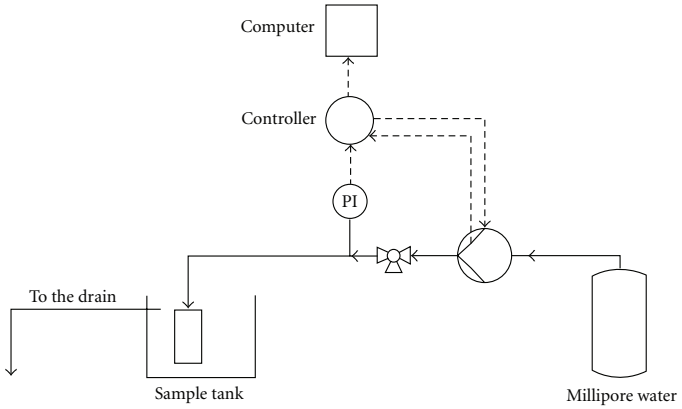

Figure 1: Equipment for measuring the water permeability of the samples.

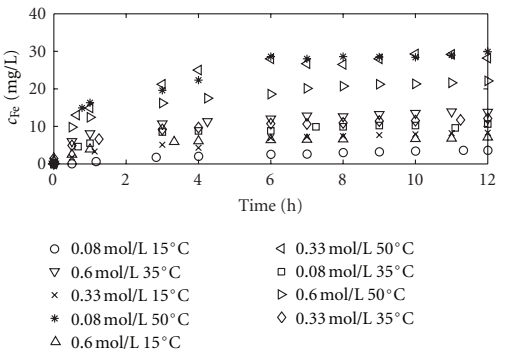

Figure 2: The concentration of dissolved Fe in the mother liqueur during the regeneration with oxalic acid at different concentrations of acid and at different temperatures.

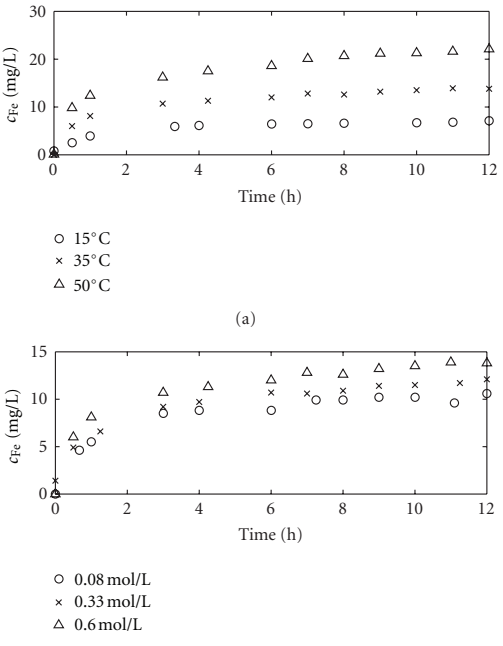

Figure 3: The individual effects of temperature (a) and acid concentration (b) on the concentration of dissolved Fe during the regeneration of the ceramic filter medium. The acid concentration in (a) was 0.60 mol/L and the temperature in (b) was 35°C.

according to temperature (Figure 2). The lowest concentration of dissolved Fe was obtained with 0.08 mol/L oxalic acid at 15°C. The dependency of the final concentration of dissolved Fe roughly followed the same trends observed in earlier studies for free particles [8]. The influence of the acid concentration was, however, questionable as the results did not show similar grouping according to the acid concentration as they did according to the temperature.

The highest concentration of dissolved Fe was observed at 50°C and the lowest at 15°C (Figure 3(a)). This observation was rather interesting as the initial hypothesis was that complete dissolution of the Fe particles would take place when the regeneration was extended for a long period of time. Here, the concentration of dissolved Fe showed signs of steady state already after roughly 3–6 hours. If complete dissolution of the Fe particles, adhered to the surface of the filter medium, indeed took place, the final concentration of Fe should not have shown a temperature dependency but rather random scattering. Scattering of the data could have been a result of differences in the samples but is, in this case, unlikely because the data seemed to group distinctively according to the different temperatures instead of scattering randomly. When dissolving in 50°C, acid concentrations of 0.08 and 0.33 mol/L yielded roughly the same final concentration of dissolved Fe whereas 0.60 mol/L showed a much lower concentration. This difference could simply be due to initial differences in the quantity of magnetite in the samples: samples regenerated in the two lower acid concentrations were more similar to each other than the one regenerated at

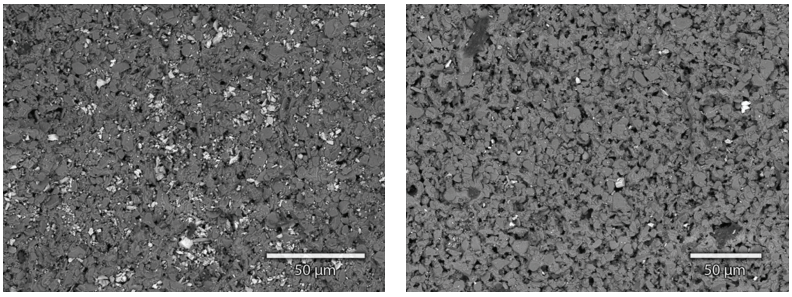

(a) (b)

Figure 4: SEM image showing particles left on the surface and between the alumina grains: (a) 0.08 mol/L oxalic acid at 15°C and (b) 0.60 mol/L oxalic acid at 50°C.

the highest acid concentration. Dissolution at 35°C yielded three almost identical dissolution curves (Figure 3(b)), where the effect of acid concentration could, however, still be seen. The highest acid concentration resulted in the highest concentration of dissolved Fe.

The kinetics of dissolution seemed to be affected by temperature as well: higher rates were observed when dissolving at a higher temperature as indicated by the slopes of the dissolution curves at the early stages of dissolution. Similar indication was found in the experiments done at different acid concentrations but the effect was again less pronounced than for the temperature.

As already previously mentioned, the samples were selected so to be as similar as possible in their chemical composition. Inspection of the surface with SEM showed that some small particles were still left on the surface of the filter medium and between the alumina grains (Figure 4).

Where lower quantities of dissolved Fe were obtained during the regeneration, more Fe_3O_4 particles were found on the surface, too. The observation further confirmed that the dissolution of the particles was dependent on the solution conditions.

3.2. Changes in the Permeability and Pore Size Distribution of the Filter Medium. Increased permeability was observed as a result of the regeneration, as was expected (Figure 5).

Whereas most of the magnetite particles were dissolved already during the first three hours of regeneration, the permeability still continued to increase until reaching a steady state between 6 and 12 h. As the dissolution of particles from the surface had stopped, possible structural changes within the filter medium could be a cause for the observation. Dissolution of any components within the filter medium could, however, most likely not be observed as the liquid which had penetrated into the structure of the filter medium during the regeneration cannot flow outwards without external pressure.

According to the experiments, the final permeability after regeneration was between 5000 and 7000 L/(m^2 h bar). These values roughly correspond to full regeneration of the filter medium. Whereas the highest concentrations of dissolved Fe were observed at the highest temperature, 50°C, the

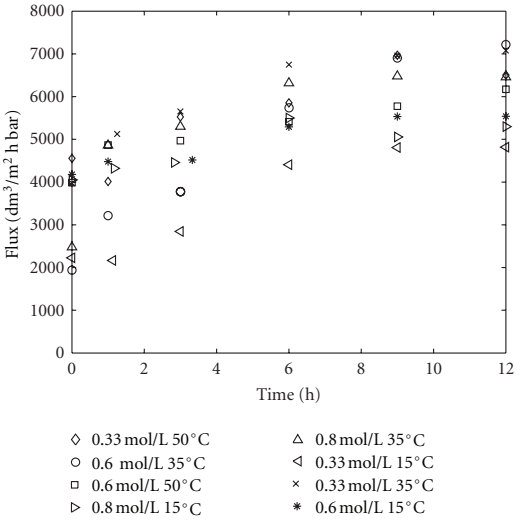

Figure 5: Permeability of the filter medium samples during the regeneration with oxalic acid. The permeability was measured at 0.5 bar pressure.

highest final permeabilities were observed at 35°C. This suggests that the dissolution of surface particles is not the only phenomenon determining the regeneration result. In general, the final permeability seemed to be dependent on the acid concentration, as the highest acid concentrations yielded the highest permeabilities at each temperature. Some discrepancies were, however, observed, for example, at 15°C 0.08 mol/L oxalic acid resulted in a higher permeability than 0.33 mol/L. Some of the differences could have been due to inherent differences in the initial permeabilities of the samples.

All the data for the pore size distributions are not presented here but only an example of the experiments done at 35°C. Similar trends were observed in all the experiments. The changes in the pore size distribution described the changes in the structure of the filter medium more accurately than the permeability. Changes in the bubble point did not

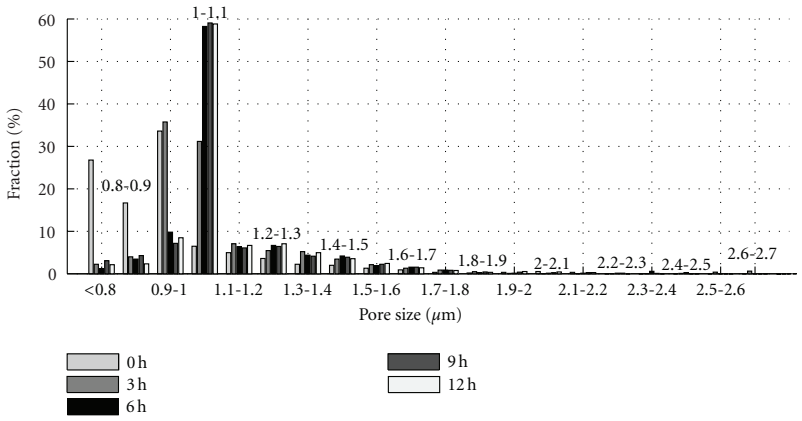

Figure 6: Changes in the pore size distribution of the filter medium during the regeneration with 0.33 oxalic acid at 35°C.

Table 1: The bubble point pressure, the corresponding bubble point pore diameter, and the median flow pore diameter for the ceramic samples before, during, and after the regeneration with oxalic acid at 35°C.

t (h)	BPP[1] (bar)	BPPD[2] (μm)	MFPS[3] (μm)
	0.08 mol/L		
0	1.33	1.55	0.63
3	0.75	2.73	0.68
6	0.74	2.79	0.70
9	0.73	2.83	0.70
12	0.74	2.78	0.69
	0.33 mol/L		
0	1.34	1.54	0.65
3	1.07	1.92	0.72
6	1.17	1.76	0.74
9	1.21	1.70	0.74
12	1.31	1.57	0.74
	0.60 mol/L		
0	1.51	1.37	0.69
3	1.48	1.40	0.75
6	1.45	1.42	0.80
9	1.45	1.42	0.81
12	1.44	1.43	0.81

[1]Bubble point pressure, [2]bubble point pore diameter, [3]mean flow pore diameter.

represent the changes in the filter medium too well, as the bubble point did not seem to change too much in all the samples (Table 1).

Some of the samples did exhibit significant decrease in the bubble point pressure but this was not the case for all of the samples which might suggest that the individual observations were most likely due to inherent differences in the samples instead of a trend. As previously mentioned the bubble point pressure only describes the size of the largest pores and might thus not be the most suitable tool to estimate the regeneration of the filter medium. The pore size distributions did, however, show significant changes in the structure of the filter medium (Figure 6).

The results showed that the fraction of the largest pores did not increase significantly which most likely explains why large changes in the bubble point pressure were not observed. The results did, however, also show that the fraction of pores in the range of 1–1.1 μm increased markedly as a result of the regeneration. In turn, the fraction of smaller pores, below 1.0 μm, decreased notably. As described earlier, the samples were wetted with ultrapure water for the porometer which could be a source for error in the calculations for the pore size distribution. However, every sample was treated in the same way and changes in the pore size distribution can be reported although absolute values might contain a small error. Distinction between surface and inner structure changes cannot be made based on the pore size distributions as the measurement only accounts for the smallest diameter of a pore whether it is the pore's surface diameter or a narrow constriction within the medium.

The regeneration of the filter medium in a large scale process is based on the combination of several actions. The use of ultrasound could significantly enhance the dissolution rate and the consequent regeneration rate of the filter medium. Ultrasound was, however, not considered here as the aim was to investigate the basic underlying phenomena of the acid regeneration and including ultrasound could have made it more difficult to interpret the results of the chemical dissolution experiments.

4. Conclusions

The dissolution of Fe_3O_4 particles and the consequent changes in the permeability and the pore size distribution of the filter medium samples were studied by regenerating the samples in oxalic acid at different temperatures.

The temperature dependency of dissolution, observed here, could indicate that the dissolution of the particles is affected by some sort of equilibrium. This observation seems

very interesting as the solubility limit for Fe_3O_4 particles is much higher than the concentrations obtained here.

Higher permeabilities were achieved at higher acid concentrations, although a direct correlation between the acid concentration and the dissolution of the particles was not found. The lowest permeabilities were obtained at the lowest regeneration temperatures, and here the removal of Fe_3O_4 from the surface correlated with permeability restoration: if the particles are not removed, the pores remain blinded. Further increase was, however, observed even after the dissolution of Fe_3O_4 particles had come to an end which suggests that something else besides the dissolution of surface particles also took place during the regeneration. No aluminium was, however, found in the liquid phase suggesting that the filter medium itself had not been dissolved.

The changes in the pore size distribution indicated the decrease of the fraction of small pores and a consequent increase in the number of slightly larger pores. Changes in the bubble point pressures were not conclusive indicating that the bubble point pressure might not be the best tool to evaluate the changes in the pore structure.

Acknowledgments

The authors would like to acknowledge the Graduate School of Chemical Engineering for funding this research. In addition, the authors are grateful to Outotec (Filters) Oy for providing the samples of the ceramic filter medium which were vital in making possible the integration between academic research and industrial relevance.

References

[1] M. A. Blesa, H. A. Marinovich, E. C. Baumgartner, and A. J. G. Maroto, "Mechanism of dissolution of magnetite by oxalic acid-ferrous ion solutions," *Inorganic Chemistry*, vol. 26, no. 22, pp. 3713–3717, 1987.

[2] R. M. Cornell and P. W. Schindler, "Photochemical dissolution of goethite in acid/oxalate solution," *Clays and Clay Minerals*, vol. 35, no. 5, pp. 347–352, 1987.

[3] M. Taxiarchou, D. Panias, I. Douni, I. Paspaliaris, and A. Kontopoulos, "Dissolution of hematite in acidic oxalate solutions," *Hydrometallurgy*, vol. 44, no. 3, pp. 287–299, 1997.

[4] G. J. Houben, "Iron oxide incrustations in wells. Part 2: chemical dissolution and modeling," *Applied Geochemistry*, vol. 18, no. 6, pp. 941–954, 2003.

[5] S. K. Mandal and P. C. Banerjee, "Iron leaching from China clay with oxalic acid: effect of different physico-chemical parameters," *International Journal of Mineral Processing*, vol. 74, no. 1–4, pp. 263–270, 2004.

[6] S. O. Lee, T. Tran, Y. Y. Park, S. J. Kim, and M. J. Kim, "Study on the kinetics of iron oxide leaching by oxalic acid," *International Journal of Mineral Processing*, vol. 80, no. 2–4, pp. 144–152, 2006.

[7] S. O. Lee, T. Tran, B. H. Jung, S. J. Kim, and M. J. Kim, "Dissolution of iron oxide using oxalic acid," *Hydrometallurgy*, vol. 87, no. 3-4, pp. 91–99, 2007.

[8] R. Salmimies, M. Mannila, J. Kallas, and A. Häkkinen, "Acidic dissolution of magnetite: experimental study on the effects of acid concentration and temperature," *Clays and Clay Minerals*, vol. 59, no. 2, pp. 136–146, 2011.

[9] R. Salmimies, M. Mannila, J. Kallas, and A. Häkkinen, "Acidic dissolution of hematite: kinetic and thermodynamic investigations with oxalic acid," *International Journal of Mineral Processing*, vol. 110-111, pp. 121–125, 2012.

[10] Y. Zhao, J. Zhong, H. Li, N. Xu, and J. Shi, "Fouling and regeneration of ceramic microfiltration membranes in processing acid wastewater containing fine TiO_2 particles," *Journal of Membrane Science*, vol. 208, no. 1-2, pp. 331–341, 2002.

[11] M. Gryta, "Effect of iron oxides scaling on the MD process performance," *Desalination*, vol. 216, no. 1–3, pp. 88–102, 2007.

[12] H. Yamamura, S. Chae, K. Kimura, and Y. Watanabe, "Transition in fouling mechanism in microfiltration of a surface water," *Water Research*, vol. 41, no. 17, pp. 3812–3822, 2007.

[13] T. Quadt and E. Schmidt, "Membranes: optimising the regeneration of ceramic membranes," *Filtration and Separation*, vol. 48, no. 6, pp. 26–28, 2011.

[14] R. Salmimies, A. Häkkinen, J. Kallas, B. Ekberg, J. P. Andreassen, and R. Beck, "Characterisation of long-term scaling effects of ceramic filter media used in the dewatering of iron ore," in *Proceedings of the Iron Ore 2011*, AusIMM, Perth, Australia, 2011.

ACTA UNIVERSITATIS LAPPEENRANTAENSIS

453. HENNALA, LEA. Kuulla vai kuunnella – käyttäjää osallistavan palveluinnovoinnin lähestymistavan haasteet julkisella sektorilla. 2011. Diss.

454. HEINIMÖ, JUSSI. Developing markets of energy biomass – local and global perspectives. 2011. Diss.

455. HUJALA, MAIJA. Structural dynamics in global pulp and paper industry. 2011. Diss.

456. KARVONEN, MATTI. Convergence in industry evolution. 2011. Diss.

457. KINNUNEN, TEEMU .Bag-of-features approach to unsupervised visual object categorisation. 2011. Diss.

458. RUUSKANEN, VESA. Design aspects of megawatt-range direct-driven permanent magnet wind generators. 2011. Diss.

459. WINTER, SUSANNA. Network effects: scale development and implications for new product performance. 2011. Diss.

460. JÄÄSKELÄINEN, ANSSI. Integrating user experience into early phases of software development. 2011. Diss.

461. KÄÄRIÄINEN, TOMMI. Polymer surface modification by atomic layer deposition. 2011. Diss.

462. KOCHURA, ALEKSEY. Growth, magnetic and transport properties of InSb and II-IV-As2 semiconductors doped with manganese. 2011. Diss.

463. PUTKIRANTA, ANTERO. Possibilities and challenges of longitudinal studies in operations management. 2011. Diss.

464. HAPPONEN, ARI. Muuttuvaan kysyntään sopeutuva varastonohjausmalli. 2011. Diss.

465. VASAVA, PARITOSH. Application of computational fluid dynamics in modelling blood flow in human thoracic aorta. 2011. Diss.

466. PURO, LIISA. Identification of extractives and polysaccharides as foulants in membrane filtration of pulp and paper mill effluents. 2011. Diss.

467. LAPPALAINEN, PIA. Socially Competent Leadership – predictors, impacts and skilling in engineering. 2012. Diss.

468. PLAMTHOTTATHIL, ANSHY OONNITTAN. Application of electrokinetic Fenton process for the remediation of soil contaminated with HCB. 2012. Diss.

469. EBRAHIMI, FATEMEH. Synthesis of percarboxylic acids in microreactor. 2012. Diss.

470. JANTUNEN, SAMI. Making sense of software product requirements. 2012. Diss.

471. VILKO, JYRI. Approaches to supply chain risk management: identification, analysis and control. 2012. Diss.

472. TANSKANEN, VESA. CFD modelling of direct contact condensation in suppression pools by applying condensation models of separated flow. 2012. Diss.

473. HUHTANEN MIKKO. Software for design of experiments and response modelling of cake filtration applications. 2012. Diss.

474. PARJANEN, SATU. Creating possibilities for collective creativity
Brokerage functions in practice-based innovation. 2012. Diss.

475. KUKKONEN, SAKU. Generalized differential evolution for global multi-objective optimization with constraints. 2012. Diss.

476. LAAKSONEN, JONNA. Tactile-proprioceptive robotic grasping. 2012. Diss.

477. KALLIO, ANNE. Enhancing absorptive capacity in a non-research and development context
An action research approach to converting individual observations into organizational awareness. 2012. Diss.

478. LÄTTILÄ, LAURI. Improving transportation and warehousing efficiency with simulation based decision support systems. 2012. Diss.

479. OYOMNO, WERE. Usable privacy preservation in mobile electronic personality. 2012. Diss.

480. LINNALA, MIKKO. Simulation and optimization tools in paper machine concept design. 2012. Diss.

481. KORPIJÄRVI, JUHA. Aging based maintenance and reinvestment scheduling of electric distribution network. 2012. Diss.

482. KORHONEN, JUHAMATTI. Active inverter output filtering methods. 2012. Diss.

483. KLODOWSKI, ADAM. Flexible multibody approach in bone strain estimation during physical activity: quantifying osteogenic potential. 2012. Diss.

484. VUORENMAA, MARKKU. Osaamisen johtaminen pk-yrityksen kansainvälisen kasvun elinkaarella. 2012. Diss.

485. RAUTIAINEN, MARITA. Dynamic ownership in family business systems – a portfolio business approach. 2012. Diss.

486. LILIUS, REIJO. THE FINNISH IT INDUSTRIES IN TRANSITION Defining and measuring the Finnish software product and IT services industries by applying theoretical frameworks . 2012. Diss.

487. TUOMINEN, PASI. The purpose of consumer co-operation: implications for the management and governance of co-operatives. 2012. Diss.

488. SAARI, ESA. Suurnopeus-turbokoneroottoreiden termodynaaminen ja mekaaninen mallinnus sekä rakenneanalyysi. 2012. Diss.

489. PAANANEN, MIKKO. On innovative search: the use of internal and external sources of innovation among Finnish innovators. 2012. Diss.

490. BELOVA, POLINA. Quasiclassical approach to the vortex state in iron-based superconductors. 2012. Diss.

491. HIETANEN, IIRO. Design and characterization of large area position sensitive radiation detectors. 2012. Diss.

492. PÄSSILÄ, ANNE. A reflexive model of research-based theatre Processing innovation of the cross-road of theatre, reflection and practice-based innovation activities. 2012. Diss.

493. RIIPINEN, TOMI. Modeling and control of the power conversion unit in a solid oxide fuel cell environment. 2012. Diss.

494. RANTALAINEN, TUOMAS. Simulation of structural stress history based on dynamic analysis. 2012. Diss.